Modelling the climate response to anthropogenic carbon dioxide emissions: time-dependent processes, commitment, and reversibility

by

Ines Dana Ehlert

M.Sc., University Potsdam, 2012
B.Sc., University Potsdam, 2008

Thesis Submitted in Partial Fulfillment of the
Requirements for the Degree of
Doctor of Philosophy

in the
Department of Geography
Faculty of Environment

SIMON FRASER UNIVERSITY
Spring 2017

Approval

Name:	**Ines Dana Ehlert**
Degree:	**Doctor of Philosophy (Geography)**
Title:	***Modelling the climate response to anthropogenic carbon dioxide emissions: time-dependent processes, commitment, and reversibility***
Examining Committee:	**Chair:** Paul Kingsbury Professor

Kirsten Zickfeld
Senior Supervisor
Associate Professor _____

Karen Kohfeld
Supervisor
Associate Professor _____

Nathan Gillett
Supervisor
Adjunct Professor _____

Pascal Haegeli
Internal Examiner
Assistant Professor
School for Resource and Environmental Management
Simon Fraser University _____

Thomas Stocker
External Examiner
Professor
Department of Climate and Environmental Physics
University of Bern _____

Date Defended: 13 April 2017

Abstract

This thesis gives insight into key aspects of the climate system response to anthropogenic carbon dioxide (CO_2) emissions. One characteristic is an approximately constant global mean surface air temperature (GMSAT) after cessation of emissions, but also changes in GMSAT to second order. Here it is shown that these second-order GMSAT changes are positive, i.e. there is a small committed warming from previous emissions, because the warming effect from declining ocean heat uptake dominates over the cooling effect from declining atmospheric CO_2. The timing of zeroing emissions or the time horizon over which the warming commitment is calculated have minor effects on this warming commitment compared to the effect of the scenario prior to cessation of emissions. Another characteristic explored is the approximately constant ratio between GMSAT change and cumulative CO_2 emissions (CE), referred to as Transient Climate Response to cumulative CO_2 emissions (TCRE). It is shown that the TCRE diverges more strongly over time from a constant value under increasing atmospheric CO_2 concentration than previously suggested. But it is approximately constant over time under constant CO_2 concentration due to cancelling effects of changes in ocean heat and carbon uptake. Applying a wide range of sub-grid ocean mixing parameterizations does not change the temporal evolution of the TCRE significantly but leads to a wide range in the TCRE value. A third characteristic explored is irreversibility of sea level rise from thermal expansion (TSLR). It is shown here that TSLR under negative emissions does not return to pre-industrial levels for centuries after atmospheric CO_2 has returned to pre-industrial concentrations. This result is robust against the choice of mixing parameter, although, generally an increased parameter leads to higher TSL rise and decline rates. The results presented in this thesis suggest that setting cumulative CO_2 emission budgets in order to not exceed a certain warming target needs to be done with caution as the TCRE varies more strongly over time than previously shown and additional committed warming may lower allowable carbon budgets. Furthermore, TSLR is not linearly related to cumulative CO_2 emissions and is slow to be reversed if net negative emissions are applied.

Keywords: Climate change; Earth system modeling; Sea level rise; Warming commitment; Transient Climate Response to cumulative CO_2 Emissions; Carbon budget

Dedication

To my mom and my grandparents.

Acknowledgements

I wish to thank my supervisor Kirsten Zickfeld very much for all her extensive support, guidance, and effort. I highly appreciated her patience for my endless questions and her support in trying to make my own steps in the research world. I further thank my supervisor committee members Karen Kohfeld and Nathan Gillett for their time, encouragement to be confident, and scientific advice. I extend my thanks to Thomas Stocker and Pascal Haegeli for their time and informative comments and Paul Kingsbury for facilitating my defense greatly.

I also wish to express my great appreciation for Michael Eby's ample support for the Uvic ESCM and scientific advice. I am also thankful for the discussion and community from Tyler Herrington, Kasia Tokarska, Margaret Valerio, Xinru Li, Claude-Michel Nzotungicimpaye, and Mehdi Aminipouri.

My most heartfelt appreciation goes out to my family, friends, and all those who supported me through my formal education, with special love and thanks to Sabine, Thilo, Sonja, and Guenther. During my doctorate studies my partner Blake always stood by my side to support me with all his effort. Thank you so much!

Finally, I wish to thank my cousin Roswitha for always welcoming me with warmth and care and also Aateka and David for their hospitality in the last critical stages of my thesis.

Table of Contents

List of Tables

List of Figures

Chapter 1

Introduction

1.1 Setting the stage

Anthropogenic emissions of carbon dioxide (CO_2) have led to an increase in atmospheric CO_2 levels to 399 ppm by 2015 (Dlugokencky and Tans, 2017). For comparison, pre-industrial CO_2 concentrations were about 280 ppm. This rise in CO_2 concentration together with smaller contributions from other radiative forcing agents have induced changes in the climate system, such as an increase in global mean temperature of 0.85°C between 1880 to 2012. Non-CO_2 radiative forcing agents include other greenhouse gases such as methane, nitrous oxide, and halocarbons, and, aerosols, some of which have a cooling effect. Other changes in the climate system induced by these radiative forcing agents are increases in extreme events, such as extreme precipitation or heat waves, declining Arctic sea ice, mass loss from Greenland and Antarctic ice sheets, and increasing sea levels by 0.19 m between 1901 and 2010. The largest contribution to this sea level rise comes from thermal expansion of the ocean (IPCC, 2013). The global mean warming by the end of this century is projected to be 0.3°C to 1.7°C for the lowest emission scenario (Representative Concetration Pathway, RCP, 2.6) and 2.6°C to 4.8°C for the highest emission scenario (RCP8.5) (the temperature changes are averages over the years 2081-2100 relative to averages over the years 1986-2005). Other projected changes are for example, increased likelihood for heat waves, increased precipitation in wet regions and decreased precipitation in dry regions, and further increases in the sea level of 0.26-0.55 m and 0.45-0.82 m by 2100 (changes are averages over the years 2081-2100 relative to averages over the years 1986-2005) for the lowest (RCP 2.6) and highest (RCP 8.5) emission scenario, respectively (IPCC, 2013).
More than half of the emitted CO_2 by human activities is taken up by carbon sinks, which is equally partitioned between the land and ocean sink (Le Quéré et al., 2016). The main mechanism for land carbon uptake is CO_2 fertilization, which is enhanced plant growth due to higher CO_2 concentration in the atmosphere (Schimel, 1995; Arneth et al., 2010). In the ocean, CO_2 dissolves with the so called buffer reaction, where CO_2 and carbonate ions are

consumed and hydrogen carbonate is produced. This reaction enables more dissolution of CO_2 in the ocean but is limited by the supply of carbonate ions (Sarmiento and Gruber, 2006). However, these uptake mechanisms of carbon will change under climate change. For example, on land, high temperatures limit plant growth in low latitudes and increase decomposition of plant matter, which increases the release of carbon from land into the atmosphere (Friedlingstein et al., 2006; Zickfeld et al., 2011). Both feedbacks weaken the land carbon uptake. Increased ocean temperatures reduce the solubility of carbon in the ocean and decrease ocean carbon uptake (Sarmiento and Gruber, 2006). Besides carbon, the ocean also takes up heat, which delays global mean warming (Hansen et al., 2005; Solomon et al., 2009) and leads to sea level rise. But also ocean heat uptake changes under global warming. For example, changes in ocean circulation under global warming shift the location of ocean heat uptake to higher latitudes, which results in a cooling effect of surface air temperatures (Winton et al., 2013).

One main question in climate change research is: what future climate changes do we expect for a certain amount of CO_2 emissions? Answering this question requires understanding of both physical and bio-geochemical processes and feedbacks. Integrating a carbon cycle into climate models (Sarmiento et al., 1998; Cox et al., 2000) allowed new insights into these processes, such as significant positive climate-carbon cycle feedbacks, irreversible global mean warming after CO_2 emissions cease or an approximately linear relationship between global mean warming and cumulative CO_2 emissions (Matthews et al., 2009; Gillett et al., 2011). These findings led to the development of the carbon budget approach, implying that there is a set amount of cumulative CO_2 emissions for a specific warming target (Zickfeld et al., 2009). This approach has been suggested to inform climate policies (Raupach et al., 2014). In the Paris agreement policy makers agreed to "Holding the increase in the global average temperature to well below 2°C above pre-industrial levels and pursuing efforts to limit the temperature increase to 1.5°C above pre-industrial level" (Paris Agreement, 2015). Applying the carbon budget approach to a warming target of 2°C relative to the period 1861-1881 results in total allowable cumulative CO_2 emissions of 1000 PgC for a 66% probability of staying below 2 °C, with more than half of this carbon budget already emitted (IPCC, 2013; Rogelj et al., 2016).

The finding that warming remains approximately constant (i.e., is irreversible) after cessation of CO_2 emissions for centuries to come (Matthews and Caldeira, 2008; Gillett et al., 2011; Solomon et al., 2009) is important as it implies that current emissions commit us to future elevated temperatures. Causes for this irreversible warming are the slow decline in atmospheric CO_2 due to its long atmospheric lifetime (Eby et al., 2009) and the ocean's thermal inertia.

To second order the global mean surface air temperature (GMSAT) continues to change after cessation of CO_2 emissions. This additional temperature change is referred to as

zero emission warming commitment (ZEC) and arises because the decline in atmospheric CO_2 (cooling effect) and the decline in ocean heat uptake (warming effect) do not exactly offset each other. The ZEC ranges from -1.2°C to 0.5°C (Zickfeld et al., 2013; Frölicher et al., 2013; Frölicher and Paynter, 2015) for a range of models and scenarios. Knowing the magnitude of the ZEC is very important if using the carbon budget approach: significant additional warming would need to be included in a warming target and would therefore lower the allowable cumulative CO_2 emissions. Different causes for the range in ZEC estimates have been suggested, such as different scenarios prior to cessation of emissions (Krasting et al., 2014; Zickfeld et al., 2013; Leduc et al., 2015), the magnitude of the forcing (Herrington and Zickfeld, 2014), and model uncertainties in physical and bio-geochemical processes (Frölicher et al., 2013; Zickfeld et al., 2013). However, a systematic study comparing a range of effects potentially influencing the ZEC has not been done. A specific effect that has not been studied is the timing of zeroing emissions, which would include a focus on comparing the effects of declining ocean heat uptake (warming effect) and declining atmospheric CO_2 concentration (cooling effect). Both of these effects decline the later emissions are zeroed, but the question remains which effect would prevail. Previous studies investigate the effect of declining ocean heat uptake but they do not study in detail the change in decline in atmospheric CO_2 (Frölicher and Paynter, 2015; Nohara et al., 2015). Another factor that has not been explored thus far is the time horizon over which the ZEC is calculated.

A to first order constant GMSAT after zeroing CO_2 emissions implies an approximately constant ratio of GMSAT change to cumulative CO_2 emissions. This approximate constancy has been found to also hold under transient warming (Matthews et al., 2009; Allen et al., 2009; Eby et al., 2009) and the ratio of GMSAT to cumulative CO_2 emissions is referred to as Transient Climate Response to cumulative CO_2 Emissions (TCRE). The cause for this approximate constancy is still under discussion and different explanations have been proposed. The constancy of the TCRE across scenarios has been explained by the following cancellation processes (Matthews et al., 2009): first, the warming per unit change in atmospheric CO_2 decreases under higher CO_2 concentrations due to the logarithmic dependency of radiative forcing, and thus temperature change, on atmospheric CO_2 concentration. Second, the fraction of carbon taken up by the ocean and land decreases under higher CO_2 concentrations (and hence leading to a warmer climate), and thus the cumulative airborne fraction (i.e., the fraction of cumulative CO_2 emissions remaining in the atmosphere) increases for higher atmospheric CO_2 concentrations. Matthews et al. (2009) explain the constancy of the TCRE over time with a cancellation of a cooling effect due to uptake of atmospheric CO_2 by carbon sinks and a warming effect due to a reduced ocean heat uptake efficiency (i.e., ocean heat uptake per unit change in GMSAT). This cancellation process has been suggested to be caused by ocean heat and carbon flux being determined by the same deep ocean mixing processes (Matthews et al., 2009; Solomon et al., 2009). Other

studies (Goodwin et al., 2015; MacDougall and Friedlingstein, 2015) use different theoretical approaches to describe the TCRE and also conclude that the cancellation of the effects of ocean heat and carbon uptake on the TCRE causes its approximate constancy.
There are reasons to question this hypothesis as there are significant differences in the processes involved in ocean heat and carbon uptake. For example, ocean heat and carbon have opposite vertical gradients, which has an effect on the regions of heat and carbon uptake from the atmosphere into the ocean. Ocean carbon increases with depth due to the soft tissue pump, whereby carbon is consumed at the ocean surface by phytoplankton and transported into deeper ocean after the plankton dies and decomposes or is consumed by zooplankton and sinks down as fecal pellets. The ocean is warmed from the top and thus ocean heat content decreases with depth. Therefore, regions of deep ocean upwelling are regions of ocean heat uptake but carbon release from the ocean into the atmosphere. Furthermore, the spatially uniform atmospheric CO_2 concentration is in contrast to the strong equator-to-pole gradient of air temperature. This contrast has an effect as both air-sea fluxes of heat and carbon depend on the air-sea surface difference in either temperature (for heat flux) or partial pressure of CO_2 (for carbon flux).
Understanding the mechanism causing the TCRE to be approximately constant is an important factor in establishing the scientific foundation for the carbon budget approach. Furthermore, comparisons of climate models show that there are inter-model differences in the TCRE. The fifth Assessment Report of the Intergovernmental Panel on Climate Change (IPCC) gives a range for the TCRE of 0.8-2.5°C per 1000 PgC based on results from CMIP5 (Fifth Coupled Model Intercomparison Project) models and observational constraints (Collins et al., 2013; Frölicher and Paynter, 2015). These inter-model differences are due to differences in both physical and bio-geochemical processes (Gillett et al., 2013; MacDougall et al., 2017). One source for uncertainty that affects both physical and bio-geochemical processes via ocean heat and carbon uptake is sub-grid scale ocean mixing, which needs to be parametrized in ocean models. The effect of ocean mixing on the TCRE has not been studied.

As mentioned above, the carbon budget for the 2°C target relative to the period 1861-1880, gives a total CO_2 budget of 1000 PgC for a probability of 66% to not exceed the target (IPCC, 2013). 555 PgC have already been emitted between 1870 and 2015 (Le Quéré et al., 2016), i.e., more than half of the allowable cumulative emission budget for a 2°C target. With continuously increasing global emissions (Boden et al., 2016) the chance of attaining this warming target with emissions reduction efforts alone is decreasing. The challenge of attaining the target is heightened by the fact that current emission reduction pledges under the Paris Agreement from the high emitting countries USA, China, and European countries are not strong enough to reach the 2°C target while leaving room for reasonable emissions from other countries (Peters et al., 2015). Therefore, many emission

scenarios for the future that stay below this warming target include negative emissions after reaching a peak in emissions (Smith et al., 2016). Negative emissions means that CO_2 is artificially removed from the atmosphere such that atmospheric CO_2 declines more rapidly than would be the case with natural removal processes alone. The option of deploying negative emission technologies raises the question of reversibility of anthropogenic climate change, i.e., to which extent it is possible to return to the pre-industrial or another "safe" (defined by socially and politically measures) state of the climate system by artificially lowering atmospheric CO_2 concentrations. Specific questions are: Is it possible to restore GMSAT to pre-industrial levels and on which time scales? How much would the decline in GMSAT lag behind the decline in atmospheric CO_2 concentration? On which time scales are other aspects of climate change such sea level rise reversible?

Reversibility of GMSAT change on human time scales has been shown in previous studies (Tokarska and Zickfeld, 2015; Boucher et al., 2012). However, other climate variables, such as ocean temperature, change on longer time scales and may therefore not be reversible on timescales relevant to human civilization. One aspect that is linked to ocean temperature is the reversibility of thermal expansion of the ocean. Ocean heat uptake acts on long time scales due to the ocean's large heat capacity, therefore sea level continues to rise after zeroed emissions despite an approximately constant GMSAT (Zickfeld et al., 2013). But if instead of zeroing emissions, negative emissions are applied that lead to a strong decline in atmospheric CO_2 concentration and declining GMSAT, can sea level rise induced by thermal expansion decline? Boucher et al. (2012) and Tokarska and Zickfeld (2015) find this thermal expansion to be irreversible on decadal to centennial time scales for most scenarios tested. Bouttes et al. (2013, 2015) and Zickfeld et al. (2013), however, find a reversible thermosteric sea level rise on longer (centennial to millennial) time scales. There are only a few studies investigating the mechanism of this reversibility. Thermosteric sea level rise varies among models (Zickfeld et al., 2013), which could, among other factors, be caused by differences in sub-grid scale ocean mixing parametrization as it affects the timescale of ocean heat uptake and release and the distribution of heat in the ocean. The effect of applying different parameterizations of ocean mixing has not been examined yet.

1.2 Research questions

The goal of this thesis is to elucidate key aspects of the century-scale climate response to anthropogenic carbon dioxide emissions, such as the proportionality of change in global mean surface air temperature to cumulative CO_2 emissions, the warming commitment following cessation of CO_2 emissions, and the reversibility of anthropogenic climate change. An important part in investigating these responses is the role of the ocean as it is a very large carbon and heat reservoir. Motivated by the research gaps identified in the previous section the following specific research questions will be addressed in this thesis:

1. Zero emissions warming commitment (ZEC)
   (a) What determines the warming commitment after cessation of CO_2 emissions?
   (b) What is the effect of thermal equilibration (declining ocean heat uptake) and bio-geochemical equilibration (declining carbon uptake) on this warming commitment?
2. Transient Climate Response to cumulative CO_2 Emissions (TCRE)
   (a) Which physical processes determine the approximate constancy of the TCRE?
   (b) What is the sensitivity of the approximate constancy of the TCRE to different representations of ocean mixing?
3. Reversibility of thermosteric sea level rise
   (a) Is sea level rise due to thermal expansion reversible and on which time scale?
   (b) What are the physical mechanisms that determine this reversibility?
   (c) What is the effect of different representations of ocean mixing on the reversibility of ocean thermal expansion?

These research questions will be explored using a modelling approach. The model used is an Earth system model of intermediate complexity, which allows to simulate climate processes on multi-centennial time scales. For the investigation of the effects of ocean heat uptake and the associated thermal inertia, such long time scales are necessary.

1.3 Thesis structure

This thesis is a paper-based thesis where Chapters 2, 3, and 4 comprise individual articles published in or submitted to peer-reviewed journals. The thesis is structured as follows:

Chapter 2 investigates what determines the ZEC. Specific aspects that are being studied are the timing of zeroing CO_2 emissions, different CO_2 concentrations prior to cessation of CO_2 emissions, and the time horizon over which the ZEC is being calculated. Investigating the timing of zeroing emissions includes studying the effects of declining atmospheric CO_2 concentrations and ocean heat uptake in determining the sign of the ZEC. The strength of the effects these different aspects on the ZEC of are being compared and the implications of the findings for the carbon budget approach are being discussed.

Chapter 3 examines causes for the approximate constancy of the TCRE over time and the sensitivity of this approximate constancy to ocean mixing. A theoretical description of the TCRE is being proposed to uncover the role of ocean heat and carbon uptake in the approximate constancy of the TCRE.

Chapter 4 explores the reversibility of sea level rise due to thermal expansion and the effects of ocean mixing on this reversibility. Physical mechanisms explaining this reversibility are explored.

Chapter 5 summarizes the conclusions of this thesis, states the significance of the findings, and gives an outlook for future research.

Chapter 2

What determines the warming commitment after cessation of CO_2 emissions?

This chapter is based on the journal article:
Dana Ehlert, Kirsten Zickfeld, What determines the warming commitment after cessation of CO_2 emissions?, *Environmental Research Letters*, 12 015002, 2017.
I designed the research, performed the model simulations and analysis for this research and wrote the manuscript. Kirsten Zickfeld had the research idea, supported the analysis and interpretation of results and edited the manuscript.

Abstract Previous studies have shown that global mean surface air temperature remains elevated after cessation of CO_2 emissions. However, studies differ in whether temperature continues to increase, slowly decreases, or remains constant after cessation of emissions. An understanding of this committed warming is of importance because it has implication for the estimation of carbon budgets compatible with temperature targets. Here, we investigate the effect of the state of thermal and bio-geochemical equilibration at the time emissions are set to zero on the committed warming as the latter is determined by the balance of these two equilibration processes. We find that the effect of thermal equilibration, expressed as fraction of realized warming, dominates over the bio-geochemical equilibration, expressed as ratio of the airborne fraction to the equilibrium airborne fraction. This leads to a positive warming commitment, and a commitment that declines the later emissions are zeroed along a trajectory of constant atmospheric CO_2 concentration. We furthermore show that the scenario prior to zeroed emissions has the strongest effect on the warming commitment, compared to the time of zeroed emissions and the time horizon over which the commitment is calculated.

2.1 Introduction

Previous studies have shown that the global mean surface air temperature (GMSAT) remains elevated for several centuries (Matthews and Caldeira, 2008; Gillett et al., 2011; Solomon et al., 2009) after CO_2 emissions are set to zero. The GMSAT change remains approximately constant to first order in most studies (Cao and Caldeira, 2010; Zickfeld et al., 2012). However, to second order GMSAT increases or decreases after emissions are zeroed, depending on the model used (Zickfeld et al., 2013; Frölicher et al., 2013). This committed change in GMSAT from previous emissions, referred to as zero emission warming commitment (ZEC), is important because it has implications for the carbon budget approach. This approach is based on the finding that the long-term warming is dependent only on the cumulative CO_2 emissions and is independent of the emission pathway, implying that there is a fixed amount of cumulative emissions for a certain temperature change target (Matthews et al., 2009; Zickfeld et al., 2009). If there were significant GMSAT increase after emissions cease, this warming commitment would need to be considered and the allowable cumulative emissions would be lower in order to reach the same target.

The ZEC varies largely in sign and magnitude across studies. Gillett et al. (2011) and Zickfeld et al. (2012) showed a ZEC of -0.6°C to 0.1°C for the first-generation Canadian Earth System Model (for the SRES A2 scenario and a range of scenarios with cumulative CO_2 emissions of 2500 PgC) whereas Frölicher and Joos (2010); Frölicher et al. (2013); Frölicher and Paynter (2015) find a ZEC of -0.5°C to 0.2°C for the National Centre for Atmospheric Research Climate System Model (for the SRES A2/B1 scenarios and a pulse emission of 1800 PgC) and a ZEC of 0.37°C to 0.5°C for the Earth System Model from the Geophysical Fluid Dynamics Laboratory (ESM GFDL) (for idealized 1% increase scenario to 745 ppm of atmospheric CO_2 and pulse emission of 1800 PgC). The range of the ZEC for the different models are due to different scenarios prior to cessation of emissions and setting emissions to zero at different atmospheric CO_2 concentrations. Zickfeld et al. (2013) showed a warming commitment of -1.2°C to 0.6°C for a number of Earth System Models of Intermediate Complexity (EMICs) using the same scenario. This EMIC range is biased towards negative values as slightly negative instead of zero emissions were prescribed in this study, resulting in a more rapid decrease in atmospheric CO_2. These ZEC ranges show that there is no systematic difference in the ZEC depending on whether an EMIC or an ESM is used, as suggested by Frölicher and Paynter (2015). Previous studies indicated that ZEC differences arise from different scenarios prior to cessation of emissions, including different rates and total amounts of emissions (Krasting et al., 2014; Zickfeld et al., 2013; Leduc et al., 2015), the consideration of different forcing agents (Matthews and Zickfeld, 2012; Zickfeld et al., 2013), the magnitude of the forcing (Herrington and Zickfeld, 2014), and model uncertainties in physical and biogeochemical processes (Frölicher et al., 2013;

Zickfeld et al., 2013).

The time at which emissions are zeroed along a constant CO_2 concentration trajectory and the time-span over which the commitment is calculated may also contribute to the differences in the warming commitment but have not been explored previously. The effect of the timing at which emissions cease is not straightforward, as the ZEC is an interplay between physical and bio-geochemical processes. When emissions are zeroed, ocean heat uptake declines which leads to an increase in surface air temperature. This warming effect is counteracted by a decline in atmospheric CO_2 concentration due to continuous uptake of carbon by the land and the ocean, which has a cooling effect. Based on the ocean's thermal inertia (Hansen et al., 1985) alone, one would expect the ZEC to decrease the later emissions are zeroed along a constant concentration trajectory because the ocean heat uptake declines less. However, atmospheric CO_2 concentrations after emissions are zeroed also decline less the later emissions are zeroed. The ZEC will be determined by the balance of the two processes and it is not immediately clear which one dominates. Previous studies investigate the effect of declining ocean heat uptake but they do not study in detail the change in decline in atmospheric CO_2 (Frölicher and Paynter, 2015; Nohara et al., 2015).

The goal of this study is to explore in depth the effect of both thermal and bio-geochemical equilibration and the amount of forcing on the ZEC using the University of Victoria Earth System Climate Model (UVic ESCM). We design two sets of CO_2 scenarios that differ in the time emissions are set to zero along a constant CO_2 concentration trajectory, and the peak CO_2 concentration (and hence radiative forcing). Such a simulation setup allows us to isolate the effect of the state of equilibration on the ZEC.

2.2 Model and Simulations

2.2.1 Model

We carried out all simulations using the University of Victoria Earth System Model, version 2.9 (UVic ESCM 2.9), an Earth system model of intermediate complexity (EMIC). The three main physical components are an atmosphere energy balance model, a general ocean circulation model, and a land surface scheme. The atmosphere is described by a vertically integrated energy-moisture balance model, including water vapour, planetary long wave, and dynamic wind feedbacks. All components have a resolution of 1.8°(meridional) x 3.6°(zonal). The model does not include an ice sheet model and we only discuss the sea level rise due to thermal expansion of the ocean. UVic ESCM also includes land, ocean, and ocean sediment coupled carbon cycle components, which enable to prescribe CO_2 emissions directly instead of CO_2 concentrations.

The ocean is described via the Geophysical Fluid Dynamic Laboratory (GFDL) Modular

Ocean Model (MOM), a 3D general circulation model with 19 vertical layers (Weaver et al., 2001) . The MOM is coupled to a dynamic sea ice model, a sediment model, an inorganic carbon cycle model, and a marine biology model (Schmittner et al., 2005). The land is modeled via a simplified version of the land surface scheme MOSES (Met Office Surface Exchange Scheme) (Meissner et al., 2003; Cox et al., 1999), which is coupled to the dynamic vegetation model TRIFFID (Top-down Representation of Interactive Foliage and Flora Including Dynamics) (Cox, 2001).

2.2.2 Simulations

The UVic ESCM is spun up for 6000 years under pre-industrial (year 1800) conditions. After the model is fully equilibrated, it is forced with idealized scenarios with a 1% yearly increase in atmospheric CO_2 concentration until doubling (2xCO2) and quadrupling (4xCO2) of the pre-industrial concentration. Starting from these CO_2 concentration levels a cessation of CO_2 emissions is prescribed in 100 year intervals (Figure 2.1a and 2.2a). The simulations are named according to the simulation year emissions are set to zero, i.e., 2xCO2_70 until 2xCO2_770 and 4xCO2_140 until 4xCO2_840. Atmospheric CO_2 is the only forcing in these simulations. Within each simulation set, either 2xCO2 or 4xCO2, simulations differ in the state of thermal and bio-geochemical equilibration of the climate system at the time emissions are set to zero and in the cumulative emissions (Figure 2.1a and 2.2a). Holding atmospheric CO_2 constant allows for (small) CO_2 emissions that results in different cumulative emissions by the time emissions are set to zero (1138-1926 PgC and 2881-3843 PgC for the 2xCO2 and 4xCO2 scenarios, respectively). Other aspects, such as radiative forcing at time of zeroed emissions, are the same. Therefore, this unique simulation set up allows for a detailed examination of the effect of the state of equilibration on the ZEC.

2.3 Results

2.3.1 Climate system response

In our scenarios, an increase in atmospheric CO_2 is prescribed, followed by setting CO_2 emissions to zero along a constant CO_2 concentration trajectory. As soon as CO_2 emissions stop, atmospheric CO_2 declines due to carbon uptake by land and ocean (Figures 2.1a and 2.2a). Within each simulation, the rate of this CO_2 decline decreases over time. The change in the rate of atmospheric CO_2 decline is associated with different time scales of carbon uptake processes on land and in the ocean, as discussed below. Additionally, atmospheric CO_2 concentration declines less between simulations the later emissions are zeroed.
Despite declining CO_2 concentration, GMSAT anomaly continues to rise slightly once emissions cease in all simulations (Figure 2.1b, and 2.2b). This warming after zeroed emissions

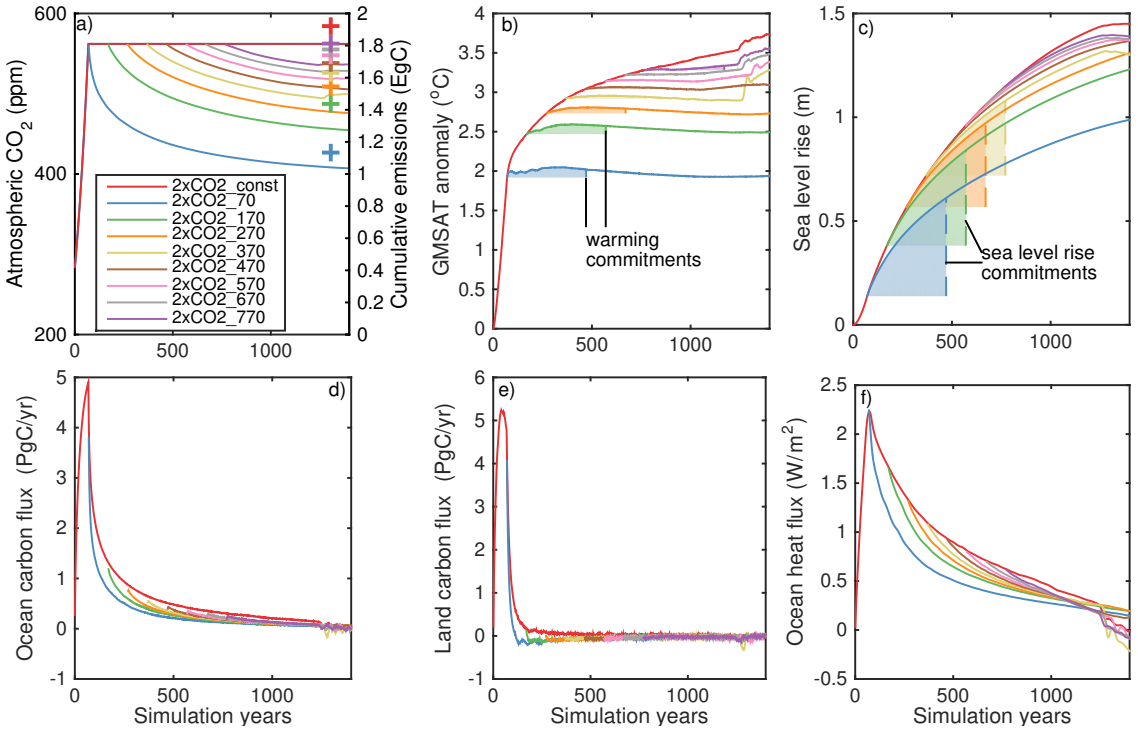

Figure 2.1: Atmospheric CO_2 concentration and cumulative CO_2 emissions at the time emissions are set to zero (crosses, 1 EgC=1000 PgC) (a), global mean surface air temperature (GMSAT) anomaly (relative to year 0) (b), sea level rise (relative to year 0) due to thermal expansion (c), carbon fluxes (d,e), and ocean heat flux (f) for a 1% yearly increase of CO_2 until doubling of pre-industrial concentration and zeroed emissions in 100 year intervals. Positive fluxes indicate uptake of heat or carbon by the ocean or land. GMSAT anomaly and thermosteric sea level rise values of the shaded areas (vertical dashed lines) show the commitments for GMSAT anomaly and sea level rise as shown in Figure 2.4.

declines between simulations the later emissions are zeroed (Figure 2.4a). The discontinuities in GMSAT anomaly and other variables towards the end of some simulations are caused by flushing events in the Southern Ocean in the UVic ESCM which depend on the level of atmospheric CO_2 (Meissner et al., 2008). In these events the model abruptly transitions into a stage of strong deep water formation in the Southern Ocean, which leads to outgassing of carbon into the atmosphere, decreased sea ice coverage, and increased air temperature.

Sea level rise due to thermal expansion of the ocean continues after emissions cease in all simulations (Figures 2.1c and 2.2c). The increase rate in thermosteric sea level rise diminishes the later emissions are zeroed. Therefore sea level rise after cessation of emissions is smaller the later emissions are zeroed (Figure 2.4b).

In order to understand which aspects determine the warming commitment it is important to understand how ocean heat uptake and ocean and land carbon uptake evolve as ocean heat uptake affects GMSAT directly and land and ocean carbon uptakes affect atmospheric CO_2

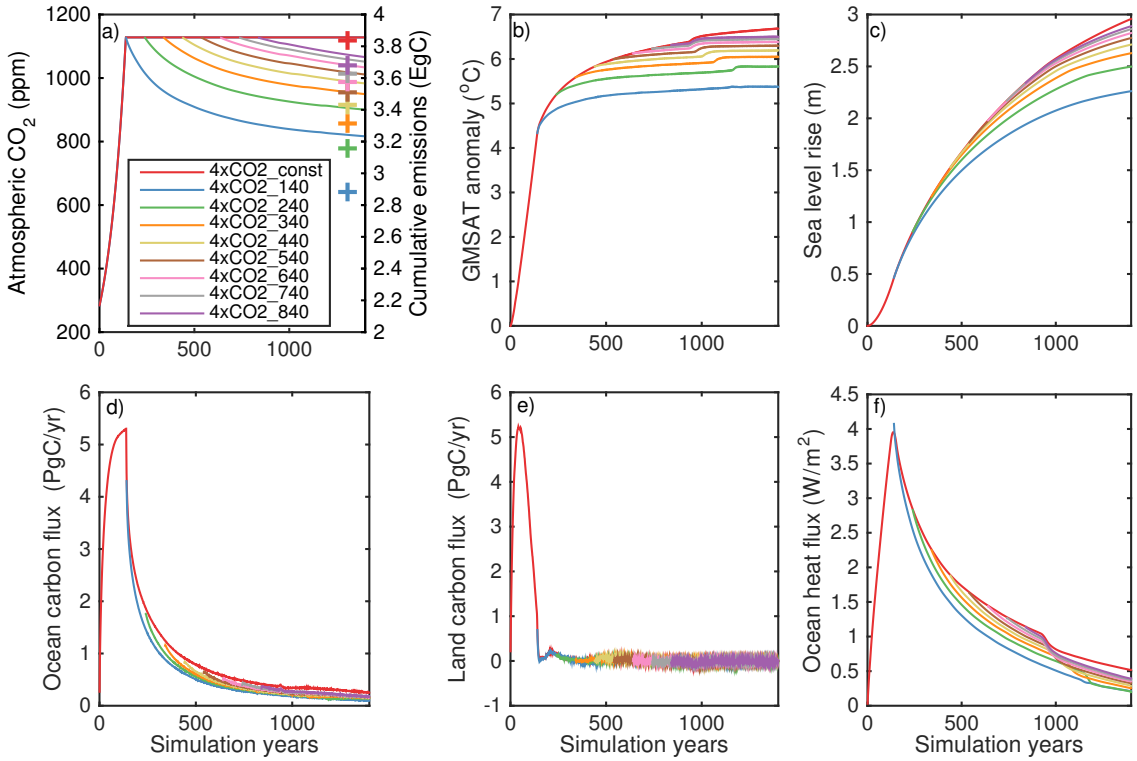

Figure 2.2: Atmospheric CO_2 concentration and cumulative CO_2 emissions at the time emissions are set to zero (crosses, 1 EgC=1000 PgC) (a), global mean surface air temperature (GMSAT) anomaly (relative to year 0) (b), sea level rise (relative to year 0) due to thermal expansion (c), carbon fluxes (d,e), and ocean heat flux (f) for a 1% yearly increase of CO_2 until quadrupling of pre-industrial concentration and zeroed emissions in 100 year intervals. Positive fluxes indicate uptake of heat or carbon by the ocean or land. Jumps in ocean fluxes and GMSAT anomaly are due to internal model variability.

and in turn radiative forcing and GMSAT. Ocean heat and carbon fluxes decline while atmospheric CO_2 is held constant and decline more strongly over time after cessation of emissions within each simulation (Figures 2.1d,f and 2.2d,f). Land and ocean carbon uptake together affect the airborne fraction (defined as ratio of change in atmospheric carbon burden to cumulative CO_2 emissions) and atmospheric CO_2 concentration after cessation of emissions and thus radiative forcing. The land carbon uptake already starts declining shortly before reaching doubling of pre-industrial CO_2 concentration due to positive climate-carbon cycle feedbacks, such as decreased net primary productivity in lower latitudes or increased soil respiration under rising temperatures (Friedlingstein et al., 2006; Zickfeld et al., 2011). Therefore, in the first zeroed emissions simulation of the 2xCO2 simulations (2xCO2_70) the land carbon flux is still relatively high. Together with high ocean carbon uptake, this high land uptake results in a strong decline in airborne fraction after cessation of emissions (Figure 2.3b) and low warming commitment for this simulation (Figure 2.5a). For all other simulations, land carbon flux is very close to zero once emissions cease. The differences

in the decline between ocean heat and carbon flux, together with the close to zero land carbon uptake after zeroed emissions have implications on how ocean heat uptake declines compared to the decline in radiative forcing. The implications for the ZEC are discussed in Section 2.3.3.

2.3.2 Thermal and bio-geochemical equilibration

In the following we explore how close the system is to thermal and bio-geochemical equilibration at the time CO_2 emissions are set to zero and to what extent the state of equilibration determines the sign and magnitude of the warming commitment.

The state of thermal equilibration is expressed in terms of the realized warming fraction, defined as the ratio of GMSAT anomaly to instantaneous equilibrium temperature, which is a commonly used measure (Solomon et al., 2009). The higher the realized warming fraction, the closer the system is to thermal equilibrium. The equilibrium temperature is calculated using $T_{eq}(t) = RF(t)/\lambda$ where T_{eq} is the equilibrium temperature at time t, RF is the radiative forcing at time t, and λ is the climate feedback parameter. For both 2xCO2 and 4xCO2 simulations, the simulations in which emissions cease later are closer to thermal equilibrium at the time of zeroed emissions (Figure 2.3a). The realized warming fraction at the time of zeroed emissions is 0.5-0.9 and 0.6-0.8 for 2xCO2 and 4xCO2 simulations, respectively. Thus the 4xCO2 simulations have a smaller range but are generally further away from thermal equilibrium than the 2xCO2 simulations (compare continuous and dashed lines in Figure 2.3a).

The deviation of the cumulative airborne fraction (AF) from the equilibrium cumulative airborne fraction (AF_{eq}) is used as a measure for the state of bio-geochemical equilibration (Figure 2.3b). The AF indicates the fraction of cumulative anthropogenic emissions that remains in the atmosphere and is determined by the carbon uptake mechanisms, which act on varying time scales. The main processes that are important on the time scales discussed here are land carbon uptake (1-100 year time scale), dissolution of CO_2 into the ocean mixed layer and mixing of carbon into deeper ocean layers (10-1000 years time scale), and reaction of dissolved carbon with calcium carbonate in sea sediments (1000-10,000 years) (Archer et al., 2009; Ciais et al., 2013). Carbon uptake by land weathering (acting on 10,000-100,000 year time scales) plays only a minor role on the time scales considered here. In previous studies (Solomon et al., 2009; Eby et al., 2009; Frölicher and Paynter, 2015), the AF after 10,000 years was taken as AF_{eq}, which does not take weathering into account.

We follow this approach here and use the year 10,000 values given by Eby et al. (2009) for the UVic ESCM. Eby et al. (2009) show that the AF_{eq} (value at year 10,000) is cumulative emission but not emission path dependent. The AF_{eq} for the 2xCO2 simulations is ∼20%, the AF_{eq} for the 4xCO2 simulations is ∼25% (grey lines in Figure 2.3b). These values agree with the theoretically derived value of 20% by Solomon et al. (2009). At the time of

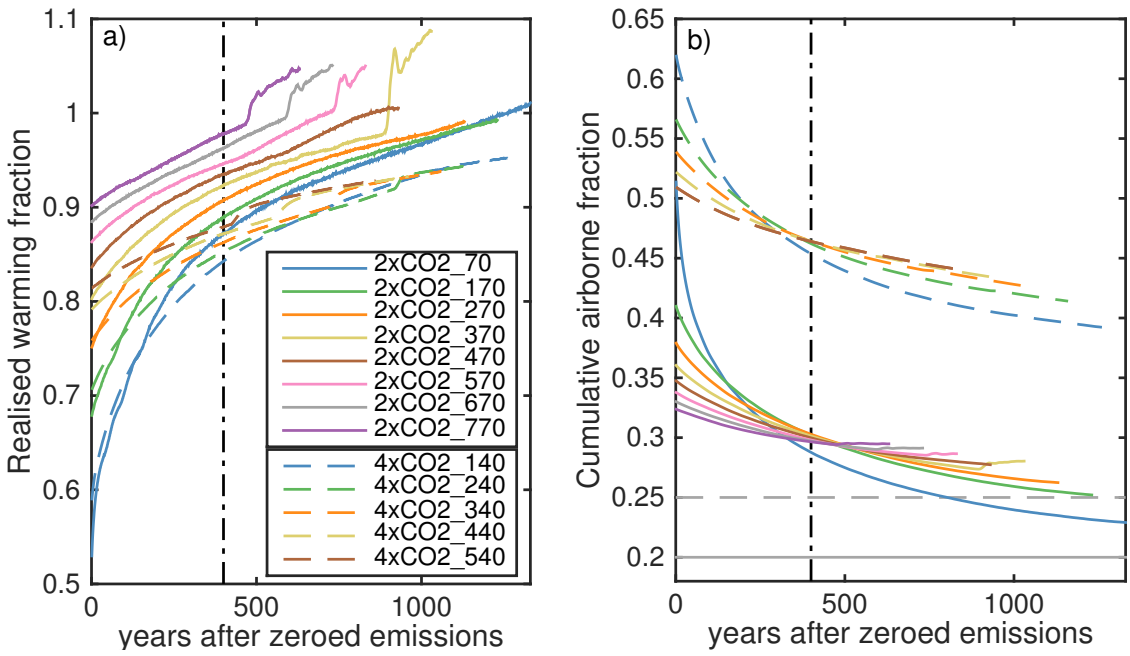

Figure 2.3: a) Realized warming fraction, defined as the ratio of GMSAT anomaly to equilibrium temperature change for the radiative forcing at each point in time. b) Airborne fraction, i.e., the ratio of change in atmospheric carbon burden over cumulative emissions. The horizontal grey lines, continuous and dashed, are the equilibrium airborne fraction for 2xCO2 and 4xCO2 simulations, respectively. The equilibrium airborne fraction is the year 10,000 value given by Eby et al. (2009). Year zero is the year at which emissions ceased and the vertical dot-dashed line indicates the time at which the commitments are calculated (400 years after cessation of emissions). For 4xCO2 simulations 4xCO2_640, 4xCO2_740, 4xCO2_840 are not shown as in those simulations the equilibration process is disturbed due to model internal variability within 400 years after zeroed emissions.

zeroed emissions, the AF is lower for simulations in which emissions cease later in time indicating that the system is closer to bio-geochemical equilibration (Figure 2.3b). However, the decline rate of the AF is higher the earlier emissions cease because atmosphere and ocean carbon reservoirs are less in equilibrium with atmospheric CO_2 and therefore land and ocean carbon uptake is higher. Thus, from 400-500 years after cessation of emissions onwards the AF is higher the later emissions cease. The 2xCO2 and 4xCO2 simulations reach an AF at the year of zeroed emissions of 30-50% and 50-60% respectively. Thus both 2xCO2 and 4xCO2 simulations are still quite far from biogeochemical equilibrium and the simulations within 2xCO2 and 4xCO2 sets do not converge to the same value.

Comparing the realized warming fraction and how close the AF is to its equilibrium value at time of zeroed emissions, the system seems to be closer to thermal equilibrium than to bio-geochemical equilibrium. However, this difference in equilibration time scale is inherent to the definition of the AF_{eq} as we include long time scale ocean sediment processes of the carbon cycle by choosing the year 10,000 value as the AF_{eq}. Thus the thermal equilibra-

tion is faster than the bio-geochemical equilibration due to the long time scales of sediment carbon cycle processes.

2.3.3 Zero emission warming commitment

In the following we discuss the ZEC and the connection to the equilibration of the climate system. We evaluate the zero emission commitment in this study by calculating the difference of a variable (GMSAT anomaly and sea level rise due to thermal expansion) between the time of setting emissions to zero and 400 years later. If we use commitment in the following, we refer to the zero emission commitment described above and ZEC refers to the zero emission warming commitment as the change in GMSAT anomaly. The ZEC is always positive (Figure 2.4a) and it is higher for 4xCO2 simulations than for 2xCO2 simulations (4xCO2 ZEC=0.2-0.9°C, 2xCO2 ZEC=0-0.1°C). Furthermore, the ZEC declines for simulations with emissions zeroed later in time for both 2xCO2 and 4xCO2 simulations. Only between the last three 2xCO2 simulations, the ZEC increases again. Similarly, the thermosteric sea level rise commitment declines for simulations with emissions zeroed later in time (Figure 2.4b).

As discussed above, the ZEC results from a balancing process between the decline in ocean heat uptake (warming effect) and the decline in radiative forcing due to declining CO_2 concentrations (cooling effect). The decline in ocean heat uptake depends on the state of thermal equilibration of the system, i.e., the more the system is equilibrated, the lower the decline in ocean heat uptake and the smaller is the warming effect from this decline. The degree of decline in atmospheric CO_2, on the other hand, is dependent on the state of bio-geochemical equilibration, i.e., the more the system is equilibrated, the smaller is the ocean carbon uptake and thus a smaller decline in atmospheric CO_2 and radiative forcing, implying a smaller cooling effect. A positive ZEC, as found in our simulations, indicates that the effect of decline in ocean heat uptake after emissions cease dominates over the effect of decline in radiative forcing within each simulation. Thus the effect of the thermal equilibration dominates over the effect of bio-geochemical equilibration within each simulation.

In the following we show that the dominance of thermal equilibration also explains the decrease in ZEC for simulations where CO_2 emissions are set to zero later with a few exceptions in the 2xCO2 simulations.

The decline in radiative forcing diminishes the later emissions are zeroed along a constant CO_2 trajectory because the decrease in carbon uptake diminishes the later emissions cease (Figure 2.4c). The decline in ocean heat uptake also diminishes the later emissions are zeroed and it diminishes more strongly between simulations than the decline in radiative forcing (compare slopes of continuous and dashed line in Figure 2.4d). Therefore, the warming effect of the decline in ocean heat uptake decreases more strongly relative to the cooling

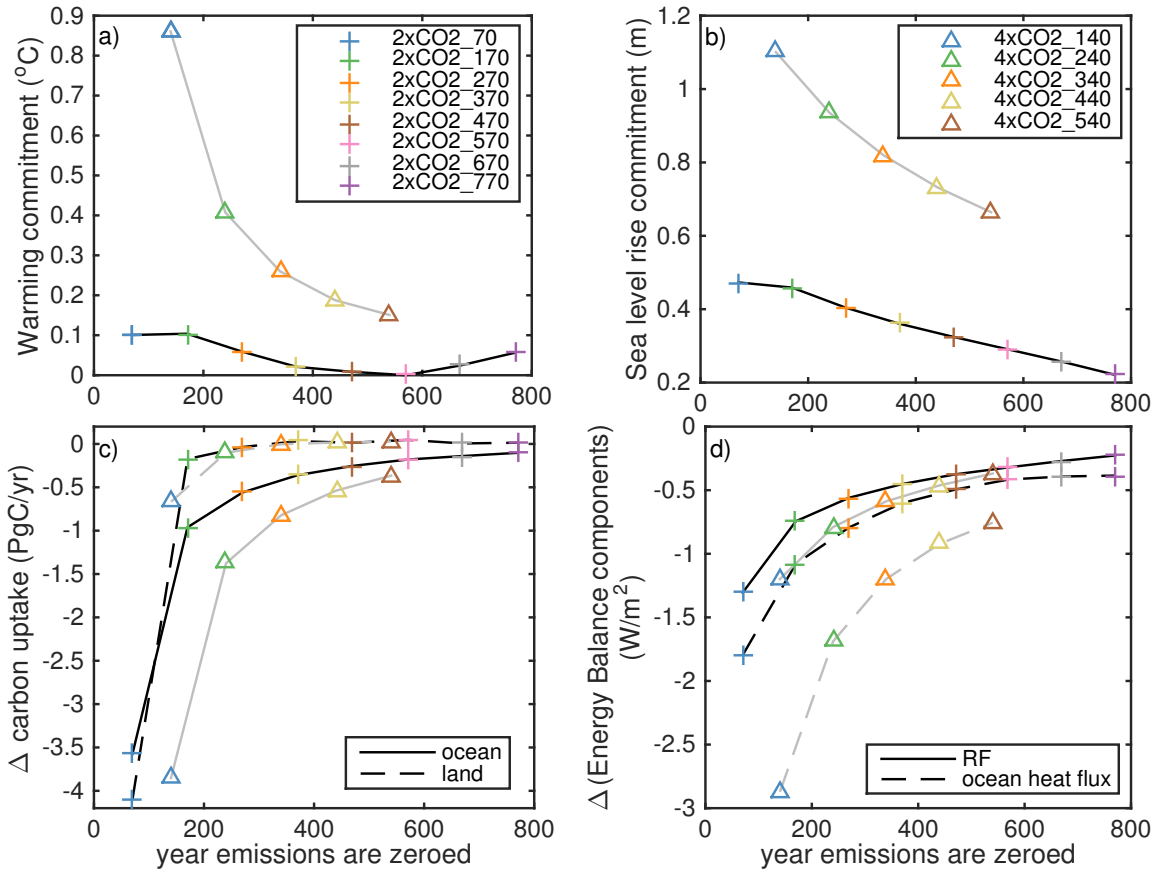

Figure 2.4: Warming commitment (a), thermosteric sea level rise commitment (b), residual change in land and ocean carbon uptake(c), and residual change in radiative forcing and ocean heat uptake (d) over 400 years after zeroed emissions for 1% yearly atmospheric CO_2 increase until 2x (black lines) and 4x (grey lines) pre-industrial CO_2. Each data point is a different simulation, where the year on the x axes indicates the year at which emissions are set to zero. The colors of each marker correspond to the simulations as seen in Figures 2.1 and 2.2. Carbon and heat uptake and radiative forcing decline over time. Therefore their residual changes are negative and their magnitude decreases between the simulations. The last three simulations of the 4xCO2 simulations are not shown as the equilibration process is interrupted due to internal model variability within 400 years after zeroed emissions.

effect from declining radiative forcing and the ZEC declines the later emissions are zeroed. There are two exceptions from this decline in ZEC in the 2xCO2 simulations. Firstly, the ZEC increases between the last three 2xCO2 simulations (Figure 2.4a), which is due to an approximately constant decline in ocean heat uptake between those simulations while the decline in radiative forcing continues to decrease (the continuous black line in Figure 2.4d still changes while the dashed black line is constant). The second exception is approximately constant ZECs between the first two 2xCO2 simulations due do similarly strong changes in ocean heat uptake decline and radiative forcing decline between those simulations. The

stronger decline in radiative forcing after zeroed emissions in the first 2xCO2 simulation is probably due to a higher land carbon uptake in this simulation. Thus to summarize the ZEC depends on both the thermal and bio-geochemical equilibration. The effect of thermal equilibration dominates in most simulations but for the last three 2xCO2 simulations the change in ocean heat uptake is the same and the change in bio-geochemical equilibration between the simulations dominates, which leads to an increase in the ZEC between these simulations.

Scenarios within each simulation set that differ in the timing of zeroing emissions also differ with regard to cumulative emissions (Figure 2.1a, 2.2a). Separating the effect of the state of equilibration and cumulative emissions is difficult. Previous studies (Herrington and Zickfeld, 2014; Leduc et al., 2015) that explored the warming commitment under different scenarios did not separate the effects of the total amount and the rate of emissions. Therefore, scenarios with higher cumulative emissions, linked to higher ZEC (at least for cumulative emissions above 2400 EgC), also entail higher emission rates and a stronger disequilibrium. Based on our current understanding of the coupled climate-carbon cycle system we expect that under higher cumulative emissions carbon sinks will be closer to saturation, which leads to lower CO_2 uptake. This lower CO_2 uptake entails lower cumulative emissions while atmospheric CO_2 is prescribed and a slower decline in atmospheric CO_2 once emissions are zeroed. The slower decline results in a higher ZEC. Thus, when only taking differences in cumulative emissions into account we would expect the ZEC to increase the later emissions are zeroed. However, ZEC are mostly deceasing the later emissions are zeroed suggesting that the effects of increased cumulative emission and bio-geochemical equilibration are less dominant than the effect of thermal equilibration. The sea level rise commitment is not affected by different cumulative emissions within each simulation set as the radiative forcing does not vary.

In addition to the time at which emissions are zeroed, the ZEC is also dependent on the CO_2 concentration scenario prior to zeroed emissions, which affects the state of equilibration, the radiative forcing, and cumulative emissions. For the 4xCO2 simulations the ZEC is 0.15-0.86°C whereas the 2xCO2 ZEC stays very low at 0.0-0.10°C (Figure 2.4a). This large difference in ZEC can be explained with a lower realized warming fraction at the time of zeroed emissions under higher CO_2 concentration (Figure 2.3a) and thus a stronger decline in ocean heat uptake. Furthermore, higher cumulative emissions together with climate carbon cycle feedbacks from increased temperatures due to increased radiative forcing lead to more saturated carbon sinks. This saturation entails a slower decline in CO_2 concentration after zeroing emissions and thus a larger ZEC. However, a higher AF relative to its AF_{eq} value for the 4xCO2 simulations compared to the 2xCO2 simulations at the time of zeroed emissions (Figure 2.3b) indicates a lower state of bio-geochemical equilibration. This lower

state of equilibration results in a stronger decline in CO_2 concentration leading to a lower ZEC. In total the effects of thermal equilibration and higher cumulative emissions dominate over the effect of bio-geochemical equilibration.

Thus far we have defined the ZEC between the time of zeroed emissions and 400 years after zeroed emissions. However, many studies differ in duration over which the commitment is calculated. Figure 2.5 shows warming and sea level rise commitments calculated as change over 100, 400, 700, and 900 years after cessation of emissions. This range of duration for calculating the commitment reflects the range in the existing literature (Lowe et al., 2009; Zickfeld et al., 2013; Frölicher and Paynter, 2015). Calculating ZEC only over 100 years for the 4xCO2 simulation gives significantly lower ZECs relative to the ZECs calculated over longer duration. For time horizons of 400 to 900 years the ZEC declines slightly for 2xCO2 simulations and increases slightly for 4xCO2 simulations the longer the time horizon over which the commitment is calculated whereas the sea level rise commitment increases significantly for both 4xCO2 and 2xCO2 simulations.

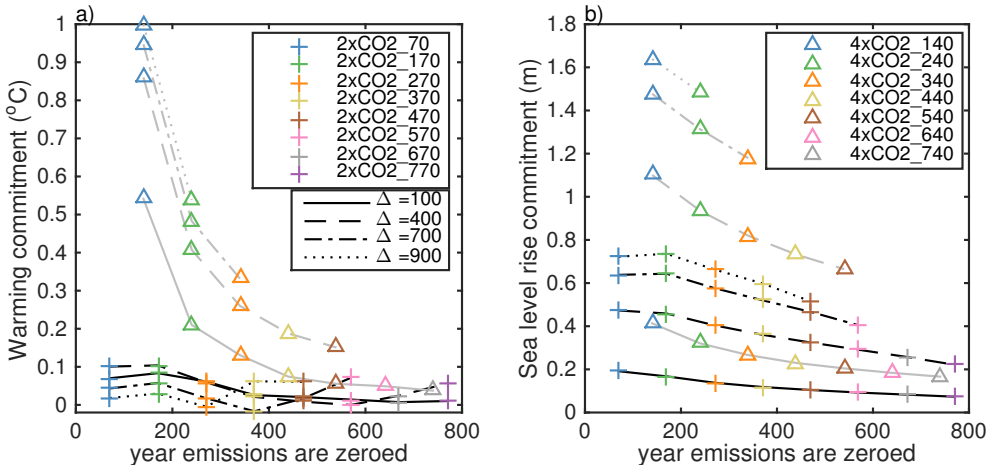

Figure 2.5: ZEC (a) and thermosteric sea level rise commitment (b) calculated as the change over 100, 400, 700, and 900 years after cessation of emissions.

2.4 Discussion

A positive warming commitment for the UVic ESCM is consistent with other studies using the same model, as long as the emissions are positive prior to cessation of emissions (Cao and Caldeira, 2010; Matthews and Zickfeld, 2012). However, sign and magnitude of the warming commitment is highly model dependent (Frölicher et al., 2013; Zickfeld et al., 2013). Frölicher and Paynter (2015) suggest that EMICs have a negative ZEC and all ESM have a positive ZEC. We do not agree with this assessment, for the following three reasons. Firstly, there are ESMs that have negative ZEC in some studies (Gillett et al., 2011;

Zickfeld et al., 2012; Frölicher and Joos, 2010; Frölicher et al., 2013), depending on the scenario prior to setting emissions to zero, as discussed in Section 4.1. Secondly, Frölicher and Paynter (2015) compare their results with the warming commitment for the EMICs from Zickfeld et al. (2013), where slightly negative as opposed to zero emissions are prescribed, which leads to a low bias in the warming commitment for some EMICs as shown for the UVic ESCM (see supplementary material). Thirdly, consistent with other studies (Cao and Caldeira, 2010; Matthews and Zickfeld, 2012) we show that the UVic ESCM, as an EMIC, has a positive ZEC. We caution against generalizing results to all EMICs, as this group of models is very heterogeneous (some are coarse resolution ESMs, whereas others are box models).

Most studies show small positive or negative ZECs (see Section 4.1), which indicates that little additional warming after zeroed emissions needs to be taken into account when estimating the cumulative CO_2 emissions compatible with climate targets. Only studies using the ESM GFDL Frölicher and Paynter (2015) find high ZECs under low warming scenarios (0.5°C ZEC for 2°C warming). Our analysis show a negligible warming commitment for CO_2 concentrations up to doubling of the pre-industrial CO_2 concentration or RCP4.5 concentrations after year 2200, whereas they show a significant warming commitment for quadrupling of pre-industrial concentrations or RCP8.5 concentrations after year 2200 (see supplementary material). An implication of this is that additional warming may not have to be considered for low climate targets (1.5°C to 2°C), whereas it may have to be considered for high targets.

2.5 Conclusions

In this study we investigate the effect of different factors on the zero emission warming commitment, including the effect of the state of thermal and bio-geochemical equilibration at the time emissions are set to zero, the CO_2 concentration level, and the time horizon over which the commitment is calculated. Previous studies have investigated the effect of thermal equilibration (Frölicher and Paynter, 2015) but this study is the first one to our knowledge that investigates the effect of bio-geochemical equilibration as well. Both thermal and bio-geochemical equilibration have to be taken into account when discussing the ZEC as the commitment is determined by the warming effect from declining ocean heat uptake, associated with the state of thermal equilibration, and the cooling effect of declining atmospheric CO_2, which is affected by declining carbon uptake, and thus the state of bio-geochemical equilibration. The warming commitment is positive in all simulations, which implies that the warming effect of decline in ocean heat uptake dominates over the cooling effect of decline in atmospheric CO_2 and thus decline in radiative forcing.

Furthermore we find that the warming commitment declines the later emissions cease along a trajectory of constant atmospheric CO_2 concentration. This implies that the decrease in

declining ocean heat uptake (decline in warming effect) dominates over the decrease in declining radiative forcing (decline in cooling effect). Thus the state of thermal equilibration, expressed as the realized warming fraction, has a stronger effect on the ZEC than the state of bio-geochemical equilibration, expressed as the ratio of airborne fraction to equilibrium airborne fraction. However, the warming commitment increases again once it declines to zero in the 2xCO2 simulations indicating the state of bio-geochemical equilibration dominates over the state of thermal equilibration in these cases. This behavior of the ZEC could be model dependent as the warming commitment in general is very model dependent as physical and bio-geochemical processes and their balance differ between models. Another factor that varies between simulations are the cumulative CO_2 emissions. Higher cumulative emissions for simulations with emissions zeroed later could lead to increasing ZEC or, rather, ZEC decreasing less if carbon sinks saturate. However, we expect this effect to be small relative to the effect of thermal equilibration.

To summarize, the warming commitment is higher for higher CO_2 concentrations prior to cessation of emissions, the earlier emissions are zeroed in time, and the longer the duration over which the commitment is calculated. Whereas the first factor, the concentration prior to zeroed emissions, has a strong effect on the commitment, the time at which emissions are zeroed and the time period over which the commitment is calculated have only a small effect on the warming commitment. Thus, when comparing warming commitments from different studies we recommend only comparing studies with the same or similar scenarios prior to zeroed emissions whereas the other two factors might not have to be taken into account or could be adjusted by using our results. Furthermore, we find significant ZEC for high CO_2 concentration scenarios (4xCO2 ZEC=0.2-0.9°C, RCP8.5 ZEC= 0.2-0.6°C) but small ZECs for lower concentration scenarios (2xCO2 ZEC=0-0.1°C, RCP4.5 ZEC=0.07-0.2°C). This implies that for low concentration scenarios no additional warming may need to be taken into account when estimating the cumulative CO_2 emissions compatible with climate targets, whereas additional warming may have to be considered for high concentration scenarios.

2.6 Supplementary material

Simulations using Representative Concentration Pathways.

2.6.1 Simulations

In order to investigate the climate change commitment under more realistic scenarios, simulations are performed using the Representative Concentration Pathways (RCP) 4.5, 6.0, and 8.5 and their extensions until calendar year 2300 (Meinshausen et al., 2011) which

include greenhouse gases (CO_2 and non CO_2), aerosols, and land use change as anthropogenic forcings. For these simulation UVic ESCM is spun up under year 850 conditions, then integrated until year 2005, as described in the EMIC inter-comparison project (Eby et al., 2013; Zickfeld et al., 2013), and subsequently forced using the RCP4.5, RCP6.0, and RCP8.5. Starting in year 2150 for RCP4.5 and RCP6.0 and year 2250 for RCP8.5, all forcings are constant. CO_2 concentrations at that time are 543 ppm for RCP4.5, 752 ppm for RCP6.0, and 2251 ppm for RCP8.5. The constant aerosol and non-CO_2 greenhouse gas forcings are -0.08 Wm^{-2} and 0.87 Wm^{-2}, -0.10 Wm^{-2} and 0.97 Wm^{-2}, -0.1 Wm^{-2} and 2.0 Wm^{-2} for RCP4.5, RCP6.0, RCP8.5 respectively. From year 2200 for RCP4.5 and 6.0 and from year 2300 for RCP8.5 CO_2 until year 2900 emissions are zeroed in 100 year intervals while all other forcings remain constant.

2.6.2 Results and discussion

In the following section we discuss the effect of the timing of zeroed emissions and the scenario prior to zeroed emissions on the climate change commitment using the Representative Concentration Pathways (RCPs) as described above. Generally, the ZEC and the thermosteric sea level rise commitment for the RCP simulations behave very similarly to the 1% yearly increase idealized simulations discussed above (Figure 2.6). This similarity is not intuitive as the RCP simulations also included non-CO_2 forcers, which can add additional warming with further consequences to carbon-cycle-climate feedbacks. As in the idealized simulations, we observe always a positive ZECs. Furthermore, both ZEC and sea level rise commitment decline between simulations with CO_2 emissions zeroed later in time and the commitments are higher for higher CO_2 concentrations prior to setting CO_2 emissions to zero.
Furthermore, the warming commitment for RCP4.5 shows a similar behavior as the commitment for the 2xCO2 simulations; the RCP4.5 warming commitments decline with emissions zeroed later in time and approach a lower most value but increase slightly thereafter (Figure 2.6a, continuous line). The only difference to the 2xCO2 simulations is that the lower most warming commitment is not zero in the RCP4.5. This non-zero value is probably due to the constant non-CO_2 forcers which add additional warming.

In an EMIC intercomparison study, Zickfeld et al. (2013) compare the warming commitment for simulations following the RCPs followed by prescribing pre-industrial emissions in year 2300. For RCP4.5, RCP6.0, and RCP8.5 they find a warming commitment range of 1.0°C to 0.3°C, -1.2°C to 0.4°C, and -0.7°C to 0.6°C over all EMICs and warming commitments of -0.4°C, -0.06°C, and 0.5°C for UVic ESCM alone. Our ZEC for the RCPs simulation with zeroed emissions at year 2300 are 0.1°C, 0.3°C, and 0.6°C for RCP4.5, RCP6.0, and RCP8.5, respectively. Thus our ZECs are higher than the commitments for

UVic ESCM from Zickfeld et al. (2013) because Zickfeld et al. (2013) prescribe negative pre-industrial emissions for UVic ESCM and we set emissions to zero. Other models in the EMIC inter-comparison study have negative pre-industrial emissions, thus it is reasonable to believe that the warming commitment range given by Zickfeld et al. (2013) is biased low when comparing it to ZEC.

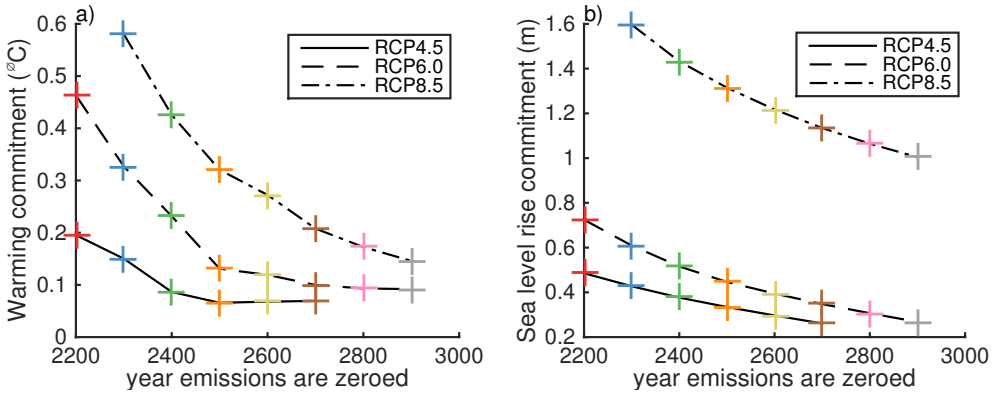

Figure 2.6: Warming commitment (a) and thermosteric sea level rise commitment (b) calculated as change in global mean surface air temperature and thermosteric sea level rise over 400 years after zeroed emissions for RCP4.5, RCP6.0, and RCP8.5. Each data point is a different simulation, where the year on the x axes indicates the year at which emissions are set to zero.

Chapter 3

The sensitivity of the proportionality between temperature change and cumulative CO_2 emissions to ocean mixing

This chapter is based on the journal article:
Dana Ehlert, Kirsten Zickfeld, Michael Eby, Nathan Gillett, The sensitivity of the proportionality between temperature change and cumulative CO_2 emissions to ocean mixing, *Journal of Climate*, 30, 2921-2935, doi: 10.1175/JCLI-D-16-0247.1, 2017.
I designed the model simulations with support from Michael Eby, performed the simulations, analysed and interpreted the simulation results with support from Kirsten Zickfeld, Michael Eby, and Nathan Gillet, and wrote the manuscript with edits from Kirsten Zickfeld, Michael Eby, and Nathan Gillett.

Abstract The ratio of global mean surface air temperature change to cumulative CO_2 emissions, referred to as Transient Climate Response to Cumulative CO_2 Emissions (TCRE), has been shown to be approximately constant on centennial time scales. The mechanisms behind this constancy are not well understood, but previous studies suggest that compensating effects of ocean heat and carbon fluxes, which are governed by the same ocean mixing processes, could be one cause for this approximate constancy. This hypothesis is investigated by forcing different versions of the University of Victoria Earth System Climate Model, which differ in the ocean mixing parameterization, with an idealized scenario of 1% annually increasing atmospheric CO_2 until quadrupling of the pre-industrial CO_2

concentration and constant concentration thereafter. The relationship between surface air warming and cumulative emissions remains close to linear but the TCRE varies between model versions, spanning the range of 1.2-2.1°C EgC^{-1} at the time of CO_2 doubling. For all model versions, the TCRE is not constant over time while atmospheric CO_2 concentrations increase. It is constant after atmospheric CO_2 stabilizes at 1120 ppm, due to compensating changes in temperature sensitivity (temperature change per unit radiative forcing) and cumulative airborne fraction. The TCRE remains approximately constant over time even if temperature sensitivity, determined by ocean heat flux, and cumulative airborne fraction, determined by ocean carbon flux, are taken from different model versions with different ocean mixing settings. This can partially be explained with temperature sensitivity and cumulative airborne fraction following similar trajectories, which suggests ocean heat and carbon fluxes scale approximately linearly with changes in vertical mixing.

3.1 Introduction

Recent literature has shown an approximately linear relationship between global warming and cumulative CO_2 emissions (Matthews et al., 2009; Allen et al., 2009; Eby et al., 2009). The ratio between global mean temperature change and cumulative emissions is referred to as transient climate response to cumulative CO_2 emissions (TCRE) but has also been called carbon-climate response (CCR) in earlier literature (Matthews et al., 2009). A useful application of the approximate constancy of the TCRE, especially for climate policy, is setting total allowable cumulative emissions to meet global warming targets (Zickfeld et al., 2009; Raupach et al., 2014). The Fifth Assessment Report of the Intergovernmental Panel on Climate Change gives a range for the TCRE of 0.8-2.5°C per 1000 PgC based on results from CMIP5 (Fifth Coupled Model Intercomparison Project) models and observational constraints (Collins et al., 2013; Frölicher and Paynter, 2015). The TCRE differs between models as it includes both the physical and biogeochemical uncertainties of the models, which makes it a useful benchmark for model intercomparison (Collins et al., 2013; Bindoff et al., 2013).

For any one specific model the TCRE is approximately constant over time and across CO_2 emissions with certain limitations to that constancy for different models. The limits of this approximate constancy have been studied in terms of cumulative CO_2 emissions and emission rates. Earlier studies suggest strongest divergence from a constant value occurs under very low cumulative emissions (<1000 PgC) because the signal to noise ratio is too low (Gillett et al., 2013) and very high cumulative emissions (>3000 PgC) because the effect of saturating radiative forcing is stronger than the saturation of carbon sinks (Gillett et al., 2013; Herrington and Zickfeld, 2014). However, a recent study suggests that a large decrease in the TCRE for high cumulative emissions is only associated with some models of intermediate complexity and the TCRE remains close to constant for most models (includ-

ing the UVic ESCM) for cumulative emissions of up to 5000 PgC (Tokarska et al., 2016). The TCRE is also not constant for stabilization of the climate system over several thousand years (Collins et al., 2013; Frölicher and Paynter, 2015). In some models the TCRE is also not constant under very high emissions rates, like an instantaneous quadrupling of pre-industrial atmospheric CO_2 concentrations (Gillett et al., 2013). Additionally, the TCRE may vary to second order for some models with emission rate. Krasting et al. (2014) find that the TCRE is highest for low and high emission rates (2 $GtCyr^{-1}$ and 25 $PgCyr^{-1}$) but is lower for current emission rates (5-10 $PgCyr^{-1}$), while Herrington and Zickfeld (2014) find a decrease in TCRE with increasing emissions rates. Thus the TCRE may be scenario dependent in some climate models but these variations are smaller than inter-model variation in the TCRE (Krasting et al., 2014; Herrington and Zickfeld, 2014; Leduc et al., 2015). Zickfeld et al. (2016) show that the TCRE is not constant when positive CO_2 emissions are followed by net-negative CO_2 emissions because of the lagged response of the deep ocean. The physical explanation for the approximate constancy of the TCRE remains under discussion and different explanations have been proposed. Matthews et al. (2009) separate the TCRE into airborne fraction of cumulative CO_2 emissions (change in atmospheric carbon burden per unit change in cumulative emissions) and temperature change per unit change in atmospheric carbon burden. Using these two ratios, Matthews et al. (2009) explain the constancy TCRE with two cancellation processes: First, the approximate constancy of the TCRE across scenarios is due to the cancellation of an increase in the airborne fraction of cumulative emissions with increase in emission rate, which means more warming, and a saturation of radiative forcing from CO_2 with increasing atmospheric CO_2, which means less warming. The cumulative airborne fraction increases at higher emissions because the carbon uptake rate by land and ocean decreases. Second, the approximate temporal constancy of the TCRE is due to the cancellation of a decrease in airborne fraction of cumulative emissions over time, i.e., less warming, and an increase in temperature change per unit change in atmospheric CO_2, meaning more warming. Matthews et al. (2009) and Solomon et al. (2009) suggest that the second cancellation process could be due to ocean heat and carbon fluxes being determined by the same deep ocean mixing processes. Goodwin et al. (2015) show a cancellation over time of the sensitivity of surface warming to radiative forcing and the sensitivity of radiative forcing to cumulative emissions due to compensating effects of ocean heat and carbon fluxes on the climate. The sensitivity of surface warming to radiative forcing increases over time due to decreasing ocean heat uptake per unit radiative forcing, i.e., more warming. At the same time the sensitivity of radiative forcing to cumulative emissions decreases over time, because the radiative forcing is directly proportional to undersaturated oceanic carbon and oceanic carbon content gets closer to equilibrium with the atmospheric carbon content. It should be noted that Goodwin et al. (2015) focus their discussion on the time after emissions are set to zero, when the climate system is not externally forced anymore and approaches equilibrium, i.e., ocean heat and carbon fluxes

are declining. Another study by Williams et al. (2016) expands the Goodwin et al. (2015) approach to simulations that include non-CO_2 forcers along with CO_2 forcing. Williams et al. (2016) find close to constant, but slightly increasing TCRE for two earth system models on long time scales. On decadal time scales they find strong temporal variations in the TCRE due to non-CO_2 forcers.

MacDougall and Friedlingstein (2015) suggest that for constant CO_2 emission rates, the cumulative airborne fraction is approximately constant over time and that the constancy of the TCRE is due to the cancellation within the physical response of the climate system. They argue that the decline in ocean heat flux rate over time and diminished radiative forcing per unit atmospheric CO_2 increase have opposite effects on temperature and cancel each other out. A constant cumulative airborne fraction does not seem plausible as this would imply a constant temperature change per unit change in atmospheric CO_2 which has been shown to not be the case (Gregory et al., 2015). Other studies using the same climate model further showed an increase in cumulative airborne fraction over time, especially for higher constant emission rates (Herrington and Zickfeld, 2014; Leduc et al., 2015). For exponentially increasing CO_2 emission rates over time, MacDougall and Friedlingstein (2015) suggest that while emission rates increase the ocean heat uptake rate increases, which has a cooling effect, and the ocean carbon uptake fraction (change in ocean carbon per cumulative emissions) declines, which leads to a higher cumulative airborne fraction of CO_2 and thus higher radiative forcing and more warming. They conclude that their finding supports the hypothesis of the TCRE being constant due to ocean heat and carbon fluxes being governed by the same process of deep ocean mixing. However, the role of ocean heat flux in the constancy of the TCRE is not addressed in depth.

The commonly given hypothesis of the same mechanism governing ocean heat and carbon fluxes causing an approximately constant TCRE can be questioned as there are important differences in the location and magnitude of ocean heat and carbon fluxes and the processes by which they are affected. For example, under a warming climate, changes in ocean circulation affect ocean heat storage more strongly than ocean carbon storage because changes in ocean circulation shift ocean heat uptake to higher latitudes, which increases the cooling effect of the heat flux. Global redistribution of ocean carbon, on the other hand, has no effect on ocean carbon uptake (Winton et al., 2013). This is partially due to the different boundary conditions for ocean heat and carbon uptake; atmospheric surface temperature has a strong meridional gradient whereas atmospheric CO_2 is equally distributed over the globe. Furthermore, only ocean carbon flux is directly affected by marine biology and carbonate chemistry. Additionally, the sea-air equilibration time scale is around nine month for carbon but only less than a month for heat (Frölicher et al., 2015).

In order to gain further understanding of the physical and biogeochemical processes determining the constancy of the TCRE the effect of ocean mixing parameterization on ocean heat and carbon fluxes and in turn on the TCRE is explored in this study. This also enables

an investigation of the hypothesis that the TCRE is approximately constant due to ocean heat and carbon fluxes being governed by the same deep ocean mixing. Ocean mixing from small-scale circulation processes, that cannot be resolved in climate models, must be parameterized. Changing this ocean mixing parameterization will affect how tracers, such as heat and carbon, are distributed within the ocean and at the ocean surface, which in turn affects ocean heat and carbon uptake. This study will also explore the sensitivity of the TCRE to ocean mixing, which may be helpful in explaining the differences in the TCRE between models.
Section 3.2.1 describes the model used, Section 3.2.2 introduces the performed simulations, and 3.2.3 explains the analytic framework applied to the simulation results. The results of the model simulations are presented in Section 3.3, including a discussion of the effect of ocean mixing on ocean heat and carbon fluxes, differences in the TCRE between mixing settings, and the temporal evolution of the TCRE. Section 3.4 presents our conclusions.

3.2 Methods

3.2.1 Model description

For this study the University of Victoria Earth System Climate Model, version 2.9 (UVic ESCM 2.9) was used. It consists of the following coupled components: a fully dynamic ocean circulation model, an energy-moisture balance atmosphere model, a dynamic-thermodynamic sea ice model, and a land surface and terrestrial vegetation model. It also includes land, ocean, and ocean sediment carbon cycle components. All components have a resolution of 1.8°(meridional) x 3.6°(zonal). Due to the simple atmosphere, this model is considered to be an Earth system model of intermediate complexity (Eby et al., 2009).
The atmosphere is represented by a vertically integrated energy-moisture balance model. It includes water vapour feedback, planetary long wave feedback, and dynamic wind feedbacks but no cloud feedbacks. Clouds are however represented in the atmosphere's albedo.
The land is modelled via a simplified version of the land surface scheme MOSES (Met Office Surface Exchange Scheme) (Meissner et al., 2003; Cox et al., 1999), which is coupled to the dynamic vegetation model TRIFFID (Top-down Representation of Interactive Foliage and Flora Including Dynamics) (Cox, 2001). The ocean is represented via the Geophysical Fluid Dynamic Laboratory (GFDL) Modular Ocean Model (MOMv2.2), which is a 3D general circulation model. It consists of 19 layers with variable thickness, ranging from 50 m at the top to 518 m at the bottom, and a total depth of 5396 m (Weaver et al., 2001). The ocean model is coupled to a dynamic-thermodynamic sea ice model, wherein sea ice is affected by ocean dynamics, atmospheric wind fields and phase-transitions (Weaver et al., 2001). Furthermore, the ocean module includes inorganic and organic carbon cycle components. The inorganic carbon component mainly describes the change in inorganic ocean carbon from of sea-air carbon flux and precipitation/evaporation, transport, and seawater carbon

chemistry (Ewen et al., 2004). The organic cycling of carbon is modelled via a marine ecosystem model that includes nutrient supply, phytoplankton, zooplankton, and detritus (NPZD) (Schmittner et al., 2005). Sediment processes are represented using an oxic-only model of sediment respiration (Archer, 1996).

Ocean mixing is described via momentum diffusivity (or viscosity) and tracer diffusivity (Weaver et al., 2001). In the following, ocean mixing always refers to the mixing of tracers. This tracer mixing can be described either in horizontal/vertical or isopycnal (along surface of constant density)/diapycnal direction. Either a horizontal or an isopycnal-mixing scheme can be used, which accounts for diffusion along isopycnals, also referred to as Redi diffusion. A parameterization for meso-scale eddies (Gent & McWilliams thickness diffusion) (Gent and Mcwilliams, 1990; Weaver et al., 2001) can be added to the isopycnal-mixing scheme. The Gent & McWilliams thickness diffusivity accounts for mixing due to baroclinic instability in areas where isopycnals are tilted.

Due to isopycnal slope limitations in the ocean model, there is no practical difference between vertical and diapycnal mixing and so a vertical mixing scheme is always applied. The vertical tracer diffusivity can be described with three different schemes: 1. vertically and laterally constant, 2. increasing with depth but laterally constant (Bryan & Lewis parameterization) (Weaver et al., 2001), and 3. tidal mixing scheme, where mixing due to the dissipation of tidal energy at topography is added to constant background diffusion parameter (Schmittner et al., 2005). The default option in the model is isopycnal mixing with the Gent & McWilliams parameterization (diffusivities of 800 m^2s^{-1}) for meso-scale eddies and Bryan & Lewis scheme for the vertical tracer diffusivity (diffusivity of 0.3-1.3 cm^2s^{-1}) (Weaver et al., 2001).

3.2.2 Experiment design

Different model versions were generated by changing the ocean mixing parameterization for tracer mixing (Table 3.1). The ocean mixing parameters are chosen to achieve an alteration of the ocean fluxes that is as large as possible while keeping the model stable and not necessarily to use parameters that closely reproduce observed ocean tracer distributions. However, to ensure the model does not transition into a different ocean circulation state we monitored the location of deep water formation. The default vertical mixing scheme in the UVic ESCM is the Bryan & Lewis parameterization, which has lower vertical diffusivity (k_v) in the upper ocean and higher vertical diffusivity in the deeper ocean. When moving to higher or lower parameter values, the shape of the curve of k_v over depth was maintained but the curve was shifted to higher or lower values, by changing the values of the vertical mixing parameter k_v as shown in Table 3.1. Values were set to range between 0.1 cm^2s^{-1} (upper ocean) and 1.5 cm^2s^{-1} (deep ocean) but the difference between lower and upper value of k_v was maintained. Different model versions were created by changing to a vertically constant

mixing parameter and varying this parameter between 0.05 cm^2s^{-1} and 1.0 cm^2s^{-1} or by using the tidal mixing scheme (Schmittner et al., 2005) in which the background diffusion parameter ($k_{v,tidal}$) was changed. The values for the background diffusivity in the tidal mixing scheme were chosen based on Schmittner et al. (2009), Goes et al. (2010), and Ross et al. (2012) with a range between 0.1 cm^2s^{-1} and 0.45 cm^2s^{-1}. Mixing along isopycnals was also varied. The parameter for diffusion along isopycnals and eddy thickness diffusion were changed individually and together between 400 m^2s^{-1} and 2400 m^2s^{-1}. Traditionally, parameters for both mixing types were set to the same value. However, recent studies suggest that the diffusion along isopycnals might be higher (as seen in measurements) than the eddy thickness diffusion (Gnanadesikan et al., 2015a). Both, lower eddy thickness diffusion and same values for both parameters are used in this study.

All model versions are spun up for 6000 years with prescribed constant atmospheric CO_2 concentration at pre-industrial levels. Initialized from this pre-industrial equilibrium state, all model versions are forced with a yearly 1% increase in atmospheric CO_2 levels up to a quadrupling of the pre-industrial atmospheric CO_2 concentration (simulation years 0-139), followed by constant atmospheric CO_2 concentration (simulation years 140-1200). All other anthropogenic and natural forcings were held constant at pre-industrial levels. As atmospheric CO_2 levels were prescribed, CO_2 emissions were diagnosed from the rate of increase in atmospheric CO_2 and land and ocean carbon fluxes.

For a comparison of the different climate states between the model versions the pre-industrial global mean surface air temperature (SAT), maximum meridional overturning circulation (MOC), and ocean carbon storage are given in Table 3.1. In the following all comparisons are made to the values for the default mixing setting. Strongest changes occur under changes in vertical mixing parameter, but not mixing scheme. Increased vertical mixing leads to a higher global mean SAT, stronger MOC, and lower ocean carbon storage. A stronger MOC leads to less sea ice, and a lower surface albedo, which in turns leads to higher temperatures. Increased mixing along isopycnals leads to negligible change in ocean carbon storage, global mean SAT, and MOC. Lower eddy thickness diffusivity leads to negligible changes in global mean SAT, slightly decreased ocean carbon storage, and a slightly increased MOC. When both mixing along isopycnals and eddy thickness diffusivity are increased global mean SAT does not change but MOC decreases and ocean carbon storage increase. Effect of changes in ocean mixing on the MOC are discussed in detail by Schmittner and Weaver (2001). Though they used a different model, we observe similar effects of changes in mixing on the MOC. At the end of the spin-up the global distribution of ocean heat uptake is similar between model versions but the global distribution of ocean carbon uptake differs slightly (see supplementary material, Figures 3.8 and 3.9). For low vertical mixing, irrespective of the mixing scheme, carbon uptake into the ocean increases relative to the model version with default mixing setting in the southern Pacific and Atlantic along a band between the southern tip of Africa, S-America and Australia. But parallel to this band is also an increase

of carbon flux into the atmosphere from the ocean. Outgassing of carbon decreases in the equatorial Pacific with decreasing vertical mixing. Outgassing increases in the Southern Ocean, south of Australia, under increased isopycnal diffusivity.

Table 3.1: Description of different model versions and their names as referred to in the text and figures. A_h is the diffusivity along isopycnals, $A_{thkdiff}$ is the eddy thickness diffusivity as introduced by Gent and Mcwilliams (1990), and k_v is the vertical diffusivity. Pre-industrial state of the different model versions are shown exemplarily for the following variables: global mean surface air temperature (SAT), Meridional Overturning Circulation (MOC) and the given values refer to the maximum of the stream function, C_O is the total ocean carbon storage.

Experiment	A_h (m^2s^{-1})	A_{thkdff} (m^2s^{-1})	vertical mixing scheme	k_v (cm^2s^{-1})	SAT (°C)	MOC (Sv)	C_O (PgC)
default	800	800	Bryan & Lewis	0.3-1.3	13.39	21.6	37297
$k_{v,const}0.05$	800	800	vertically constant	0.05	12.89	9.8	37910
$k_{v,const}0.3$	800	800	vertically constant	0.3	13.33	21.4	37386
$k_{v,const}1.0$	800	800	vertically constant	1.0	16.67	32.3	36229
$k_{v,B\&L}$low	800	800	Bryan & Lewis	0.1-1.1	13.16	12.7	37919
$k_{v,B\&L}$high	800	800	Bryan & Lewis	0.5-1.5	13.52	25.8	36820
$k_{v,tidal}0.1$	800	800	tidal	0.1	13.15	14.4	37753
$k_{v,tidal}0.2$	800	800	tidal	0.2	13.32	19.3	37511
$k_{v,tidal}0.45$	800	800	tidal	0.45	13.49	25.8	36854
A_h2400	2400	800	Bryan & Lewis	0.3-1.3	13.44	20.2	37300
$A_{thkdff}400$	800	400	Bryan & Lewis	0.3-1.3	13.44	23.9	37120
$A_hA_{thkdff}1600$	1600	1600	Bryan & Lewis	0.3-1.3	13.35	16.6	37596

3.2.3 Theoretical framework for the TCRE

In order to investigate which variables affect the TCRE and how these variables differ between model versions we write the TCRE as:

$$TCRE = \frac{\Delta T}{CE} = \frac{\Delta C_A}{CE}\frac{RF}{\Delta C_A}\frac{\Delta T}{RF} \tag{3.1}$$

where ΔC_A is the change in atmospheric carbon in PgC, CE are the cumulative CO_2 emissions in PgC, RF is the radiative forcing in Wm^{-2}, and ΔT is the change in global mean surface air temperature in °C.

The airborne fraction of cumulative emissions (ΔC_A/CE) can be rewritten as a function of the ocean carbon uptake fraction (ΔC_O/CE) and land carbon uptake fraction (ΔC_L/CE) using the carbon budget equation $CE = \Delta C_A + \Delta C_O + \Delta C_L$, where ΔC_O and ΔC_L are the change in ocean and land carbon reservoirs:

$$\frac{\Delta C_A}{CE} = 1 - \left(\frac{\Delta C_O}{CE} + \frac{\Delta C_L}{CE}\right) \tag{3.2}$$

Using an energy balance equation for global mean temperature change:

$$\Delta T = 1/\lambda(1 - \frac{N}{RF})RF \tag{3.3}$$

where λ is the feedback parameter in $\mathrm{Wm^{-2}K^{-1}}$ and N is the net heat flux into the climate system in $\mathrm{Wm^{-2}}$, the TCRE can be expressed as:

$$TCRE = \left(1 - \frac{\Delta C_O + \Delta C_L}{CE}\right) \frac{RF}{\Delta C_A} \frac{1}{\lambda} \left(1 - \frac{N}{RF}\right) \tag{3.4}$$

The first term in Equation 3.4 is the cumulative airborne fraction, i.e., the fraction of cumulative CO_2 emissions that remains in the atmosphere and is not taken up by land and ocean sinks. The second term, $\mathrm{RF}/\Delta \mathrm{C}_A$, is the radiative forcing sensitivity to an increase in CO_2 in the atmosphere. The last term of Equation 3.4, $1/\lambda$(1-(N/RF)), is the temperature sensitivity. If the radiative forcing is taken at the time of doubling of the pre-industrial atmospheric CO_2, this term multiplied with the radiative forcing is the Transient Climate Response (TCR). The TCR describes the physical response of the climate system to CO_2 forcing and is a useful metric to compare the physical response of different climate models. Equation 3.4 shows the effect of ocean heat and carbon uptake on the TCRE. The TCRE depends directly on ocean heat uptake but it also depends on the change in the land and ocean carbon reservoirs, i.e., the integrals of the carbon fluxes in and out of these reservoirs.

3.3 Results and Discussion

3.3.1 Effect of ocean mixing on ocean heat and carbon fluxes in forced simulations

Forcing the different model versions with increasing atmospheric CO_2 levels results in different heat and carbon fluxes between the model versions (see Figure 3.1a,b). In all simulations, globally averaged ocean heat and carbon uptake increase while atmospheric CO_2 levels rise and decrease after atmospheric CO_2 is stabilized. Increased vertical mixing leads to an increase in ocean heat and carbon uptake as higher vertical mixing increases the rate of mixing between the mixed layer and the deeper ocean (compare highest and lowest vertical diffusion parameter for each mixing scheme, i.e., dark blue, dark purple, and green curves to light blue, light purple, and light green curves in Figure 3.1a,b). Deep ocean water is cold and less equilibrated with increasing atmospheric CO_2 levels, thus heat and carbon uptake increase. Increased ocean heat and carbon uptake and a less stratified ocean due to increased vertical mixing have also been shown in other studies (Goes et al., 2010; Olson et al., 2012; Schmittner et al., 2009). However, these studies only used the tidal mixing scheme. If CO_2 emissions are prescribed and atmospheric CO_2 can evolve freely, increased ocean heat and carbon uptake due to increased vertical mixing have been shown to contribute equally to reduced warming (Schmittner et al., 2009). Correspondingly, decreased vertical mixing results in decreased ocean heat and carbon uptake. Interestingly, ocean heat and carbon uptakes correlate linearly with the vertical mixing parameter within each mixing setting (Figure 3.2).

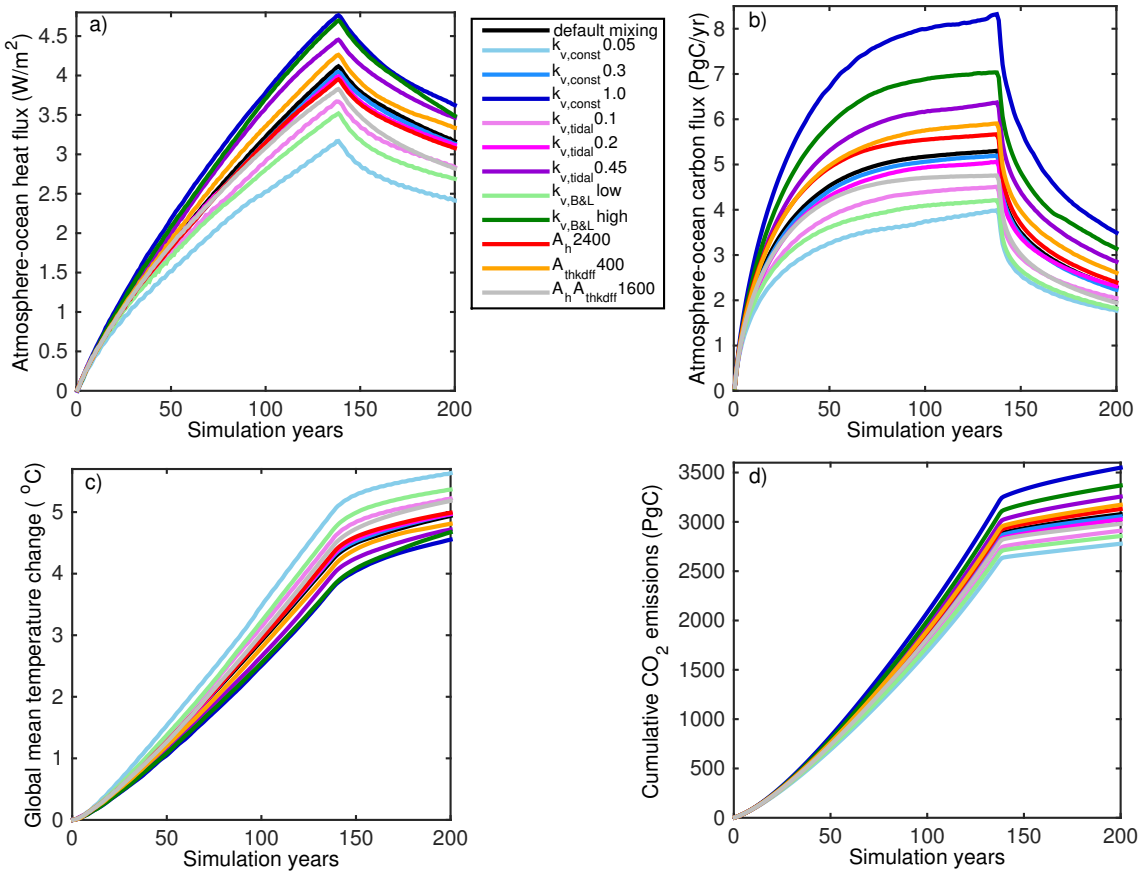

Figure 3.1: Global mean ocean heat (a) and carbon (b) fluxes for the model versions with different mixing settings, under increasing atmospheric CO_2 levels (year 0-139) and 50 years of constant atmospheric CO_2. Positive fluxes indicate uptake of heat or carbon by the ocean, i.e., a flux from the atmosphere into the ocean. Global mean surface air temperature change relative to year 0 (c) and cumulative CO_2 emissions (d) for the different model versions, under increasing atmospheric CO_2 levels (year 0-139) and 50 years of constant atmospheric CO_2. Model versions with higher ocean heat and carbon fluxes have lower warming and stronger increases in cumulative emissions. Changes in vertical mixing (blue and green curves) have a stronger effect on temperature change and cumulative emissions than changes in mixing along isopycnals (yellow and red curves) compared to the default setting (black curve).

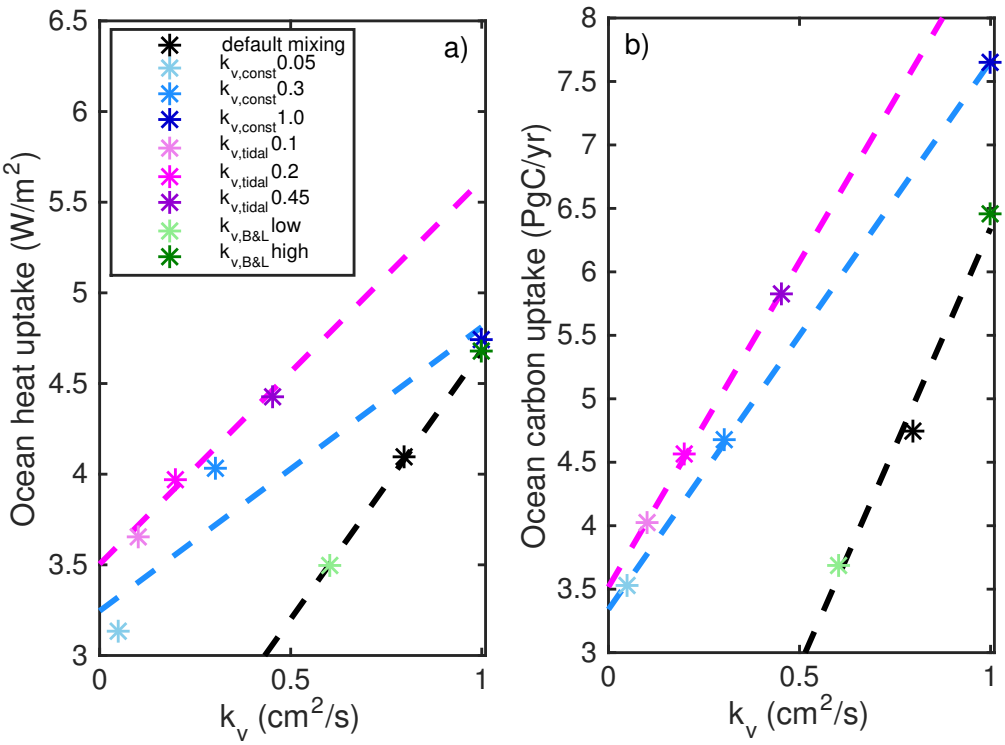

Figure 3.2: Ocean heat (a) and carbon (b) uptake at year 140 as function of vertical mixing parameter k_v. The black, blue, and pink lines are the linear correlations (ordinary least square regression) between the ocean uptake and the mixing parameter for Bryan & Lewis, vertically constant, and tidal mixing scheme, respectively. The r-square values are 0.99 ($p \leqslant 0.09$) for all correlations except for the correlation of constant vertical mixing and ocean heat uptake, where r-square is 0.91 ($p=0.13$). Therefore, the correlations are strong and significant, except in the latter case.

Lower eddy thickness diffusivity leads to increased overturning circulation (Gnanadesikan, 1999) which leads to slightly increased ocean heat and carbon uptake compared to the default setting (compare yellow curve to black curve in Figure 3.1a,b). Increased diffusivity along isopycnals leads to the smallest difference in heat and carbon uptake relative to the default setting compared to changes in the other mixing parameters even though the relative changes in the diffusion parameter compared to the default setting are the strongest for the parameter of diffusion along isopycnals. A slightly higher increase in ocean carbon flux and slightly lower increase in ocean heat flux compared to the default setting can be observed (compare red curve to black curve in Figure 3.1a,b). Changes in ocean heat and carbon uptake, relative to the uptake in the default mixing setting, are opposite in sign and the change in ocean carbon flux is stronger in magnitude than the change in ocean heat flux. One possible explanation for lower ocean heat uptake compared to the default setting under increased atmospheric CO_2 is that increased mixing along isopycnals leads

to a warmer surface ocean at higher latitudes, which in some areas leads to an increase in ocean heat loss, especially in the north Atlantic. A meridional redistribution of temperature in the surface ocean affects ocean heat flux but a redistribution of carbon does not affect ocean carbon flux because atmospheric temperature has a meridional gradient and atmospheric carbon is globally equally distributed. An explanation for the slight increase in ocean carbon uptake could be changes in marine biology. Simulations with increased isopycnal diffusivity show less carbon outgassing and increased net primary productivity rates in the upwelling regions of the East equatorial Pacific, as more nutrients are available at the surface. Thus the increase in globally averaged ocean carbon uptake could be explained with changes in ocean biology, which only affects ocean carbon but not ocean heat uptake. Increased ocean carbon uptake under increased diffusivity along isopycnals, partially due to increased biological carbon storage, has also been found in another study using a complex earth system model (Gnanadesikan et al., 2015b).

Increasing both mixing along isopycnals and eddy thickness diffusivity (simulation $\mathrm{A}_h\mathrm{A}_{thkdff}1600$) leads to a decline in both ocean heat and carbon uptake. Assuming that changes in ocean heat and carbon uptake due to variations in the eddy thickness diffusivity are symmetric, increased eddy thickness diffusivity would lead to decreased ocean heat and carbon uptake, but increased diffusion parameter along isopycnals leads to lower ocean heat uptake and higher ocean carbon uptake. The changes in ocean heat and carbon uptake in $\mathrm{A}_h\mathrm{A}_{thkdff}1600$ show that changes in the eddy thickness diffusivity outweigh changes in the diffusion parameter along isopycnals. This result agrees with another study (Gnanadesikan et al., 2015b).

Our results suggest that changes in eddy thickness diffusivity, vertical mixing parameter and/or vertical mixing scheme scale ocean heat and carbon uptake up or down but do not significantly affect the temporal evolution of the uptake.

3.3.2 Effect of different mixing settings on the TCRE

Differences in ocean heat and carbon uptake lead to different TCRE values between model versions. Higher ocean heat uptake leads to less surface air warming because more heat is taken up by the ocean. This can also be seen in Equation 3.3. Higher ocean carbon uptake leads to higher cumulative emissions because if more carbon is taken up by the ocean, more carbon can be emitted in order to reach the same atmospheric CO_2 level.

For both higher vertical mixing and lower eddy thickness diffusivity, ocean heat and carbon uptake increase, resulting in a lower temperature change and higher cumulative emissions (see Figure 3.1c,d). As the TCRE is defined as temperature change per cumulative emissions, TCRE values decrease for these mixing changes (see Figure 3.3b). Lower vertical mixing leads to higher TCRE values because the effects of changes in vertical mixing are symmetric. Increased isopycnal diffusivity leads to a marginally lower increase in heat flux and a slightly stronger increase in ocean carbon flux. This leads to a marginally stronger

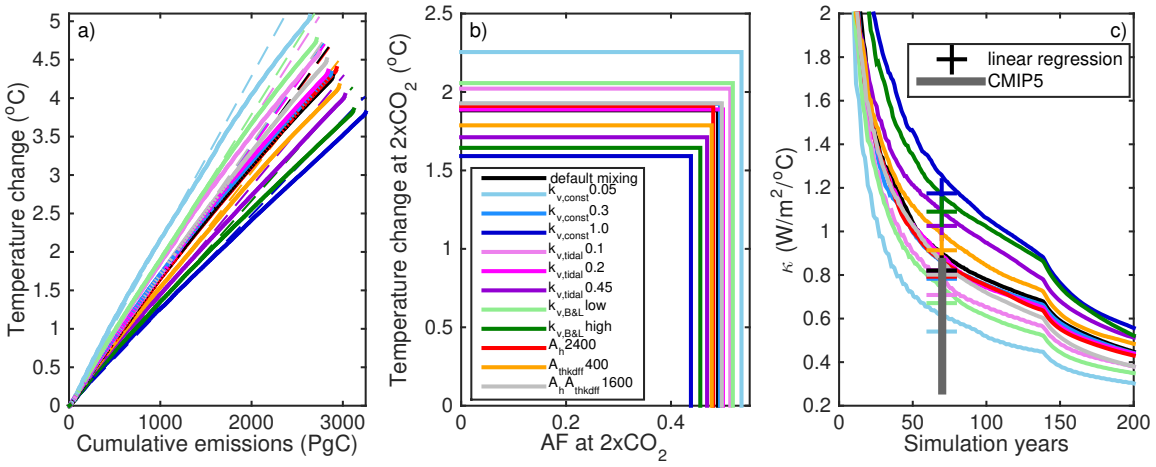

Figure 3.3: a) Global mean surface air temperature change (as shown in Figure 3.1c) versus cumulative CO_2 emissions over the time period of increasing CO_2 concentration (simulation years 0-139). The slope of the curves is the TCRE, with a steeper slope indicating a higher TCRE value. The dashed lines are hypothetically constant TCRE values, using the TCRE value at the time of doubling atmospheric CO_2 levels. b) Temperature change (relative to simulation year 0) at time of doubling of CO_2, referred to as transient climate response (TCR), versus the cumulative airborne fraction (AF) at the time of CO_2 doubling for different model versions. c) Ocean heat uptake efficiency κ, defined as ratio of net heat flux into the climate system (note that the latter is different from the ocean heat flux shown in Figure 3.1, which is averaged over the surface area of the ocean rather than the entire Earth surface) to global mean surface air temperature change, over time. The efficiency is only shown for 60 years after quadrupling of atmospheric CO_2 is reached for readability reasons but the efficiency continues to decline for all model version under constant atmospheric CO_2. The grey bar indicates the CMIP5 ocean heat uptake efficiency range (Kuhlbrodt and Gregory, 2012) and the crosses indecate the ocean heat uptake efficiency, both calculated via a ordinary least squares regression between net heat flux into the climate system and global mean surface air temperature change over the first 70 simulation years.

warming and slightly larger cumulative emissions. In total the TCRE is lower, thus the increase in cumulative emission dominates over the increase in warming (compare black line to red line in Figures 3.1, 3.3a).

The total range of the TCRE for all model versions at the time of CO_2 doubling is 1.2-2.1°CEgC^{-1}. Changes in the vertical mixing parameters (Figure 3.3a, green, blue, and purple curves) have a much stronger effect on the TCRE than changes in isopycnal mixing even though relative changes in the mixing along isopycnals are 300% (relative to the default value of A_h) and 200% for vertical mixing (relative to the center value of k_v,const). A stronger effect on ocean variables from changes in vertical mixing than from changes in isopycnal mixing are plausible as changes in vertical mixing have a strong effect on the density structure of the ocean.

This range in the TCRE is similar to the range in TCRE for CMIP5 models of 0.8-

2.4°CEgC^{-1} (Gillett et al., 2013) and the most likely range of 0.8-2.5°CEgC^{-1} given in the Fifth Assessment Report of the IPCC (Collins et al., 2013). However, this should not imply that the TCRE spread between CMIP5 models is solely caused by variations in ocean mixing parameterization as a number of aspects, specifically in biogeochemical processes and the climate feedback parameter, are involved in the CMIP5 model TCRE range (MacDougall et al., 2017).

Plotting the temperature change at the time of doubling CO_2, a measure also referred to as Transient Climate Response (TCR), versus the airborne fraction of cumulative CO_2 emissions (AF) at the time of doubling CO_2, gives insights into the contribution of changes in the physical and the biogeochemical parts of the climate system towards the changes in the TCRE (see Figure 3.3b). The TCR is a measure of the physical response of the climate system to rising CO_2 levels and is affected by the effect of ocean heat flux on temperature and physical climate feedbacks. The AF is affected by both marine and terrestrial biogeochemical processes, and thus is a measure of the biogeochemical response of the climate system. The boxes in Figure 3.3b representing AF and TCR for each model version are nested. This means that changes in the TCR and in the AF, i.e., variations in physical and biogeochemical processes between model versions, affect variations in TCRE in the same direction. The exceptions are changes in the mixing along isopycnals, as under this mixing setting changes in the TCR are smaller and opposite in sign compared to changes in the AF. This goes along with minimal changes in the ocean heat uptake and slightly stronger changes in ocean carbon uptake (see Figure 3.1a,b red curve) for increased diffusivity along isopycnals.

The ocean heat uptake efficiency, defined as the ratio of net heat flux into the climate system to change in global mean surface air temperature, is another factor affected by ocean mixing. A decrease in ocean heat uptake efficiency means an increase in the TCR (Kuhlbrodt and Gregory, 2012) and thus the TCRE. The ocean heat uptake efficiency increases for higher vertical mixing, and for lower eddy thickness diffusivity (Figure 3.3c), which corresponds to a decreased TCR and TCRE (Figure 3.3a,b). Kuhlbrodt and Gregory (2012) link a high ocean heat uptake efficiency to a less stratified ocean as more heat can be transported into the deeper ocean. This link holds true for both increased vertical mixing and decreased eddy thickness diffusivity. Decreased eddy thickness diffusivity leads to steeper isopycnal layers, especially in the Southern Ocean, and thus a weak stratification. The efficiency range given by Kuhlbrodt and Gregory (2012) is 0.27-0.83 Wm^{-2} °C^{-1}, which is calculated as ordinary least squares regression between net heat flux into the climate system and global mean surface air temperature change over the first 70 years of a 1% CO_2 increase simulations. We find a range of 0.54-1.17 Wm^{-2} °C^{-1} for an efficiency calculated the same way as for the CMIP5 models, with a value of 0.82 Wm^{-2} °C^{-1} for the default mixing setting (Figure 3.3c).

3.3.3 Evolution of the TCRE over time

Even with strong changes in ocean mixing parameters, the relationship between global mean temperature change and cumulative emissions remains close to linear within each mixing setting (see Figure 3.3a). However, when looking at how the TCRE evolves over time, the TCRE is not constant while atmospheric CO_2 increases (up to 20% divergence from time-mean TCRE value) in our model, but it is approximately constant (maximum 5% divergence from time-mean TCRE value) while atmospheric CO_2 is constant (see Figure 3.4a). Our finding of a non-constant TCRE under increasing CO_2 concentration differs from the finding by Matthews et al. (2009) despite using the same model and prescribing a 1% atmospheric CO_2 increase because we apply a tighter definition of constancy and increase the time scale of our simulations beyond 70 years. Considering a longer time scale emphasizes variation when the TCRE is plotted over time (compare Figure 3.4a in this chapter and Figure 2a in Matthews et al. (2009)). To further investigate which parts of the climate system contribute to the constancy of the TCRE over time or lead to divergence from a constant value, we consider the separation of the TCRE into the three terms given in Equation 3.1. The first term in Equation 3.1, the cumulative airborne fraction AF (ΔC_A/CE), is determined by the response of the ocean and land carbon sinks. The second term in Equation 3.1 is the radiative forcing per unit change in atmospheric carbon (RF/ΔC_A), which expresses the radiative properties of CO_2. This term, referred to as radiative sensitivity from here on, follows a logarithmic relationship as the radiative forcing depends logarithmically on atmospheric CO_2 levels. The third term in Equation 3.1 is the temperature sensitivity (ΔT/RF), i.e., the amount of warming per unit radiative forcing. This sensitivity depends on climate feedbacks and ocean heat uptake and can be analytically described by the last two terms in Equation 3.4.

Equation 3.1 is applied to the simulations results in order to investigate the time dependency of AF, radiative sensitivity, and temperature sensitivity and their role in the constancy of the TCRE. The discussion of the temporal evolution of AF, radiative sensitivity, temperature sensitivity, and the TCRE is separated in 1) the time period of increasing atmospheric CO_2 concentration (simulation year 0-139), and 2) the time period of constant atmospheric CO_2 concentration (simulation year 140-1200), when the system equilibrates to a new state and CO_2 emissions are very low.

Increasing atmospheric CO_2 concentration For all mixing settings the AF reaches a minimum and then increases again (see Figure 3.5a). It almost instantly reaches a value of around 0.7 and then declines to 0.5 at around year 40 and increases again to around 0.55-0.7. The AF can be expressed in terms of ocean and land uptake fraction, i.e., the fraction of cumulative CO_2 emissions absorbed by the land/ocean (see Equation 3.2). The ocean carbon uptake fraction increases strongly at the beginning of the simulations and

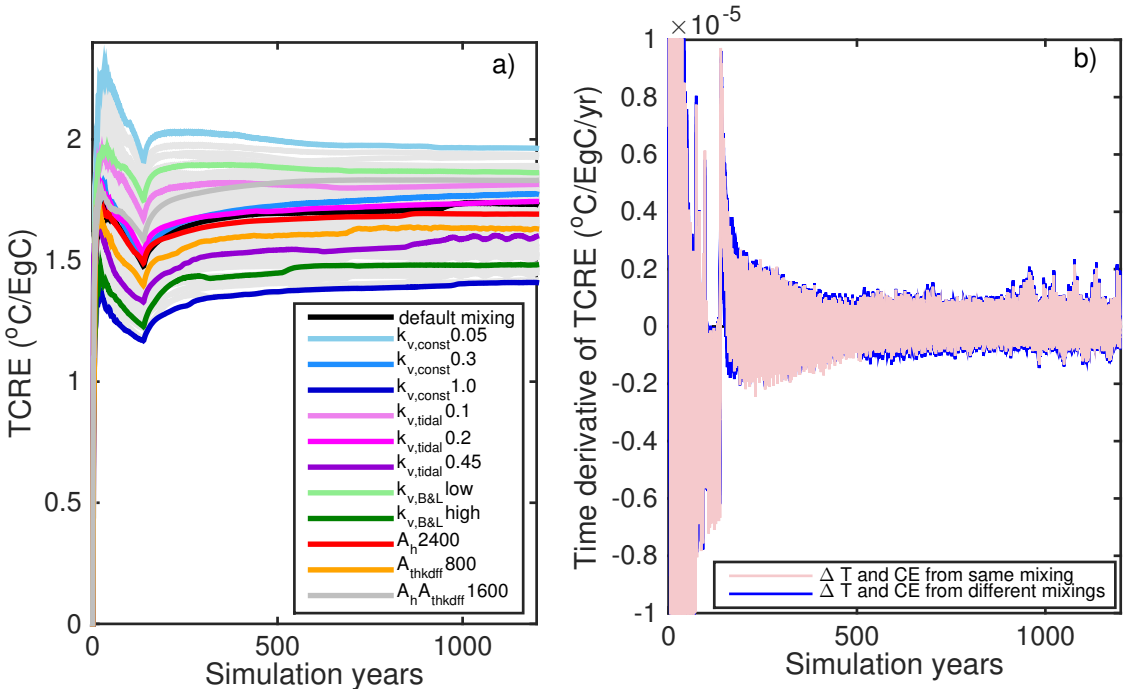

Figure 3.4: a) TCRE over time for different model versions. TCRE over time, with temperature change and cumulative emissions taken from model versions with different ocean mixing settings, is shown in light grey in the background. b) Time derivatives of the TCRE with cumulative CO_2 emissions CE and global mean surface air temperature ΔT from the same model version (all model versions are shown in pink) and with CE and ΔT from different model versions (all combinations are shown in blue).

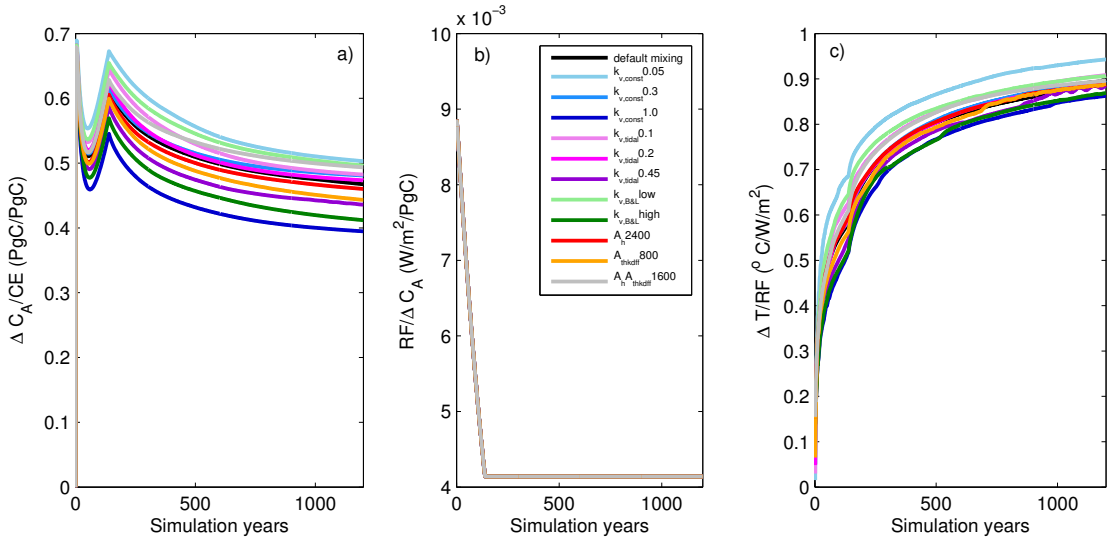

Figure 3.5: Variation of the terms of the TCRE over time: $\Delta C_A/CE$ (cumulative airborne fraction), $RF/\Delta C_A$ (radiative sensitivity), and $\Delta T/RF$ (temperature sensitivity), where ΔC_A is the change in atmospheric carbon burden, CE are the cumulative CO_2 emissions, RF is the radiative forcing, and ΔT is the global mean temperature change.

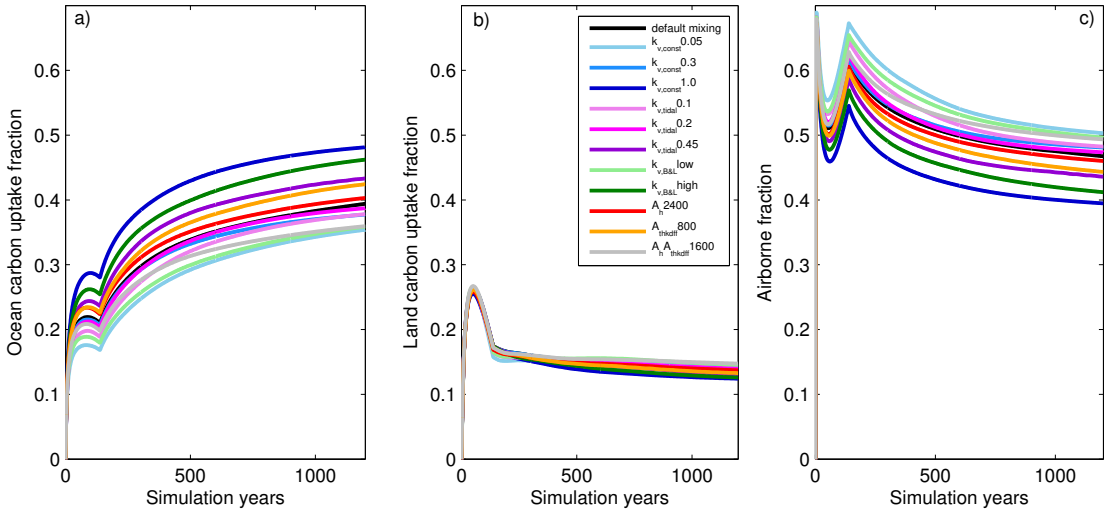

Figure 3.6: Ocean carbon uptake fraction ($\Delta C_O/CE$), land carbon uptake fraction ($\Delta C_L/CE$), and cumulative airborne fraction ($\Delta C_A/CE$) over time. $\Delta C_{A,O,L}$ is the change in atmospheric, ocean, and land carbon, respectively, and CE are the cumulative CO_2 emissions.

then declines slightly (see Figure 3.6a). In contrast, the land carbon uptake fraction first increases over time and then declines strongly (see Figure 3.6b) due to saturation of land carbon sinks. The saturation of the land carbon sinks can be explained with climate-carbon cycle feedbacks, such as decreased net primary productivity in lower latitudes due to high temperatures or increased soil respiration under rising temperatures (Friedlingstein et al., 2006; Zickfeld et al., 2011). Thus, variations in the AF over time within each model version are mostly caused by the increase and decline of the land carbon uptake fraction. It should further be noted that the ocean carbon uptake fraction varies significantly between model versions but the land carbon uptake fraction has only small variations between model versions. The land carbon uptake fraction does vary between model versions because the temperature differs, which has an effect on vegetation growth and soil respiration and in turn on land carbon uptake.

In contrast to the AF, radiative and temperature sensitivities decrease/increase monotonically. The radiative sensitivity declines over time (see Figure 3.5,b) as the rate of increase in radiative forcing declines with increasing CO_2 levels. The temperature sensitivity increases over time (see Figure 3.5c). Using Equation 3.3, this can be explained with a decrease of heat flux into the ocean per unit radiative forcing. Thus over the time of increasing atmospheric CO_2, AF, radiative sensitivity, and temperature sensitivity vary. The variations in these three terms do not compensate each other very well, resulting in the TCRE increasing first for one or two decades and then decreasing over time (see Figure 3.4a). While the TCRE increases, the increase in temperature sensitivity dominates, as the other two terms

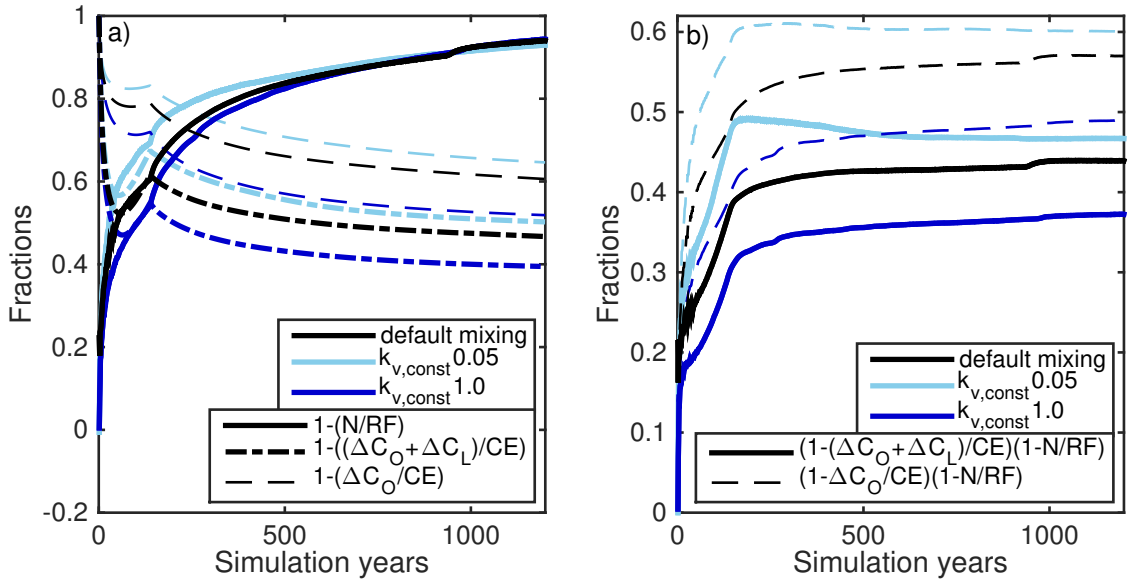

Figure 3.7: Terms in the equations for TCRE (Equation 3.4) affected by ocean heat and carbon fluxes. a) One minus the ratio of net heat flux into the climate system (N, note that it differs from the ocean heat flux shown in Figure 3.1, which is averaged over the surface area of the ocean rather than the entire Earth surface) and radiative forcing (RF); one minus ΔC_O/CE, the ocean carbon uptake fraction, or $(\Delta C_O + \Delta C_L)$/CE, the combined carbon uptake fraction for land and ocean. b) Terms in the equations for the TCRE containing ocean heat flux and ocean carbon flux, the latter one indirectly via ΔC_O (change in ocean carbon).

of the TCRE decline over that time frame. As the TCRE starts declining, the decline in radiative sensitivity becomes dominant.

As all three terms of the TCRE vary, it could still be that the terms affected by ocean heat and carbon uptake cancel each other out. However, this is not the case (see Figure 3.7). The decline in heat flux per radiative forcing dominates over the increase in ocean carbon uptake fraction or land and ocean carbon uptake fraction added together (see Figure 3.7a, showing the terms containing ocean heat flux per radiative forcing and carbon uptake fractions which are opposite in sign to ocean heat flux per radiative forcing and carbon uptake fractions). Therefore, both terms of the TCRE containing ocean heat and carbon flux together, i.e., multiplied with each other, increase while atmospheric CO_2 increases (see Figure 3.7b) and the effects of ocean heat and carbon uptake on the TCRE do not compensate each other.

The result that all three responses in the TCRE vary is consistent with the findings by MacDougall and Friedlingstein (2015) for exponentially increasing emission rates (the simulations presented here also have increasing emissions rates).

Constant atmospheric CO_2 concentration While atmospheric CO_2 levels are constant (year 140-1200) the radiative sensitivity is constant, the cumulative AF declines, and the temperature sensitivity increases (see Figure 3.5). The cumulative AF changes mostly due to an increase in the ocean uptake fraction; the land uptake fraction exhibits only minimal variations over time while atmospheric CO_2 levels are constant (see Figure 3.6). The TCRE abruptly increases at year 140 (see Figure 3.4a) because the emission rates change abruptly from increasing emission rates of up to 30 $PgCyr^{-1}$ to close to zero emissions. After an adjustment time of about a decade the TCRE is approximately constant (see Figure 3.4a) due to a compensation between the decline in AF and the increase in temperature sensitivity. The AF only varies due to changes in ocean carbon uptake and the temperature sensitivity changes only due to changes in the ocean heat flux (see Equation 3.4). Ocean carbon uptake declines, which leads to a less strong increase in the ocean carbon uptake fraction and thus a decrease in the airborne fraction. The decrease in ocean heat uptake leads to a stronger increase in temperature change and thus an increase in the temperature sensitivity. Hence the effects of ocean heat and carbon uptake have opposite effects on the TCRE. This suggests that the approximate constancy of the TCRE is caused by the compensation of the terms of the TCRE including ocean heat and carbon fluxes (see Equation 3.4 and Figure 3.7). This compensation is independent of whether land carbon uptake is taken into account or not because the land uptake fraction does not change over time. The constancy of the land uptake fraction, however, may be model dependent. These results agree with the findings by Goodwin et al. (2015) and confirm the hypothesis that the compensating effects of ocean heat and carbon flux on the climate system lead to an approximately constant TCRE over time.

That ocean heat and carbon uptakes compensate each other despite the differences between them indicates that those differences (listed in the introduction in detail and summarized below) have secondary effects under constant atmospheric CO_2 concentrations. The time scales of air-sea equilibration are nine month for carbon but less than a month for heat. Both equilibration time scales are short compared to the decadal to centennial timescales considered in this study. The effects of ocean biology and solubility on ocean carbon uptake are difficult to diagnose but these effects appear to be relatively small while atmospheric CO_2 is constant. The effect of changes in ocean circulation on redistribution of heat and carbon and in turn on their air-sea fluxes together with the differences in the atmospheric boundary conditions could be small under constant forcing. However, this effect could play a role under increasing atmospheric CO_2 concentration where the effects of ocean heat and carbon uptake do not cancel each other out. It should be noted though that the effect of changes in ocean circulation on ocean heat uptake may be smaller in the UVic ESCM than in atmosphere ocean general circulation models (AOGCMs) as changes in cloud cover increase the cooling effect from changes in ocean heat uptake due to changes in ocean circulation (Trossman et al., 2016) and the UVic ESCM does not include changes in clouds. Thus it

could be that in AOGCMs the TCRE is not constant under constant forcing, at least while there is still an effect from changes in ocean circulation, as these changes in ocean circulation have a stronger effect on the ocean heat uptake than ocean carbon uptake and their effects on temperature (Winton et al., 2013). For example, Frölicher and Paynter (2015) show a non-constant TCRE for the Earth System Model (ESM) from the Geophysical Fluid Dynamics Laboratory (GFDL) from direct simulations and for other CMIP5 AOGCMs by temporally extending CMIP5 simulations using a theoretical approach.

The paragraphs above discuss to which extent and why the TCRE remains approximately constant over time within each mixing setting. Temporal variations in the TCRE, and compensating mechanism leading to an approximately constant TCRE over time while atmospheric CO_2 is constant, remain surprisingly consistent across model versions (see Figures 3.4a and 3.5). In order to further test whether variations in mixing parameters cause compensating variations in ocean heat and carbon fluxes such that the TCRE remains constant, the TCRE is calculated using global mean temperature change from one model version and cumulative emissions from a different model version. We sampled over all possible combinations of temperature change and cumulative emissions (see Figure 3.4a, grey shading) in such a way that for each ratio between temperature change and cumulative emissions, heat and carbon fluxes are affected by different ocean mixing settings. We find that the temporal evolution of the TCRE does not change significantly (see Figure 3.4a, grey shading, 3.4b) despite temperature change being affected by e.g. low ocean heat flux and cumulative emissions being affected by high ocean carbon flux or vice versa. The time derivative of the TCRE (see Figure 3.4b) is used as a measure of the constancy of the TCRE over time. This derivative is largely insensitive to whether temperature change and cumulative emissions are taken from the same or different model versions because the rate of change of the AF and the temperature sensitivity over time are similar enough between mixing settings (curves in Figure 3.5a,c are approximate multiples of each other). These similarities in the temporal evolution of the AF and the temperature sensitivity between model versions with different mixing setting suggest that changes in ocean heat and carbon fluxes scale linearly with changes in vertical diffusivity (which have the largest effect on ocean heat and carbon fluxes). We show a linear correlation between ocean heat and carbon uptake and vertical diffusivity within each vertical mixing scheme (Figure 3.2). This leads to higher (lower) ocean heat and carbon uptake and lower (higher) global mean temperature change and higher (lower) cumulative emissions, but does not affect the trajectories of these variables. Therefore, the magnitude of the TCRE is affected if temperature change and cumulative emissions are taken from different simulations but the TCRE remains approximately constant over time. This linear scaling between diffusivities and ocean heat and carbon fluxes might be specific to the UVic ESCM as mixing parametrization and effects on the fluxes may vary.

3.4 Conclusion

Different model versions of the University of Victoria Earth System Climate Model are generated by changing the ocean mixing parameterization. These model versions are forced with a 1% per year increase in atmospheric CO_2 until quadrupling of the pre-industrial CO_2 concentration and constant concentration thereafter. Despite significant changes in ocean mixing between model versions, the relationship between temperature change and cumulative emissions remains close to linear within each model version (see Figure 3.3a). However, the magnitude of the TCRE differs between model versions with a total range of the TCRE at the time of CO_2 doubling of 1.2-2.1°CEgC^{-1}. These differences in the TCRE are due to changes in both the physical and biogeochemical response of the system as the two components of the TCRE, the AF at the time of CO_2 doubling and the TCR, change in the same direction in each model version, i.e., a larger AF is associated with a larger TCR and vice versa (see Figure 3.3b). Variations in the vertical ocean mixing lead to stronger changes in heat and carbon fluxes, and thus in the TCRE, than changes in mixing along isopycnals (see Figure 3.1a,b). Therefore, constraining the vertical ocean mixing parameterization could help constrain the TCRE. Thus a next step could be to run historical simulations with the different model versions, in order to compare them to observational data such as surface air temperature data or ocean tracer distributions.

The TCRE is approximately constant while atmospheric CO_2 concentrations are constant (5% variation from mean TCRE value) but it is not constant (up to 20% deviation from mean TCRE value) while atmospheric CO_2 increases (see Figure 3.4a). Separating the TCRE into AF, radiative sensitivity (radiative forcing per unit change in atmospheric CO_2), and temperature sensitivity (temperature change per unit radiative forcing), reveals that all three sensitivities vary while atmospheric CO_2 concentration increase but changes in temperature sensitivity and AF compensate each other in all model versions while atmospheric CO_2 concentrations are held constant (see Figure 3.5). This compensation is due to the compensating effects of ocean heat and carbon fluxes on the TCRE. The TCRE remains approximately constant even if the temperature sensitivity and AF, which are determined by ocean heat and carbon fluxes respectively, are taken from model versions with different ocean mixing settings. This could be explained with temperature sensitivity and AF having similar trajectories under different mixing settings. This suggests that changes in ocean heat and carbon fluxes scale linearly with changes in vertical mixing (see Figure 3.2). The effects of changes in mixing along isopycnals on ocean heat and carbon fluxes, and in turn on temperature sensitivity and AF, are too small to affect the temporal constancy of the TCRE.

In summary, the responses of ocean heat and carbon fluxes do not compensate each other very well and the TCRE is not constant while atmospheric CO_2 concentrations increase, or more generally while emission rates vary strongly, but is approximately constant while

atmospheric CO_2 is constant. This constancy of the TCRE arises due to compensating effects of ocean heat and carbon fluxes. The land carbon uptake plays only a minor role while atmospheric CO_2 concentrations are constant as the land carbon uptake fraction exhibits only small variations. Thus for the case of constant atmospheric CO_2 our findings confirm the hypothesis that the evolution of ocean heat and carbon fluxes over time is similarly determined by vertical mixing processes, leading to compensating changes in temperature sensitivity and AF, and an approximately constant TCRE.

3.5 Supplementary material

Global distribution of ocean heat (Figure 3.9) and carbon (Figure 3.8) fluxes at the end of the spin up simulations.

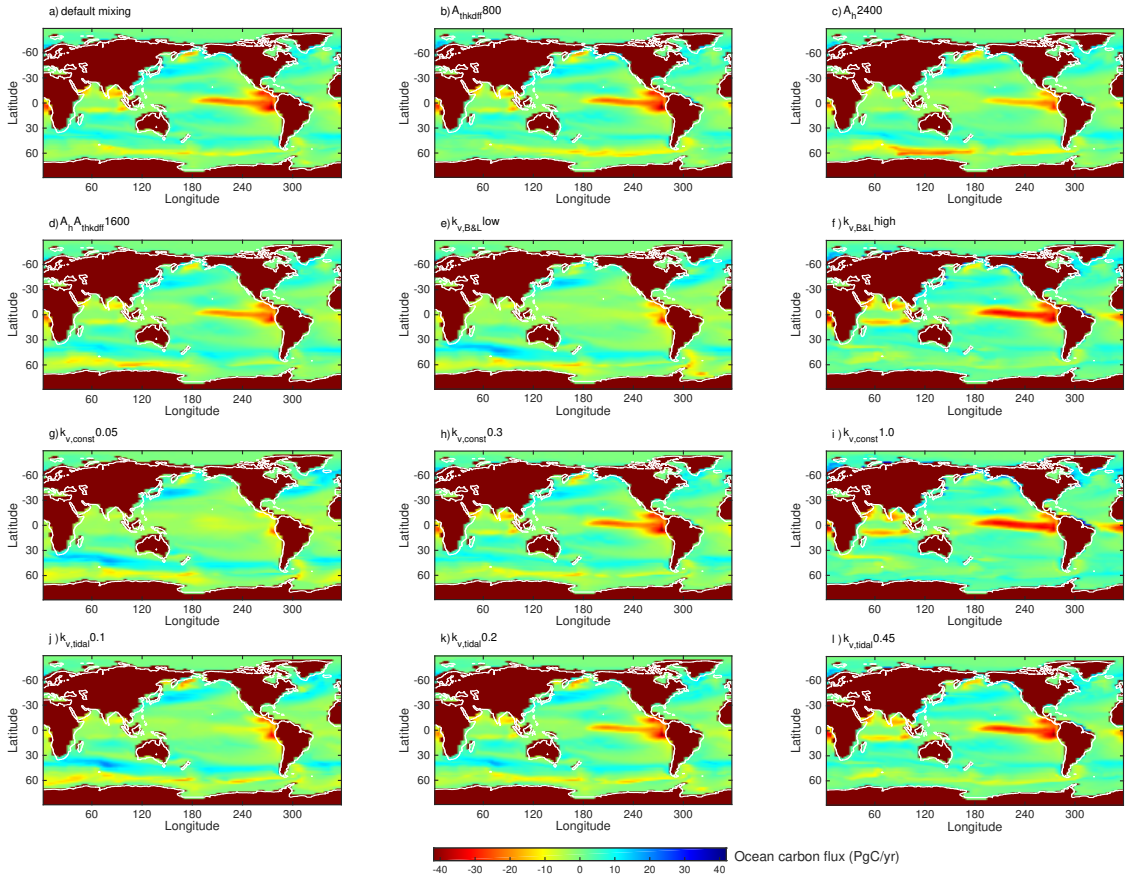

Figure 3.8: Air-sea dissolved inorganic carbon flux at the end of the spin up simulation. Positive numbers are uptake of carbon by the ocean.

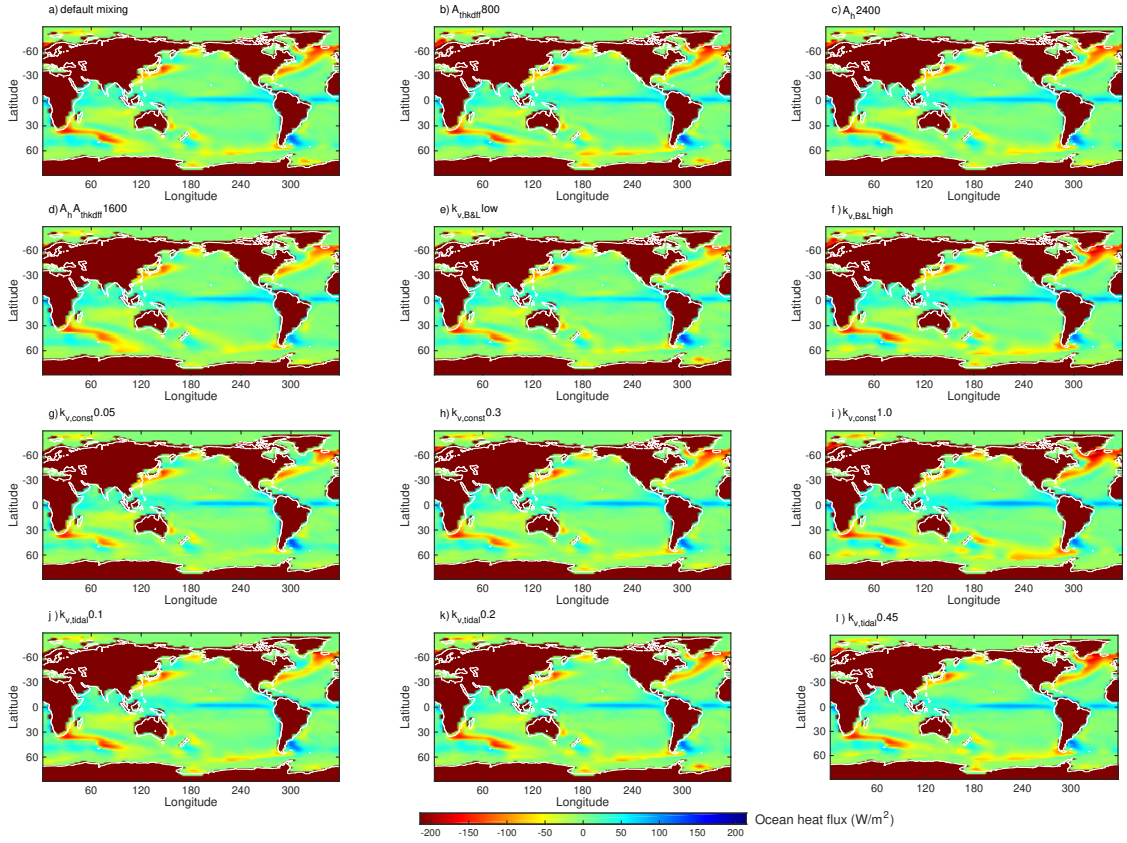

Figure 3.9: Air-sea heat flux at the end of the spin up simulation. Positive numbers are uptake of heat by the ocean.

Chapter 4

Irreversible ocean thermal expansion under negative CO_2 emissions

Abstract In the Paris Agreement in 2015 countries agreed on holding global mean surface air warming well below 2°C but the emission reduction pledges under that agreement are not ambitious enough to meet this target. Therefore, the question arises whether restoring a state of the climate system related to this target after exceeding it by artificially removing CO_2 from the atmosphere is possible. One important aspect regards the reversibility of ocean heat uptake and the associated sea level rise, which have very long (centennial to millennial) response time scales. In this study the response of sea level rise due to thermal expansion (TSLR) to a 1% yearly increase of atmospheric CO_2 up to a quadrupling of the pre-industrial concentration followed by a 1% yearly decline back to the pre-industrial CO_2 concentration is examined using the University of Victoria Earth System Climate Model (UVic ESCM). We find that TSLR continues for several decades after the CO_2 concentration starts to decline and that sea level does not return to pre-industrial levels centuries after atmospheric CO_2 has returned to pre-industrial concentrations. This finding is independent of the strength of vertical sub-grid scale ocean mixing. Furthermore, TSLR rises faster than it declines in response to a symmetric rise and decline in atmospheric CO_2 concentration partly because the deep ocean continues to warm for centuries after atmospheric CO_2 returns to pre-industrial concentrations. Both rise and decline rate in sea level change due to thermal expansion increase with increasing vertical mixing. Exceptions from this behaviour arise if the overturning circulation in the North Atlantic and Southern Ocean intensifies beyond initial levels stronger in model versions with lower vertical mixing, which leads to rapid cooling of the deep ocean.

4.1 Introduction

Policy makers agreed to "Holding the increase in the global average temperature to well below 2°C above pre-industrial levels and pursuing efforts to limit the temperature increase to 1.5°C above pre-industrial levels" under the Paris Agreement in 2015 (Paris Agreement, 2015). But the national pledges under this agreement are not sufficient to meet this target (Peters et al., 2015; Rogelj et al., 016a). At the same time, global mean temperature would remain elevated even if all CO_2 emissions were to cease (Matthews and Caldeira, 2008; Gillett et al., 2011; Matthews and Zickfeld, 2012; Zickfeld et al., 2013), implying that the mere cessation of emissions would not enable recovery of a warming target after exceeding it. Therefore, the idea has been discussed of artificially removing CO_2 from the atmosphere, a measure referred to as "negative emissions", with a number of techniques such as reforestation or direct air capture (Smith et al., 2016). It should be noted though that none of these techniques has yet been applied on a large scale (Fuss et al., 2016; Smith et al., 2016). However, most future scenarios not exceeding the 2°C warming target include such negative emissions and show a peak and decline in atmospheric CO_2 stronger than would be observed from only zeroing emissions (Smith et al., 2016). For example, the only Representative Concentration Pathway not exceeding 2°C, RCP 2.6, includes negative CO_2 emissions (Meinshausen et al., 2011). This decline of the radiative forcing induced by negative CO_2 emissions raises the question of reversibility of anthropogenic climate change, i.e., to what extent it is possible to revert to either a pre-industrial climate or another warming target such as 2°C and the related climate state by artificially removing CO_2 from the atmosphere. Previous studies have shown that global warming is reversible on human time scales but lags the CO_2 decline due to the ocean's thermal inertia (Boucher et al., 2012; Tokarska and Zickfeld, 2015; Zickfeld et al., 2016). Other aspects, such as precipitation or sea ice, also decline but lag the temperature response (Boucher et al., 2012). The effectiveness of negative emissions to lower atmospheric CO_2 is impeded as CO_2 outgases from natural carbon sinks in reaction to the negative emissions. This outgassing increases with increasing negative emissions, thus negative emissions become less effective the higher they get (Tokarska and Zickfeld, 2015). The total negative emissions are higher than the total positive emissions for reverting to the same CO_2 concentration if the permafrost feedback, which accounts for additional carbon emissions from thawing permafrost, is included (MacDougall, 2013). Higher total negative than positive emissions, means that more carbon needs to be artificially removed from the atmosphere than was initially emitted due to the hysteresis behaviour of the permafrost carbon pool. Another important finding in the reversibility research under negative emissions is that the approximately constant ratio between temperature change and cumulative emissions differs between atmospheric CO_2 increase and decline phases. This difference would need to be taken into account when setting total allowable emissions for a certain warming target after overshoot (Zickfeld et al., 2016).

An important part of the climate system response is ocean heat uptake and the associated sea level rise. Previous studies found this thermosteric sea level rise to be irreversible (i.e., sea level does not decline) on human (decadal to centennial) time scales even if large amounts of negative CO_2 emissions are applied (Boucher et al., 2012; Tokarska and Zickfeld, 2015). However, if longer time scales are taken into account, sea level rise due to thermal expansion is reversible (Zickfeld et al., 2013). Bouttes et al. (2013) show reversibility of thermal expansion on centennial time scales. By using a 2-layer ocean model they show that the decline in thermosteric sea level in response to zeroed or negative radiative forcing (with preceding positive radiaitve forcing) is due to a strong temperature decline in the upper ocean relative to the deep ocean, which enables the release of heat. This decline in thermosteric sea level cannot be explained with a zero-layer ocean model where the ocean is modelled as an infinite heat sink, which cannot spontaneously release heat. Under negative radiative forcing Bouttes et al. (2013) find that an Atmosphere Ocean General Circulation Model (AOGCM) shows a faster ocean heat release than uptake. This asymmetric behaviour is not observed in the 2-layer model response because the heat release in this model is determined by the temperature response of the upper ocean, which reacts instantly to a change in radiaitve forcing. Thus the 2-layer model temperature response is the same for positive and negative forcing, being solely opposite in sign. In the AOGCM, however, the ocean has multiple layers with multiple time scales and under negative radiative forcing the upper layers cool very fast, which creates such a strong temperature gradient between upper and lower ocean that thermostric sea level declines faster than it rises. This asymmetry in decline and rise is strengthened by an AMOC overshoot under the negative forcing (Bouttes et al., 2015). However, a detailed explanation of the physical processes leading to a stronger sea level change due to this AMOC overshoot is not given.

Zickfeld et al. (2017) investigate the mechanisms of thermosteric sea level rise and decline induced by emissions of short-lived radiative forcing agents, such as methane, and the cessation of those emissions. The thereby induced increase and decline in radiative forcing is similar to the change in radiative forcing that can be induced by positive and negative CO_2 emissions as short-lived forcing agents decline relatively fast in the atmosphere after cessation of their emissions. Zickfeld et al. (2017) show that the rate of sea level change from thermal expansion can be approximated with the difference between radiative forcing and a term representing radiative damping to space, which corresponds to a zero dimensional energy balance model. This model shows that a negative difference between radiative forcing and GMSAT change scaled by the climate feedback parameter enables declining global mean ocean temperatures and thus declining thermosteric sea level.

Herein, we further explore the physical mechanisms that determine the reversibility of thermosteric sea level rise. In particular, we examine the sensitivity of the reversibility of thermal expansion to parameterization of sub-grid ocean mixing. This is important because parameterization of sub-grid ocean mixing is still an uncertainty in climate models

that strongly affects ocean heat uptake. Using a range of ocean mixing parameters also enables further insights into the processes involved in the reversibility of thermal expansion and the associated sea level change. We examine the reversibility of thermal expansion and the processes involved in the context of symmetrically increasing and decreasing CO_2 concentrations, as opposed to Bouttes et al. (2013, 2015) who focus mostly on the mechanisms under negative radiative forcing.
The model used for this study is a model of intermediate complexity, which enables simulations on long time scales. Section 4.2 describes this model and the simulations performed. The results of these simulations are presented in Section 4.3 and discussed in Section 4.4. In Section 4.5 the conclusion from those results are drawn.

4.2 Model and Simulations

4.2.1 Model

Simulations for this study were performed using the University of Victoria Earth System Climate Model, version 2.9 (UVic ESCM 2.9). The physical model consists of an atmosphere energy balance model, a general circulation ocean model, an ocean sediment model, and a land surface scheme. All components include coupled carbon cycle descriptions and have a resolution of 1.8°(meridional) x 3.6°(zonal). UVic ESCM is a model of intermediate complexity. The model does not include an ice sheet model and we only discuss the sea level rise due to thermal expansion of the ocean in the following sections.
The atmosphere model is a vertically integrated energy-moisture balance model, which includes dynamic wind, planetary long wave, and water vapour feedbacks. Clouds are represented in the albedo of the atmosphere but dynamic cloud feedbacks are not included.
The land is represented using a simplified version of the Met Office Surface Exchange Scheme (MOSES) (Meissner et al., 2003; Cox et al., 1999), coupled to the dynamic vegetation model TRIFFID (Top-down Representation of Interactive Foliage and Flora Including Dynamics) (Cox, 2001).
The ocean is described with a three dimensional general circulation model with 19 vertical layers. It is the Geophysical Fluid Dynamic Laboratory (GFDL) Modular Ocean Model (MOM) (Weaver et al., 2001), which is coupled to a dynamic sea ice model, a sediment model, an inorganic carbon cycle model, and a marine biology model (Schmittner et al., 2005). Sub-grid ocean mixing is described via momentum diffusivity (or viscosity) and tracer diffusivity (Weaver et al., 2001). The following discussion focuses on parametrization of tracer diffusivity and the term ocean mixing only refers to the diffusion of tracers. This diffusion of tracers is parameterized as diffusion along isopycnals (surfaces of constant density) and diffusion across isopycnals. The diffusivity along isopycnals is set to 800 m^2s^{-1} and an additional parametrization is implemented to account for instabilities where isopycnals are tilted. This additional parameter, referred to as Gent & McWilliams thickness diffu-

sivity, is also set to 800 m^2s^{-1}. Mixing across isopycnals (diapycnal mixing) is described via a vertical mixing scheme as there is no practical difference between vertical and diapycnal mixing due to isopycnal slope limitations in the ocean model. There are three vertical mixing scheme options in the UVic ESCM 2.9: a vertically and laterally constant mixing scheme, a depth-dependent but laterally constant (Bryan & Lewis) mixing scheme, and a tidal mixing scheme, where mixing due to the dissipation of tidal energy over topography is added to a constant background diffusion parameter (Schmittner et al., 2005).

4.2.2 Simulations

The UVic ESCM is spun up for 6000 years under pre-industrial (year 1800) conditions for different model versions using different vertical ocean mixing parameter values and schemes (Table 4.1). The range of mixing parameters is chosen to achieve the widest possible range in ocean heat uptake while keeping the model stable and not necessarily to use parameters that closely reproduce observed ocean tracer distributions. However, for the tidal mixing scheme the range of background diffusivities was informed by studies that aimed at finding a range that best fits tracer observations (Schmittner et al., 2009; Goes et al., 2010; Ross et al., 2012). Mixing along isopycnals only entails small variations in ocean heat uptake (Chapter 3) and is therefore set to the default value in all model versions.
The default setting has a Bryan & Lewis vertical mixing scheme and a diffusivity of 0.3 cm^2s^{-1} in the deeper ocean and 1.3 cm^2s^{-1} in the upper ocean. This range is shifted to higher values of 0.5-1.5 cm^2s^{-1} ($k_{v,B\&L}$high) and lower values of 0.1-1.1 cm^2s^{-1} ($k_{v,B\&L}$low) while the vertical distribution within these ranges remains the same. The mixing scheme was changed from Bryan & Lewis to a vertically constant mixing ($k_{v,const}$), where the diffusivity was set to a value between 0.05 cm^2s^{-1} and 1.0 cm^2s^{-1}. Additionally, a tidal mixing scheme is used ($k_{v,tidal}$) and the background diffusivity was set to a value between 0.1 cm^2s^{-1} and 0.45 cm^2s^{-1}.
All model versions are run to a pre-industrial equilibrium and subsequently forced with an idealized scenario of a 1% yearly increase in atmospheric CO_2 concentration until quadrupling of the pre-industrial concentration (simulation year 140) followed by a 1% yearly decrease until pre-industrial levels are reached (simulation year 280). The simulations are continued with constant pre-industrial CO_2 concentration for another 1120 simulation years.

4.3 Results

4.3.1 Reversibility of sea level rise

In this section we focus on the discussion of thermosteric sea level rise and decline for the default ocean mixing setting (black curves in all figures with line plots) and Section 4.3.2

Table 4.1: Description of different model versions and their names as referred to in the text and figures. k_v is the vertical diffusivity. The pre-industrial state of the different model versions is shown exemplarily for the following variables: global mean surface air temperature (SAT), Atlantic Meridional Overturning Circulation (AMOC) and the given values refer to the maximum of the overturning stream function.

Experiment	vertical mixing scheme	k_v (cm^2s^{-1})	SAT (°C)	AMOC (Sv)
default	Bryan & Lewis	0.3-1.3	13.39	21.6
$k_{v,B\&L}$low	Bryan & Lewis	0.1-1.1	13.16	12.7
$k_{v,B\&L}$high	Bryan & Lewis	0.5-1.5	13.52	25.8
$k_{v,const}$0.05	vertically constant	0.05	12.89	9.8
$k_{v,const}$0.3	vertically constant	0.3	13.33	21.4
$k_{v,const}$1.0	vertically constant	1.0	16.67	32.3
$k_{v,tidal}$0.1	tidal	0.1	13.15	14.4
$k_{v,tidal}$0.2	tidal	0.2	13.32	19.3
$k_{v,tidal}$0.45	tidal	0.45	13.49	25.8

discusses the effect of different ocean mixing settings on this reversibility. Global mean surface air temperature (GMSAT) declines shortly after a decline in CO_2 is prescribed (Figure 4.1a). Global mean thermosteric sea level (GMTSL) continues to rise for another 80 years until it starts declining (Figure 4.1b). The decline is much slower than the rise in GMTSL despite a symmetrically increasing and decreasing atmospheric CO_2 concentration. To further investigate the mechanism of the GMTSL rise and decline we investigate ocean temperature as a proxy for GMTSL as the depth profile of ocean temperature gives insight into the distribution of heat in the ocean and will enable comparison with a simple ocean model in Section 4.3.2. The choice of ocean temperature as a proxy for thermosteric sea level rise is plausible as changes in global mean ocean temperature (GMOT) and changes in GMTSL follow a similar temporal evolution (Figure 4.1b,c). The relationship between temperature and density is not entirely linear in the ocean but the non-linear part is negligible for the scope of this study.

The decline in global mean ocean temperature and thus GMTSL is very slow because the warming signal from the previous increase in CO_2 still penetrates into the deeper ocean centuries after the radiative forcing has returned to zero and heat that entered the mid ocean is mixed into the upper ocean very slowly (Figure 4.2a). Thus, despite a cooling of the upper ocean, the deep ocean is still warming, except at high latitudes where the deep ocean cools (Figure 4.3b). This cooling is likely associated with an intensification of deep and bottom water formation, which overshoots the original value after CO_2 concentrations return to pre-industrial levels (Figures 4.6 and 4.7, these responses will be discussed in further detail in Section 4.3.2). The decline in GMOT lags the decline in atmospheric CO_2 concentration and also the decline in global mean surface air temperature (GMSAT) to such an extent that even by the end of the simulation (1120 years after returning to pre-industrial atmo-

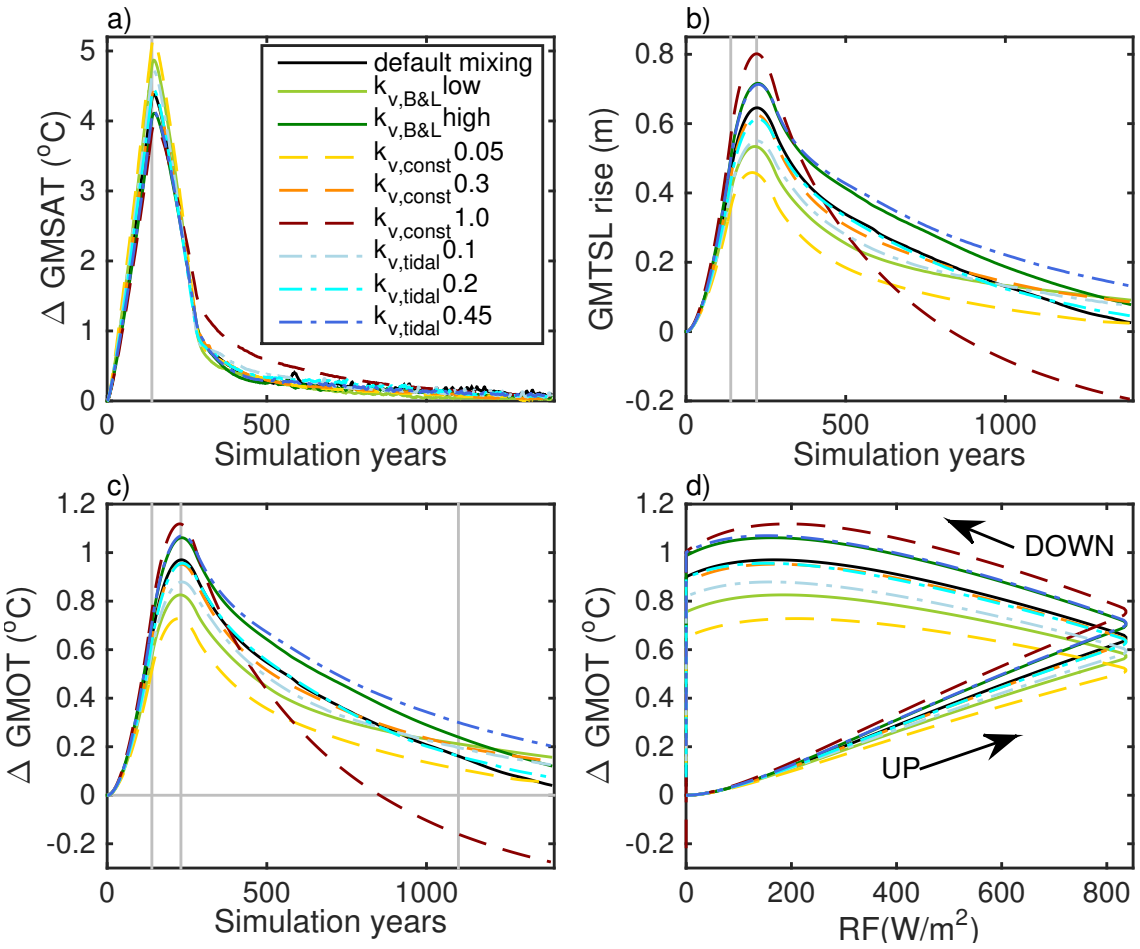

Figure 4.1: Changes in Global Mean Surface Air Temperature (a), Global Mean Thermosteric Sea Level (b), and Global Mean Ocean Temperature (c) relative to year 0 over time and change in GMOT versus radiative forcing. The first vertical grey line in panel a, b, and c indicates the time of peak atmospheric CO_2 concentration (quadrupling of pre-industrial levels, year 140). The second grey line in panel b and c indicates the time GMTSL and GMOT reach maximum values. The third grey line in panel c is the time Figures 4.2 and 4.3 refer to year 1100.

spheric CO_2 concentration) GMOT and thus thermosteric sea level have not returned to pre-industrial levels. As seen in previous literature (Boucher et al., 2012), GMOT exhibits hysteresis relative to change in radiative forcing as GMOT remains elevated despite zero radiative forcing (Figure 4.1d).

Previously it has been assumed that GMTSL change is proportional to GMSAT changes and thus to radiative forcing (Rahmstorf, 2007; Bouttes et al., 2013). However, this assumption does not hold for declining radiative forcing (Bouttes et al., 2013) and Zickfeld et al. (2017) therefore suggested the following relationship, which holds also under declining ra-

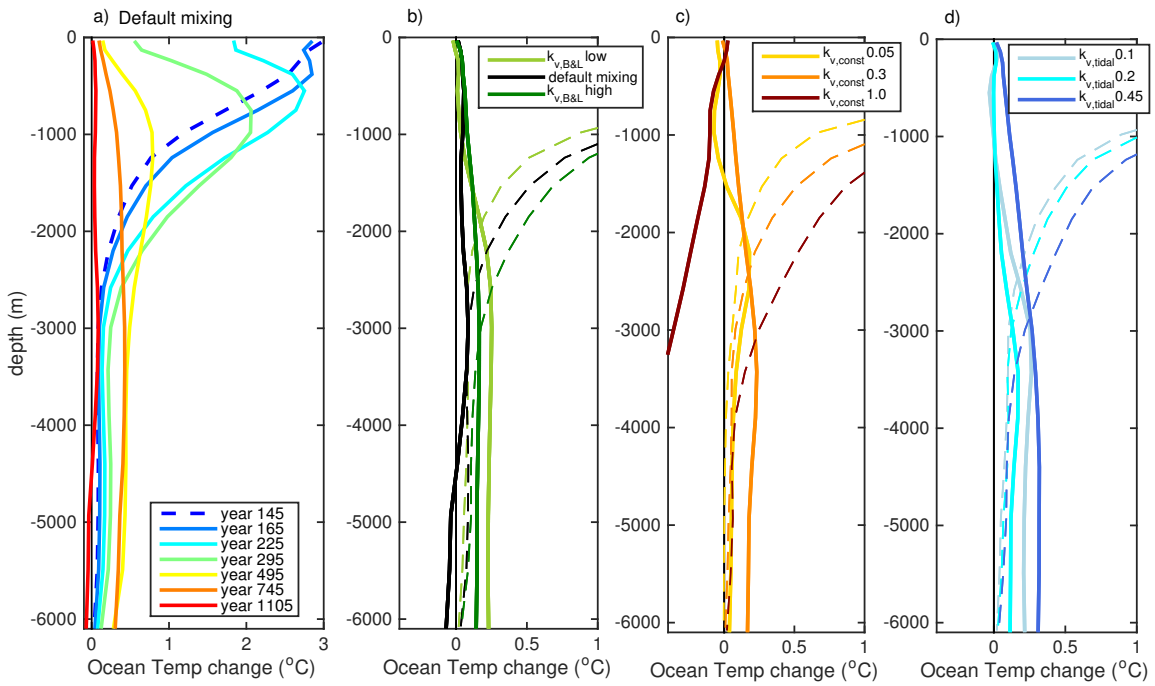

Figure 4.2: Zonal and meridional average of change in ocean temperature relative to year 0 for the model version with default mixing setting for various points in time (a). Zonal and meridional average of change in ocean temperature relative to year 0 for model versions with different ocean mixing settings for year 140 (dashed curves, year of peak forcing) and year 1100 (continuous curves, 3rd vertical grey line in figure 4.1c) for Bryan& Lewis mixing scheme (b), constant mixing scheme (c), and tidal mixing scheme (d).

diative forcing:

$$\frac{d\eta}{dt} = \alpha RF - \beta \Delta T$$

where η is the sea level rise due to thermal expansion, RF is the radiative forcing, and ΔT is the temperature change relative to a reference year. β/α is equal to the climate feedback parameter λ in $\mathrm{Wm^{-2}K^{-1}}$ by analogy of the above equation with the zero dimensional energy balance equation (i.e., dη/dt$\propto$RF-$\lambda\Delta$T). Applying this framework to the simulation results discussed here shows that while GMTSL is rising (i.e., positive time derivative) the radiaitive forcing is larger than $\lambda\Delta T$ (Figure 4.4). However, when $\lambda\Delta T$ is larger than the radiative forcing, induced by the lag of the GMSAT decline relative to the decline in radiative forcing, GMTSL declines. Thus the declines of GMOT and GMTSL are due to a negative radiation imbalance at the top of the atmosphere.

4.3.2 The effect of ocean mixing on sea level rise and its reversibility

In this section we discuss the effect of different parameters for vertical ocean mixing on GMTSL rise and decline and identify the mechanisms that lead to the differences in GMTSL among model versions with different vertical mixing parameters.

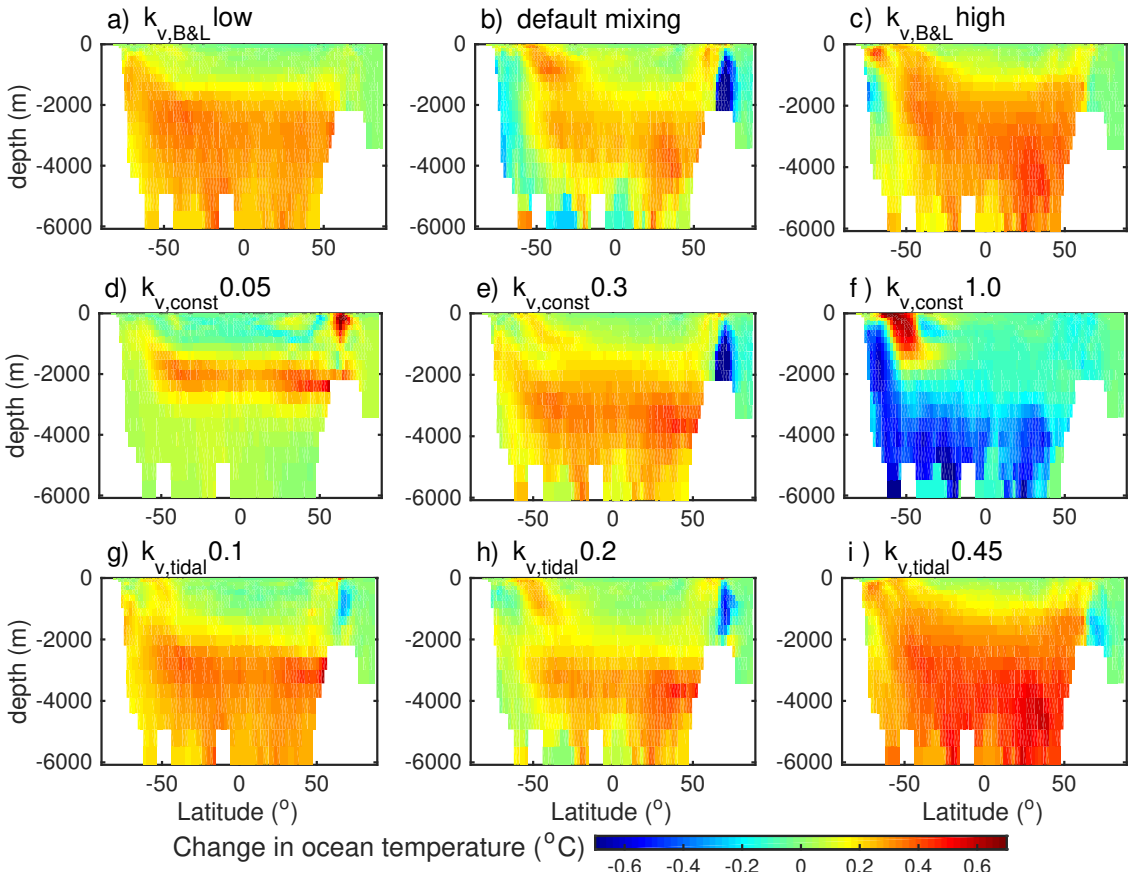

Figure 4.3: Zonal average change in ocean temperature for year 1100 relative to year 0 for the different model versions. Each row shows results for one mixing scheme (Bryan&Lewis mixing, constant mixing, tidal mixing in the 1st, 2nd, and 3rd row, respectively) and the vertical diffusivity increases from left to right.

Under increasing CO_2 concentrations, GMTSL rises faster with increasing vertical mixing parameter (Figure 4.1b,c). Peak GMTSL, which occurs around year 220 (80 years after atmospheric CO_2 started declining), ranges between 0.45 m and 0.80 m. Similarly to the increase, GMTSL and GMOT also decrease faster under increased vertical ocean mixing, with exceptions for $k_{v,B\&L}$high and $k_{v,tidal}$0.45 simulations (Figure 4.1b,c). In these simulations, GMOT decrease rate is similar to the rate in model versions with lower mixing parameters. The causes for this behaviour will be discussed later in this section.

In most cases a higher decline rate of GMOT for a model version with higher vertical diffusivity results in a crossover of the GMOT curves (Figure 4.1b,c): for example, the $k_{v,B\&L}$low simulation has a slower ocean warming than the default simulation between year 0 and year 900. However, the rate of ocean temperature decline is higher in the default simulation than in the $k_{v,B\&L}$low simulation, leading to a crossover of these two ocean temperature curves, and from around year 900 on the default simulation has lower ocean temperatures and thus a lower GMTSL.

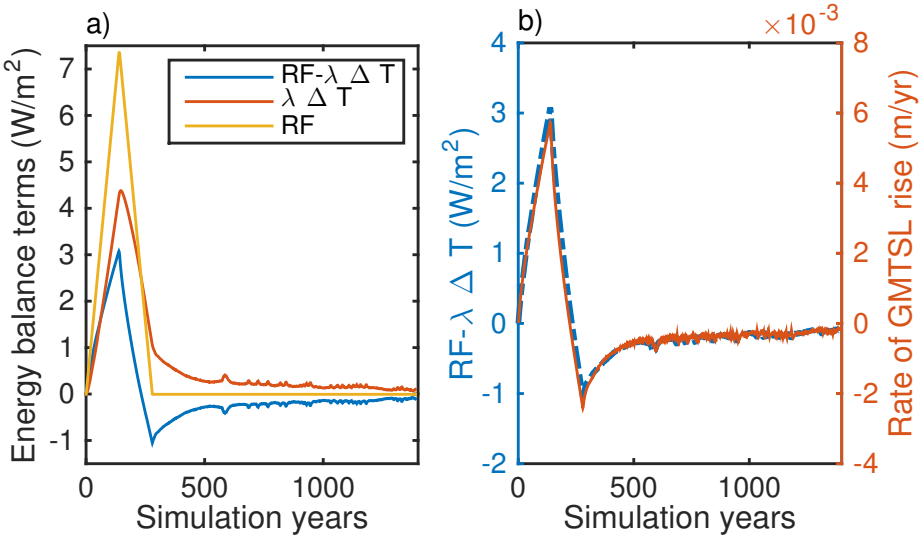

Figure 4.4: Energy balance terms calculated from the simulation data of the model version with default mixing setting. $\beta/\alpha = \lambda$ =1 $Wm^{-2}K^{-1}$ is the climate feedback parameter for the default mixing setting. ΔT is the change in global mean surface air temperature relative to year 0 and RF is the radiaitve forcing. Panel (b) compares the energy imbalance (blue y-axes and curve) to the rate of Global Mean Thermosteric Sea Level rise (red y-axes and curve).

This behaviour of faster GMOT increase and decline rates under higher mixing, including the crossover of the GMOT curves, can be explained with a 2-layer ocean model (Figure 4.5a). This model consists of an upper ocean layer and a deep ocean layer (Gregory, 2000; Bouttes et al., 2013). The upper layer is thin (depth d_u 100 m) and responds immediately to changes in forcing because it has a small heat capacity. The lower layer is thick (depth d_l 2000 m), has a high heat capacity, and thus provides the inertia of the ocean response. The heat flux between the upper and lower layer is proportional to the temperature difference between these layers. The temperature for each layer (T_u temperature upper layer, T_l temperature lower layer) can be calculated using the following equations:

$$cd_u \frac{dT_u}{dt} = RF - ck\frac{(T_u - T_l)}{0.5(d_l + d_u)} - \lambda T_u$$
$$cd_l \frac{dT_l}{dt} = ck\frac{(T_u - T_l)}{0.5(d_l + d_u)}$$

where c= 4.218*10^6 $Jm^{-3}K^{-1}$ is the volumetric heat capacity, k =1*$10^{-4}m^2s^{-1}$= 1 cms^{-1} is the thermal diffusivity between the layers, λ= 1.0 $Wm^{-2}K^{-1}$ is the climate feedback parameter, and RF (Wm^{-2}) is the surface heat flux representing the external radiative forcing, which is prescribed according to a symmetric 1% yearly increase to quadrupling pre-industrial CO_2 levels and subsequent and decrease in atmospheric CO_2, i.e., the same forcing as in the UVic ESCM simulations. Changes in mixing are achieved by changing the

thermal diffusivity k between the layers in the range from 0.05*k to 1.0*k. This range was chosen to correspond to the range in mixing parameters in the UVic ESCM simulations that leads to the widest range in GMOT.

The temperature of the upper layer reacts instantaneously to changes in the forcing (Figure

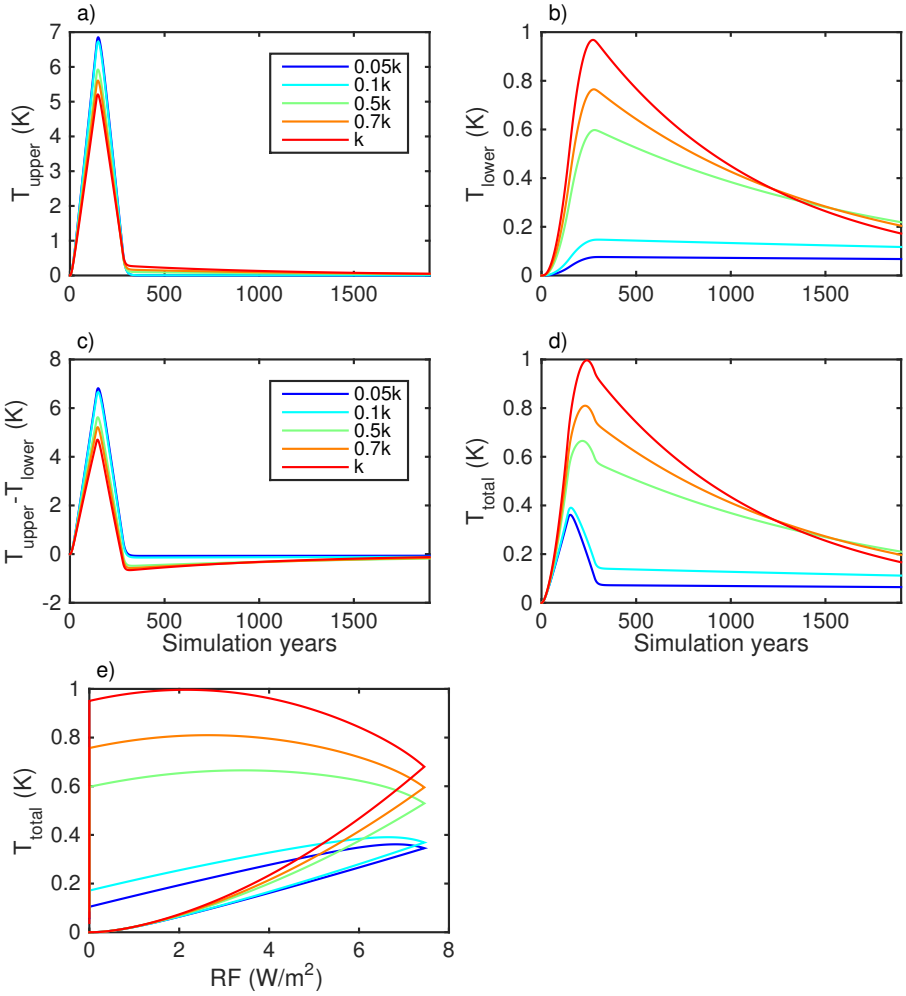

Figure 4.5: Temperature changes for the 2-layer ocean model: change in upper (T_{upper}) (a) and lower layer ocean temperature T_{lower} (b), difference in the temperature between the layers (c) and change in total ocean temperature (d, calculated as average from T_{upper} and T_{lower} weighted by the layer depth). Change in total ocean temperature versus radiative forcing (e). k=1 cm^2s^{-1} is the thermal diffusivity between the layers.

4.5a). The temperature in the lower layer lags behind the radiative forcing but also dominates the total temperature of the ocean (Figure 4.5b,d) due to its very high heat capacity relative to the heat capacity of the upper layer. Therefore, ocean heat uptake or release can be approximated by the heat exchange between the layers, which is determined by the thermal diffusivity and the temperature gradient between the layers. A higher diffusivity between the layers enables a faster heat exchange between the layers and a faster heat

uptake and release by the whole ocean as observed in the model (Figure 4.5d). However, the temperature gradient between the layers is lowest for the model version with the highest diffusivity (Figure 4.5c) implying a diminished heat exchange between the layers and a slower ocean heat uptake and release, which is the opposite from what is observed in the model. Therefore, it is the effect of the diffusion that dominates the ocean heat uptake and not the vertical temperature gradient. This 2-layer model also shows a similar hysteresis behaviour as the UVic ESCM simulation (compare Figures 4.1d and 4.5e).
One limitation of the two-layer model is that the lower layer has a too high heat capacity resulting in a very slow heat release from this layer. This is especially strong for very low diffusivity values (Figure 4.5b blue and red curve). For comparison: in a multi-layer model where heat is transferred step by step from one layer to the next, heat is more easily released because upper layers, which extend deeper than the upper layer in the 2-layer model, have a response time scale that is between that of the upper and lower layer of the 2-layer model and therefore release heat faster than the lower layer in the 2-layer model (Bouttes et al., 2013). The other limitation is that the 2-layer model has no meridional overturning circulation, which intensifies in the UVic ESCM simulations in both the Atlantic Ocean and the Southern Ocean after radiative forcing returned to zero and leads to a stronger heat release. Due to these two shortcomings the decline in ocean temperature is much slower in the 2-layer model than in the UVic ESCM and 2-layer model simulations have to be extended for 1000 years compared to the UVic ESCM simulations to observe a crossover of the ocean temperature curves.
Generally, the initial (pre-industrial) meridional overturning in both the Atlantic Ocean and the Southern Ocean increases as vertical diffusivity increases (Figure 4.6a and 4.7a) in the UVic ESCM model versions. In addition, response to the radiative forcing also differs among model versions. These differences in the overturning response likely lead to divergences between the results from UVic ESCM simulations and 2-layer ocean model simulations as will be discussed in the following.

Cases where the UVic ESCM simulations diverge from the 2-layer ocean model behaviour (i.e., similar GMOT decline in model version with higher compared to those with lower diffusivity) are the model version with default ocean mixing setting relative to the $k_{v,B\&L}$high model version and the $k_{v,tidal}0.2$ relative to the $k_{v,tidal}0.45$ model version. For each model version pair, the uptake of heat is faster for the model version with the higher mixing but the rate of heat release is approximately the same. This similar ocean heat release rate is likely caused by a stronger intensification of the overturning (in both the Atlantic Ocean and the Southern Ocean) in response to the declining forcing in the simulations with lower vertical mixing (i.e., default mixing setting and $k_{v,tidal}0.2$).
The globally averaged vertical ocean temperature profiles support the finding that higher mixing does not always entail a stronger decline in ocean temperatures (Figure 4.2b,d).

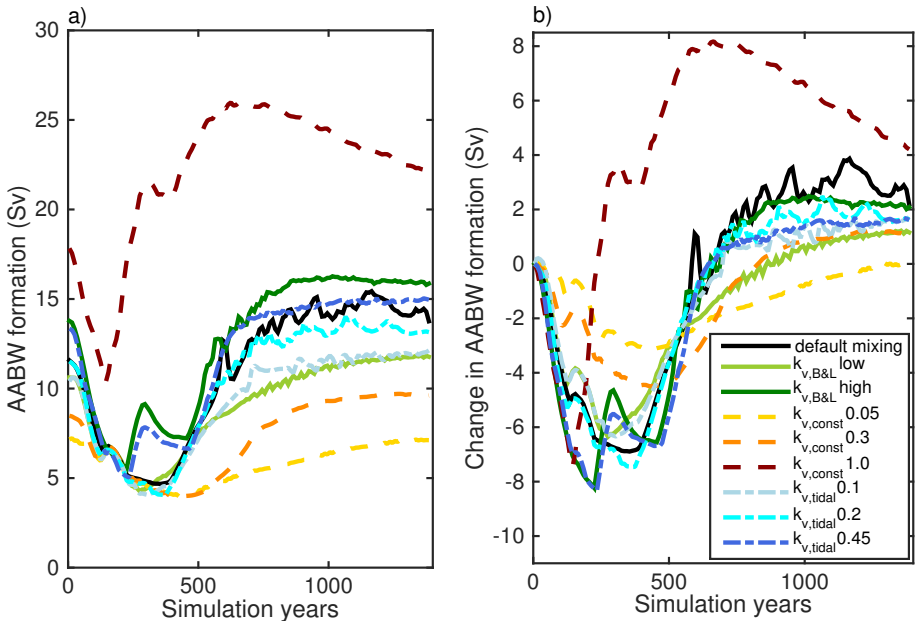

Figure 4.6: a) Antarctic Bottom Water (AABW) formation, calculated as minimum of the zonally averaged overturning stream function (averaged over the globe) below 500 m. b) Change in the AABW formation relative to year 0.

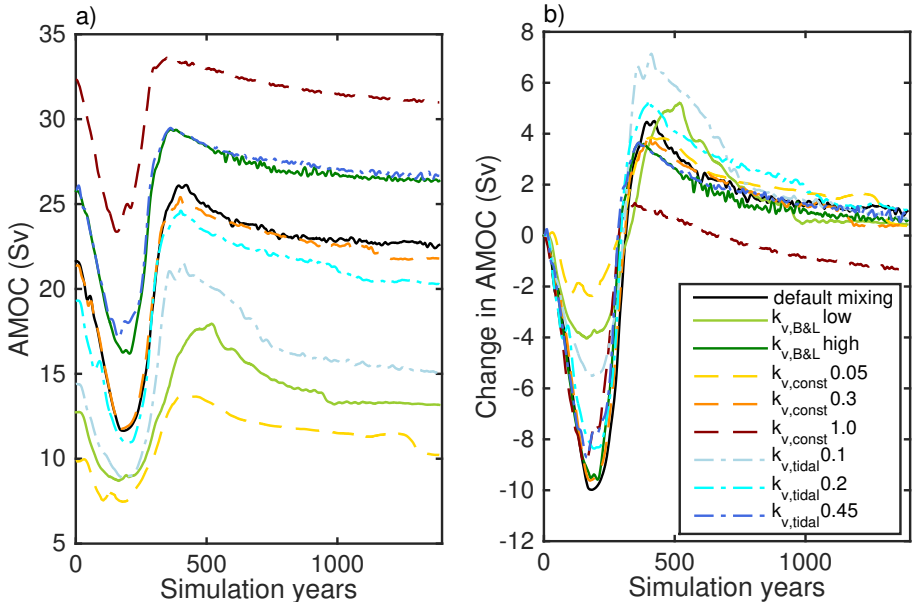

Figure 4.7: a) Atlantic meridional overturning circulation (AMOC) calculated as maximum of the zonally averaged overturning stream function in the North Atlantic. b) Change in the AMOC relative to year 0.

At year 140 (year of peak forcing), for the Bryan& Lewis mixing scheme (default mixing setting, $k_{vB\&L}$low and high) and the tidal mixing scheme ($k_{v,tidal}$), the temperature in the surface and mid-ocean increases with increasing ocean mixing. However, for year 1100 de-

fault mixing and $k_{v,tidal}0.2$ simulations have the lowest ocean temperature below a depth of around 1100 m. Interestingly, in those cases the deep ocean has also cooled more than the mid ocean, probably induced by increased Antarctic Bottom Water (AABW) formation. For the tidal mixing scheme, both simulations with the lower mixing setting ($k_{v,tidal}0.1$ and 0.2) have a stronger cooling than the simulation $k_{v,tidal}0.45$. The discussion of the overturning circulation and especially its response to the declining radiative forcing will give further insights into this behaviour.

Both Atlantic Meridional Overturning Circulation (AMOC) and AABW formation decline in response to increased atmospheric CO_2 concentrations and the associated global warming (Figures 4.6a, 4.7b). AMOC responses to global warming have been well studied and the decline in the AMOC under warming is due to surface warming and freshening of North Atlantic surface waters (Rahmstorf, 2006). The AMOC increases again in a delayed response to the decrease in radiative forcing (Figure 4.7a), which leads to a cooling of surface waters and also increase in sea ice formation that increases surface water density and thus increases the deep water formation. The AMOC even overshoots its pre-industrial strength (Figure 4.7b) due to a build up of salinity in the subtropical gyre in the northern Atlantic while AMOC is weaker (Wu et al., 2011). When the AMOC strengthens again as a response to declining surface temperature this salinity anomaly is advected northward, which results into denser water in the North Atlantic and an intensified AMOC. This AMOC overshoot has been linked to an increased rate of ocean heat release (Bouttes et al., 2015). Declining AABW formation/volume in response to anthropogenic climate change has been seen in model and observational data (Purkey and Johnson, 2012) but the causes for this response have not been explored in modelling experiments to our knowledge. It is likely linked to the decline in sea ice formation and surface warming. The AABW formation increases as a delayed response to the decreasing radiative forcing (Figure 4.6a), likely due to surface cooling and increased sea ice formation, and it also intensifies above pre-industrial levels (Figure 4.6b). However, this intensification is much smaller and slower than the AMOC overshoot. Further investigation is needed to uncover the processes that cause this intensification.

Both AMOC and AABW formation overshoot/intensify more strongly in the model versions with lower mixing setting (i.e., in the model version with default mixing relative to $k_{v,B\&L}$high, and $k_{v,tidal}0.1$ and 0.2 relative to $k_{v,tidal}0.45$), which leads to faster heat release as the exchange between deep/bottom waters and surface waters is increased. This intensification in overturning circulation likely offsets the decreased exchange between upper and deeper ocean in the model version with lower mixing (i.e., default mixing setting and $k_{v,tidal}0.2$). The cooling effect on the deep and bottom waters from stronger than pre-industrial AMOC and AABW formation is also evident in the zonally averaged ocean temperature changes (Figure 4.3), where the simulations with default ocean mixing and $k_{v,tidal}0.2$ have more cooling in the mid ocean at northern high latitudes and the deep

ocean at southern high latitudes than in the $k_{v,B\&L}$high and $k_{v,tidal}$0.45 simulations. The deep ocean cooling is less pronounced in the $k_{v,tidal}$0.2 case. Also the $k_{v,tidal}$0.1 has a very strong AMOC overshoot, which together with the lower heat uptake during the increasing forcing phase results in a stronger cooling than in the $k_{v,tidal}$0.45 simulation.
A special case is the $k_{v,const}$1.0 simulation, which has the highest vertical mixing of all simulations. Here, the GMOT and thus GMTSL decline below pre-industrial levels implying that more heat is being released than initially entered the ocean. This is most likely linked to a very strong intensification of the AABW formation under this very high mixing setting (Figure 4.6b, red curve). This assumption is supported by a strong cooling in the Southern Ocean along the path of the AABW (Figure 4.3f). The cause for this intensification would require further investigation, which is beyond the scope of this study.

4.4 Discussion

Contrary to Tokarska and Zickfeld (2015), we find that GMTSL can decline on centennial time scales despite using the same climate model. This different finding is caused by applying a stronger decline in atmospheric CO_2 than Tokarska and Zickfeld (2015). Boucher et al. (2012) use the same scenarios as in this study but only investigate decadal time scales and thus do not detect the decline in GMTSL.
There are only a few previous studies investigating the reversibility mechanisms of thermal expansion. Bouttes et al. (2013, 2015) investigate the mechanism of this reversibility for rapidly declining and negative radiative forcing and find that the reversibility in response to declining radiative forcing can be described by a 2-layer ocean model, i.e., by the heat exchange between the upper and deeper ocean. This is in agreement with our findings. Under negative radiative forcing (preceded by positive radiative forcing) they also find that an AMOC overshoot causes a faster decline in GMTSL. The extension of the zero layer ocean model (GMTSL rise rate is proportional to GMSAT) by a term to account for radiative damping (Zickfeld et al., 2017), which has been shown to explain the reversibility of thermal expansion after elimination of short-lived forcers, is invoked to explain the mechanisms of GMTSL decline. We show here that this model also explains GMTSL decline as a response to declining atmospheric CO_2 concentration from negative CO_2 emissions.
A decline of the AMOC under increased forcing is well documented in the literature (Stocker and Schmittner, 1997; Rahmstorf, 2006; Meehl et al., 2007) as well as a recovery and an overshoot of the AMOC when the forcing is reduced leading to a faster decline in GMTSL (Wu et al., 2011; Bouttes et al., 2015). Earlier studies (Knutti and Stocker, 2000; Levermann et al., 2005) found a slow increase (over several millennia) of global mean sea level after a shut down of the AMOC because the reduction of the surface temperature induced by the AMOC shutdown reduces the radiation lost to space and thereby increases ocean

heat uptake. A rapid regional thermosteric sea level increase in the North Atlantic with thermosteric sea level decrease in the Southern Ocean is also shown by Levermann et al. (2005). This slow increase of global sea level is in contrast to the link we propose whereby GMTSL changes less with a weaker AMOC. However, the mechanism between a slowdown of the AMOC and a complete shutdown could be different because a slightly weaker AMOC does not induce such strong changes in surface temperature.
A decrease of the overturning circulation in the Southern Ocean under increasing atmospheric CO_2 concentration has been documented in earlier studies (Gregory, 2000) and a decrease in AABW formation has been documented in observations (Purkey and Johnson, 2012). However, changes in circulation in the Southern Ocean, especially AABW formation, under decreasing radiative forcing and the processes involved have not been studied in detail. We find a recovery and intensification of AABW formation after radiative forcing is reduced back to zero but further investigation is needed to improve the understanding of the processes involved in the response of the AABW formation, which is beyond the scope of this study.

Shortcomings of the research presented here are that the model used (UVic ESCM 2.9) does not include an interactive ice sheet component and no interactive representation of cloud feedbacks. The lack of an interactive ice sheet component means that sea level rise and possible decline from the melting and possibly regrowing ice sheets in reaction to the increase and decline in radiative forcing is not included. The contribution to sea level rise from melting ice sheets is projected to become dominant in the future and reversibility of sea level rise from ice sheet melting would be delayed due to their long response time scales and possible threshold behaviour (Robinson et al., 2012; Church et al., 2013). However, there are large uncertainties for these contributions due to incomplete understanding of ice sheet dynamics (Church et al., 2013). No interactive representation of cloud feedbacks affects ocean heat uptake as investigations with AOGCMs have shown that changes in cloud cover enhance the cooling effect from changes in ocean heat uptake induced by changes in ocean circulation due to climate change (Trossman et al., 2016). Thus the model used here might underestimate the effect of changes in ocean circulation on ocean heat uptake under increasing atmospheric CO_2. Whether this effect between ocean heat uptake, changes in ocean circulation, and cloud cover is also in effect when the changes in ocean circulation are induced by changes in ocean mixing or how this link evolves under declining CO_2 concentration is unclear. Additionally, modelling of cloud feedbacks is still subject to great uncertainties, and thus the overall effect of their exclusion is unknown.
These shortcomings are unlikely to affect the robustness of the result that thermosteric sea level rise is not reversible on human time scales. Including the contribution from ice sheets to sea level would make sea level rise even less reversible due to the very long response timescales of ice sheet dynamics. Significant changes in the response time of thermosteric

sea level changes from including dynamic cloud feedbacks are unlikely as the associated effect on ocean heat uptake is very small, only $0.01\mathrm{Wm}^{-2}$ in a previous study (Trossman et al., 2016). Furthermore this study shows that irreversibility of GMTSL rise on human timescales is robust against the choice of vertical diffusivity.

4.5 Conclusions

In this study the reversibility of thermosteric sea level rise in response to a symmetric increase and decrease in atmospheric CO_2 concentration is examined. Furthermore, the sensitivity of this reversibility to sub-grid ocean mixing is investigated, which also gives further insight into the role of ocean circulation in this reversibility. Different versions of the UVic ESCM 2.9, which differ in the parametrization of vertical sub-grid ocean mixing, are forced with a 1% yearly increase in atmospheric CO_2 concentration until quadrupling of pre-industrial levels, followed by a 1% yearly decrease in CO_2 and constant pre-industrial CO_2 concentration thereafter. Such a strong decline in atmospheric CO_2 concentrations can only be realised with net negative CO_2 emissions, i.e., artificial removal of CO_2 from the atmosphere.

We find that thermosteric sea level is not reversible on human time scales (decadal time scales) as GMTSL rise continues for 80 years after atmospheric CO_2 concentration starts declining. The decline of GMTSL is much slower than the rise due to the thermal inertia of the ocean, which can be observed by a warming signal in the deeper ocean that persists for almost a millennium after atmospheric CO_2 concentration is restored to pre-industrial levels. Furthermore, GMTSL does not revert to pre-industrial values by the end of the simulations (1120 years after atmospheric CO_2 concentration is restored to pre-industrial levels). The release of heat by the ocean, and thus a declining GMTSL, are explained by evoking a 0-D energy balance model where the rate of GMTSL rise is linked to radiative forcing and a term representing radiative damping to space. This model shows that a declining GMTSL is enabled by radiative forcing being lower than the change in GMSAT scaled by the climate feedback parameter (Zickfeld et al., 2017).

Generally, sea level rise and decline rates in response to increasing and decreasing atmospheric CO_2 increase with higher vertical diffusivity, which can be explained with a simple 2-layer ocean model with diffusion of heat between a thin upper layer and a deep lower layer. Exceptions to this behaviour in the UVic ESCM simulations are linked to a strengthening of the meridional overturning circulation beyond pre-industrial values (inferred from AMOC and AABW formation intensification) after recovering from a decline induced by the increasing radiative forcing. Generally, this intensification in meridional overturning circulation beyond pre-industrial values is stronger in model versions with lower vertical diffusivity. In some cases this intensification is so large in the model version with lower diffusivity that it offsets the effect of decreased vertical diffusivity and GMTSL decline rates

are similar among model versions with different diffusivity values. Stronger North Atlantic deep water and AAWB formation increase the exchange of heat between the upper and the deeper ocean and the intensification of these deep and bottom water formation beyond their pre-industrial levels increases the release of heat from the ocean. Especially the intensification of AABW formation results in a cooling of the deep ocean after radiative forcing has returned to zero.

Generally, ocean thermal expansion induced by increased CO_2 concentrations does not revert to pre-industrial levels for at least a millennium after CO_2 concentration returned to pre-industrial levels irrespective of the choice of vertical diffusivity. Lower vertical diffusion in the ocean models, which may be closer to reality as it has been argued that ocean models have a too high diffusion (Hansen et al., 2011), would imply a lower GMTSL rise at first but would increase the duration of elevated sea levels after CO_2 concentrations are restored to pre-industrial levels. The reversibility of sea level rise would likely be prolonged further if sea level rise from melting ice sheets would be taken into account as ice sheets respond on even longer time scales than ocean heat uptake and their contribution to sea level rise is projected to increase in the future (Church et al., 2013; Clark et al., 2016).

Thus sea level rise from thermal expansion, and likely also from ice sheet melting, is not reversible even under strong decreases in atmospheric CO_2 far beyond time scales relevant to human civilization.

Chapter 5

Key findings and conclusions

Anthropogenic carbon dioxide (CO_2) emissions increase CO_2 concentrations in the atmosphere, which induces changes in the climate system (IPCC, 2013). The goal of this thesis is to elucidate key characteristics of the climate response to anthropogenic CO_2 emissions, such as the linear relationship between change in global mean surface air temperature and cumulative CO_2 emissions, the warming commitment following elimination of CO_2 emissions, and the reversibility of anthopogenic climate change. The following research questions have been examined using a climate modelling approach:

1. Zero emissions warming commitment (ZEC)
   (a) What determines the warming commitment after cessation of CO_2 emissions?
   (b) What is the effect of thermal equilibration (declining ocean heat uptake) and bio-geochemical equilibration (declining carbon uptake) on this warming commitment?
2. Transient Climate Response to cumulative CO_2 Emissions (TCRE)
   (a) Which physical processes determine the approximate constancy of the TCRE?
   (b) What is the sensitivity of the approximate constancy of the TCRE to different representations of ocean mixing?
3. Reversibility of thermosteric sea level rise
   (a) Is sea level rise due to thermal expansion reversible and on which time scale?
   (b) What are the physical mechanisms that determine this reversibility?
   (c) What is the effect of different representations of ocean mixing on the reversibility of ocean thermal expansion?

5.1 Zero emission warming commitment

Chapter 2 of this thesis focuses on the second-order temperature change after CO_2 emissions cease, also referred to as zero emission warming commitment (ZEC). The goal of this chapter is to explore the mechanisms that determine the ZEC.

Previous studies found a to first order constant global mean surface air temperature (GMSAT) after cessation of CO_2 emissions (Matthews and Caldeira, 2008; Gillett et al., 2011) but also second-order changes in the GMSAT (i.e., ZEC) of a range from -1.2°C to 0.5°C (Zickfeld et al., 2013; Frölicher et al., 2013; Frölicher and Paynter, 2015). Differences in the ZEC arise from different models being used, different emission scenarios and atmospheric CO_2 concentrations prior to cessation of CO_2 emissions, different timing of zeroing emissions, and different time horizons over which the ZEC is calculated (Zickfeld et al., 2013; Frölicher and Paynter, 2015; Leduc et al., 2015; Herrington and Zickfeld, 2014; Matthews and Zickfeld, 2012). Knowing the magnitude of the ZEC is important because a significant ZEC would need to be taken into account for a warming target and thus lower the allowable budget of cumulative CO_2 emissions for this warming target.

A non-zero ZEC arises from an imbalance between a warming effect from declining ocean heat uptake after elimination of CO_2 emissions (i.e., thermal equilibration) and a cooling effect from declining atmospheric CO_2 concentration. The latter is determined by land and ocean carbon uptake, which also decline after emissions cease (i.e., bio-geochemical equilibration).

This study is the first one to our knowledge that systematically investigates the effects of the timing of zeroing CO_2 emissions, CO_2 concentration prior to cessation of emissions, and time horizon over which the ZEC is being calculated. Examining the timing of zeroing emissions entails comparing the effects of bio-geochemical and thermal equilibration, as both decline the later emissions are zeroed along a trajectory of constant atmospheric CO_2 concentration. Especially the effect of bio-geochemical equilibration has not been studied in detail previously. Due to the unique study set-up (emissions are zeroed along a trajectory of constant CO_2 concentrations), the effects of the state of equilibration can be separated from other effects such as differences in radiative forcing prior to zeroed emissions.

We find that the ZEC is positive and declines the later emissions are zeroed, implying that the warming effect of thermal equilibration dominates over the cooling effect from declining atmospheric CO_2 concentration. However, under low CO_2 concentration (double the pre-industrial concentration or RCP4.5) prior to zeroing CO_2 emissions the ZEC slightly increases or is constant for emissions zeroed later in time, indicating that the decline in the cooling effect from the decline in CO_2 concentration after cessation of emissions dominates over the decline in the warming effect from the decline in ocean heat uptake.

Overall it is the effect of the scenario (i.e., the level of radiative forcing) prior to cessation of CO_2 emissions that dominates the ZEC. The timing of zeroing emissions or the time

horizon over which the ZEC is calculated only play a minor role. Thus, only ZECs with similar scenarios prior to zeroing emissions should be compared, whereas effects from choosing a different time horizon to calculate the ZEC or timing of zeroing emissions could be neglected or could be accounted for by using the results from our study.
We furthermore find significant ZECs for high CO_2 concentration scenarios prior to setting emissions to zero, such as for quadrupling of pre-industrial CO_2 concentrations or RCP 8.5 (ZECs of 0.2-0.9°C and 0.2-0.6°C for 4xCO2 and RCP8.5 respectively). Thus for these scenarios the ZEC would have to be taken into account for a warming target and the budget for allowable cumulative CO_2 emissions would have to be lowered. For lower CO_2 concentration scenarios such as doubling of pre-industrial CO_2 concentrations of RCP4.5 the ZEC is not significant (ZECs of 0.0-0.1°C and 0.07-0.2°C for doubling of CO_2 and RCP4.5 respectively) and does not need to be considered for a warming target and in setting the respective cumulative CO_2 emissions budgets.

5.2 Constancy of the TCRE

Previous studies revealed that the ratio between GMSAT and cumulative CO_2 emissions, referred to as Transient Climate Response to cumulative CO_2 Emissions (TCRE), is approximately constant over time and among scenarios (Matthews et al., 2009; Allen et al., 2009; Eby et al., 2009). This finding is useful as it implies that there is a set amount of allowable cumulative CO_2 emissions for a certain warming target (Zickfeld et al., 2009), which could be used to inform climate policies (Raupach et al., 2014). The the 2°C warming target allows a cumulative CO_2 emission budget of 1000 PgC with a 66% probability of staying below this target (IPCC, 2013), over half of which have been emitted by now (Le Quéré et al., 2016).
The reasons for this constancy are still under discussion, but a commonly given hypothesis is that the effects of ocean heat and carbon uptake cancel each other out because both are governed by the same deep ocean mixing processes and thus lead to an approximately constant TCRE over time.
In order to investigate this hypothesis and the robustness of the temporal constancy of the TCRE, different model versions of an EMIC, which differ in the parameterization of sub-grid scale ocean mixing, were produced. At the time of doubling of the pre-industrial atmospheric CO_2 concentration, the TCRE ranges from 1.2°C/EgC to 2.1°C/EgC (for comparison the CMIP5 TCRE range is 0.8-2.5°C/EgC, Gillett et al. (2013)). Changes in diapycnal or vertical mixing parameter have a much stronger effect on ocean heat and carbon uptake than changes in mixing along isopycnals. Higher vertical mixing parameter leads to increased ocean heat and ocean carbon uptake. A higher ocean carbon uptake means that more CO_2 can be emitted (i.e., higher cumulative CO_2 emissions) while reaching the same atmospheric CO_2 concentration, which has been prescribed in this study. Higher

ocean heat uptake means more heat is transferred into the ocean, which lowers surface air temperatures. Thus higher ocean heat and carbon uptake lead to decreased GMSAT change (numerator of the TCRE) and increased cumulative CO_2 emissions (denominator of the TCRE), and thus a decreased TCRE. For the temporal evolution of the TCRE we find that it deviates up to 20% from the mean value while atmospheric CO_2 concentration increases (1% yearly increase in atmospheric CO_2 until quadrupling of pre-industrial CO_2 concentration) and that the effects of ocean heat and carbon uptake on the TCRE do not cancel out each other. These are stronger variations in the TCRE than indicated previously (Matthews et al., 2009) because longer time scales are taken into account. However, under constant atmospheric CO_2 concentrations that follow the increase in CO_2 the TCRE is approximately constant (5% deviation from the mean value), which is due to a cancellation of effects of ocean heat and carbon uptake on the TCRE. This finding therefore confirms the hypothesis of ocean heat and carbon uptake causing the approximately constant TCRE, which has also been suggested by other studies (Goodwin et al., 2015; MacDougall and Friedlingstein, 2015). Despite strong differences in ocean mixing, the temporal evolution of the TCRE and cancellation effects remain similar among the model versions likely because there is a linear relationship between ocean heat and carbon uptake and strength of the vertical ocean mixing parameter.

Understanding the mechanism involved in the approximate constancy of the TCRE is important in scientifically underpinning the carbon budget approach. Few studies (Matthews et al., 2009; Goodwin et al., 2015; MacDougall and Friedlingstein, 2015) investigated the mechanism but none investigated the effect of sub-grid ocean mixing on the TCRE. The finding that strong changes in ocean mixing do not entail significant changes in the temporal evolution of the TCRE makes this temporal evolution less sensitive to uncertainties in the parametrization of sub-grid ocean mixing and increases the robustness of the temporal evolution. However, variations in the ocean mixing parameter lead to a wide range in to total value of the TCRE (0.9°C range), which is higher than the highest range due to temporal TCRE variations within a simulation under a specific mixing setting (0.36°C range if the first steep increase of the TCRE over the first decade is neglected). The strong variations in the TCRE due to mixing parameters induce uncertainties in carbon budgets related to warming targets. The temporal variations of the TCRE over time while atmospheric CO_2 increases strongly could weaken the scientific foundation of applying the carbon budget approach as a mitigation framework.

5.3 Thermosteric sea level rise reversibility

As the remaining carbon budget for a 2°C warming target is declining (Le Quéré et al., 2016) due to continuously increasing CO_2 emissions (Boden et al., 2016) and pledges for reducing emissions are not ambitious enough to match this target (Smith et al., 2016),

the application of negative CO_2 emission technologies has been suggested. Negative emissions imply artificial removal of CO_2 from the atmosphere that could enable atmospheric CO_2 concentrations to decline more rapidly than what could be achieved with cessation of CO_2 emissions alone. This raises the question of the reversibility of anthropogenic climate change under negative emissions. Previous studies found that GMSAT is reversible on human (decadal) time scales (Boucher et al., 2012; Tokarska and Zickfeld, 2015). Sea level rise due to thermal expansion is an important factor in the question of reversibility due to high impacts and the long time scales of ocean heat uptake and release. Previous studies find irreversible thermal expansion on human time scales but reversible thermal expansion on centennial time scales (Boucher et al., 2012; Tokarska and Zickfeld, 2015; Zickfeld et al., 2013; Bouttes et al., 2013).

In Chapter 4 we examine the reversibility of sea level rise due to thermal expansion in response to symmetrically increasing and decreasing CO_2 concentration and the sensitivity of this reversibility to parameterization of vertical sub-grid ocean mixing. We find that global mean thermosteric sea level (GMTSL) continues to rise for many decades after atmospheric CO_2 starts declining. But GMTSL declines thereafter and is thus reversible but only on centennial time scales. Reversibility to pre-industrial levels is estimated to be possible solely on multi-millennial time scales, thus, far beyond human time scales. Following a symmetric increase and decrease in atmospheric CO_2 concentration (1% yearly increase until quadrupling of pre-industrial CO_2 concentration and then return to pre-industrial levels at the same rate), GMTSL increases much faster than it decreases partly because the warming signal still penetrates into the deeper ocean for centuries after CO_2 concentrations return to pre-industrial levels. GMTSL rise and decline rate strengthen with increasing vertical ocean mixing parameter, which is caused by a faster exchange of heat between the mixed layer and deeper ocean. The higher decline rate of GMTSL under higher vertical mixing parameters results in lower GMTSL by the end of the simulation for model versions with higher vertical mixing, despite the fact that they initially took up more heat. Deviations from this behaviour arise where overturning circulation, in both or either the North Atlantic and the Southern Ocean, increases beyond pre-industrial strength in response to the declined atmospheric CO_2 concentration for cases with lower vertical mixing. Strongly enhanced overturning in some model versions leads to a faster cooling of the deep ocean, which offsets the reduced heat release due to a lower diffusivity.

Generally, a lower vertical ocean mixing parameter, which has been suggested to be closer to modelling the real ocean (Hansen et al., 2011, 2016), leads to a lower GMTSL during increasing atmospheric CO_2 concentrations but also slower decline in GMTSL after CO_2 concentrations decrease and possibly even higher GMTSL on centennial time scales. Thus GMTSL rise from current CO_2 emissions is likely not reversible even under negative CO_2 emissions for centuries to come.

This irreversibility is likely to be strengthened when sea level rise from ice sheet melting is

taken into account due to the long time scales of ice sheet dynamics and possible threshold behaviour (Robinson et al., 2012; Church et al., 2013; Clark et al., 2016).
There are only few studies investigating the mechanism of reversibility of GMTSL rise under negative CO_2 emissions and none to our knowledge investigating the effect of ocean mixing on this reversibility. This study gives further insight into the effectiveness of negative emissions in reversing the uptake of heat by the ocean and the associated thermal expansion. For instance, it is shown that decreased vertical mixing leads to lower GMTSL but also decreases the ability to reverse it (i.e., a lower diffusivity slows down the decline in GMTSL). Applying different ocean mixing parameters also gives insights into the effect of changes in the overturning circulation on ocean heat uptake and release. For example, the intensification of overturning in the Southern Ocean as well as AMOC overshoot could enable faster declines in GMTSL. Furthermore, there are large inter-model variations in GMTSLR reversibility (see reversibility experiments in Zickfeld et al. (2013)) and this research helps elucidate some of these differences.

5.4 General conclusions and outlook

The results from the research presented in this thesis suggest that using cumulative CO_2 emission budgets to limit warming to a specific target as a framework for climate mitigation needs to be done with caution. Reasons for caution are that the TCRE under increasing CO_2 concentration diverges more strongly from a constant value than suggested in previous studies (Matthews et al., 2009). The TCRE could also be higher than found in current studies (Gillett et al., 2013; Eby et al., 2013) because vertical ocean mixing has been suggested to be too high in current climate models (Hansen et al., 2011) and as found here, the TCRE decreases with increasing vertical mixing (Chapter 3), implying a lower carbon budget for a certain warming target. Furthermore, significant warming after zeroing emissions needs to be taken into account in scenarios with high radiative forcing (such as RCP8.5 or 1% yearly increase in atmospheric CO_2 concentration until quadrupling of pre-industrial levels) prior to setting CO_2 emissions to zero. However, additional warming is less relevant for carbon budgets related to low warming targets such as those included in the Paris Agreement (Paris Agreement, 2015).
Furthermore, other aspects of climate change, such as ocean warming and GMTSL rise, do not relate linearly to cumulative CO_2 emissions. The long time scales of ocean heat uptake and release due the ocean's high heat capacity lead to increasing GMTSL after cessation of emissions and irreversible GMTSL rise under negative CO_2 emissions on human time scales.

The following specific research directions would corroborate and expand the research findings presented in this thesis. Additional research would be useful to further systematically investigate the relationship between CO_2 concentration prior to setting emissions to

zero and the ZEC for a range of models. This would give further insight into how much warming would need to be added to a warming target. Further studies exploring in detail how changes of sub-grid ocean mixing parameterization induce changes in the geographical distribution of ocean heat and carbon uptake, changes in the geographical distribution of surface ocean tracers and sea ice, ocean circulation, and distribution of heat and carbon within the ocean would give further insights into the uncertainties due to these parameterizations. Also the behaviour of overturning circulation in the Southern Ocean under decreasing atmospheric CO_2 has not been studied to our knowledge, which is of importance as the study presented here has shown the important role of ocean circulation for ocean heat release under a scenario of declining atmospheric CO_2 concentration. Furthermore, a comparison study of present-day simulations under the different mixing parameters and schemes used in this thesis with measurements of ocean tracers, such as ocean temperature or salinity, as performed by Schmittner et al. (2009) and Goes et al. (2010), would provide insides into how realistic the chosen diffusivity parameters and their induced ranges in TCRE and projected GMTSL are.

In terms of broader future research directions, there is still a lack of understanding of which processes exactly cause the approximate constancy of the TCRE over time. For example, do specific processes that affect ocean heat and carbon uptake differently cause a strong deviation of the TCRE from a constant value while atmospheric CO_2 concentrations increase? This question is difficult to answer because separating the effect of specific mechanism, such as different time scales of sea-air equilibration for heat and carbon, different geographical distribution of ocean heat and carbon uptake, or the effect of ocean circulation on ocean heat and carbon uptake relative to the effect of different ocean mixing parameterizations, is hard to achieve. It would be useful to study the effect of changes in ocean circulation on the TCRE as these changes affect both ocean heat and carbon uptake but have a stronger effect on ocean heat uptake (Winton et al., 2013).
Another open question is how to reduce the uncertainty range of the TCRE. As the research presented here shows, ocean mixing can have a strong effect on the TCRE. Improving the parameterization of ocean mixing could help narrowing this range. One option that has been suggested and becomes partly implemented as advances in computing power permit, is to improve ocean models such that they resolve some of these mixing processes (eddy permitting or resolving ocean models, resolution of $\sim 1/3^\circ$ or lower)(Kuhlbrodt et al., 2015; Newsom et al., 2016; Williams et al., 2015; Munday et al., 2014). Long term simulations with these models, particularly if including a representation of the carbon cycle, are limited by computing power. However, such long term (centennial time scales) simulations would help understand mechanisms of ocean carbon uptake and ocean heat uptake due its long response times. Such studies could also help to understand which processes of ocean heat and carbon uptake affect the temporal evolution of the TCRE, which could in turn support

the understanding of the constancy of the TCRE. A refined understanding of ocean heat and carbon uptake would also reduce uncertainties in the ZEC, as it is dominated by the ocean heat uptake and decline in atmospheric CO_2, which is mostly determined by ocean carbon uptake. However, such studies would not be able to resolve all uncertainties in ocean heat uptake as there are also strong uncertainties in the climate feedback parameter, i.e., uncertainties in how much warming there is to expected from a certain radiaitive forcing, which also affects ocean heat uptake. It should also be noted that these eddy-permitting or eddy-resolving models still require parametrization of eddies that are smaller than mesoscale (Delworth et al., 2012), which are for example eddies that induce vertical mixing. However, these models do improve the representation of the Southern Ocean (Newsom et al., 2016). Furthermore, the research presented here only addresses CO_2 as a radiative forcing agent. However, other greenhouse gases, in particular methane, and aerosols need to be taken into account as well as they contribute to anthopogenic climate change (IPCC, 2013). Carbon budgets vary strongly depending on whether temperature changes from non-CO_2 radiative forcing agents are taken into account (Rogelj et al., 2016). Many non-CO_2 radiative forcing agents (e.g., methane), however, are short lived and their warming is emission-pathway dependent and thus a budget approach is not applicable (Smith et al., 2012). Therefore, further research is needed to understand how to consolidate the warming effects of long and short lived radiative forcing agents in order to create useful tools, similar to the carbon budgets approach, for mitigation efforts. Previously used metrics, such as the global warming potential (GWP, the warming potential of a radiative forcing agent relative to the warming potential of CO_2), treat all radiative forcing agents in the same way. This leads to significant short comings as for example, a short lived radiative forcing agent with a high specific radiative forcing (i.e., the radiative forcing per kilogram emission) has the same GWP as a long lived radiative forcing agent with a low specific radiative forcing (Shine et al., 2005). However, if emission reductions for the long lived forcing agent were replaced with emission reductions for the short lived forcing agent, as they have the same GWP, long term warming would increase as the cumulative emissions for the long lived forcing agent increase. Therefore, metrics have been suggested that treat long and short lived radiative forcing agents differently, such as using budget approaches for long lived radiative forcing agents and peak warming inferred from emission rates for short lived radiative forcing agents (Smith et al., 2012). However, the effect of the metric chosen to compare the climate effects from non-CO_2 radiative forcing agents and CO_2 on not exceeding a warming target needs to be studied in more detail. Especially, comparisons of the effects of either choosing a metric that treats all radiative forcing agents same versus one that treats long and short lived radiative forcing agents differently are needed.

Overall this thesis gives new insights into the role of ocean heat and carbon uptake in the response of the climate system to anthropogenic CO_2 emissions on centennial time

scales. The relative effects of bio-geochemical and thermal equilibration in determining the ZEC have been uncovered. The effect of changes in parameterization of sub-grid ocean mixing on ocean heat and carbon uptake and on the value and temporal evolution of the TCRE are shown. Additionally, the effect of changes in ocean mixing parameterization on the (ir)reversibility of thermal expansion is unveiled and the physical processes that govern sea level rise reversibility are elucidated.

Bibliography

Allen, M. R., Frame, D. J., Huntingford, C., Jones, C. D., Lowe, J. a., Meinshausen, M., and Meinshausen, N. (2009). Warming caused by cumulative carbon emissions towards the trillionth tonne. *Nature*, 458(7242):1163–1166.

Archer, D. (1996). A data-driven model of the global calcite lysocline. *Global Biogeochemical Cycles*, 10(3):511–526.

Archer, D., Eby, M., Brovkin, V., Ridgwell, A., Cao, L., Mikolajewicz, U., Caldeira, K., Matsumoto, K., Munhoven, G., Montenegro, A., and Tokos, K. (2009). Atmospheric Lifetime of Fossil Fuel Carbon Dioxide. *Annual Review of Earth and Planetary Sciences*, 37(1):117–134.

Arneth, A., Harrison, S. P., Zaehle, S., Tsigaridis, K., Menon, S., Bartlein, P. J., Feichter, J., Korhola, A., Kulmala, M., O'Donnell, D., Schurgers, G., Sorvari, S., and Vesala, T. (2010). Terrestrial biogeochemical feedbacks in the climate system. *Nature Geoscience*, 3(8):525–532.

Bindoff, N., Stott, P., AchutaRao, K., Allen, M., Gillett, N., Gutzler, D., Hansingo, K., Hegerl, G., Hu, Y., Jain, S., Mokhov, I., Overland, J., Perlwitz, J., Sebbari, R., and Zhang, X. (2013). Detection and Attribution of Climate Change: from Global to Regional. In Stocker, T., Qin, D., Plattner, G.-K., Tignor, M., Allen, S., Boschung, J., Nauels, A., Xia, Y., Bex, V., and Midgley, P., editors, *Climate Change 2013: The Physical Science Basis. Contribution of Working Group I to the Fifth Assessment Report of the Intergovernmental Panel on Climate Change*, pages 867–952. Cambridge University Press, Cambridge, United Kingdom and New York, NY, USA.

Boden, T., Marland, G., and Andres, R. (2016). Global, regional, and national fossil-fuel CO2 emissions. *Carbon Dioxide Information Analysis Center, Oak Ridge National Laboratory, U.S. Department of Energy, Oak Ridge, Tenn., U.S.A.*

Boucher, O., Halloran, P. R., Burke, E. J., Doutriaux-Boucher, M., Jones, C. D., Lowe, J., Ringer, M. A., Robertson, E., and Wu, P. (2012). Reversibility in an Earth System model in response to CO 2 concentration changes. *Environmental Research Letters*, 7(2):024013.

Bouttes, N., Good, P., Gregory, J. M., and Lowe, J. A. (2015). Nonlinearity of ocean heat uptake during warming and cooling in the famous climate model. *Geophysical Research Letters*, 42(7):2409–2416.

Bouttes, N., Gregory, J. M., and Lowe, J. a. (2013). The Reversibility of Sea Level Rise. *Journal of Climate*, 26(8):2502–2513.

Cao, L. and Caldeira, K. (2010). Atmospheric carbon dioxide removal: long-term consequences and commitment. *Environmental Research Letters*, 5(2):024011.

Church, J., Clark, P., Cazenave, A., Gregory, J., Jevrejeva, S., Levermann, A., Merrifield, M., Milne, G., Nerem, R., Nunn, P., Payne, A., Pfeffer, W., Stammer, D., and Unnikrishnan, A. (2013). Sea level change. In Stocker, T., Qin, D., Plattner, G.-K., Tignor, M., Allen, S., Boschung, J., Nauels, A., Xia, Y., Bex, V., and Midgley, P., editors, *Climate Change 2013: The Physical Science Basis. Contribution of Working Group I to the Fifth Assessment Report of the Intergovernmental Panel on Climate Change*, book section 13, pages 1137–1216. Cambridge University Press, Cambridge, United Kingdom and New York, NY, USA.

Ciais, P., Sabine, C., Bala, G., Bopp, L., Brovkin, V., Canadell, J., Chhabra, A., DeFries, R., Galloway, J., Heimann, M., Jones, C., Le QueÌĄreÌĄ, C., Myneni, R., Piao, S., and Thornton, P. (2013). Carbon and other biogeochemical cycles. In Stocker, T., Qin, D., Plattner, G.-K., Tignor, M., Allen, S., Boschung, J., Nauels, A., Xia, Y., Bex, V., and Midgley, P., editors, *Climate Change 2013: The Physical Science Basis. Contribution of Working Group I to the Fifth Assessment Report of the Intergovernmental Panel on Climate Change*, book section 6, pages 465–570. Cambridge University Press, Cambridge, United Kingdom and New York, NY, USA.

Clark, P. U., Shakun, J. D., Marcott, S. A., Mix, A. C., Eby, M., Kulp, S., Levermann, A., Milne, G. A., Pfister, P. L., Santer, B. D., Schrag, D. P., Solomon, S., Stocker, T. F., Strauss, B. H., Weaver, A. J., Winkelmann, R., Archer, D., Bard, E., Goldner, A., Lambeck, K., Pierrehumbert, R. T., and Plattner, G.-K. (2016). Consequences of twenty-first-century policy for multi-millennial climate and sea-level change. *Nature Clim. Change*, 6(4):360–369.

Collins, M., Knutti, R., Arblaster, J., Dufresne, J.-L., Fichefet, T., Friedlingstein, P., Gao, X., Gutowski, W., Johns, T., Krinner, G., Shongwe, M., Tebaldi, C., Weaver, A., and Wehner, M. (2013). Long-term climate change: Projections, commitments and irreversibility. In Stocker, T., Qin, D., Plattner, G.-K., Tignor, M., Allen, S., Boschung, J., Nauels, A., Xia, Y., Bex, V., and Midgley, P., editors, *Climate Change 2013: The Physical Science Basis. Contribution of Working Group I to the Fifth Assessment Report of the Intergovernmental Panel on Climate Change*, book section 12, pages 1029–1136. Cambridge University Press, Cambridge, United Kingdom and New York, NY, USA.

Cox, P. M. (2001). Description of the TRIFFID dynamic global vegetation model: Hadley Centre Technical Note 24. Hadley Centre technical note 24, Hadley Centre, Met Office, Berks, UK.

Cox, P. M., Betts, R. a., Bunton, C. B., Essery, R. L. H., Rowntree, P. R., and Smith, J. (1999). The impact of new land surface physics on the GCM simulation of climate and climate sensitivity. *Climate Dynamics*, 15(3):183–203.

Cox, P. M., Betts, R. a., Jones, C. D., Spall, S. a., and Totterdell, I. J. (2000). Acceleration of global warming due to carbon-cycle feedbacks in a coupled climate model. *Nature*, 408(6809):184–187.

Delworth, T. L., Rosati, A., Anderson, W., Adcroft, A. J., Balaji, V., Benson, R., Dixon, K., Griffies, S. M., Lee, H. C., Pacanowski, R. C., Vecchi, G. A., Wittenberg, A. T., Zeng,

F., and Zhang, R. (2012). Simulated climate and climate change in the GFDL CM2.5 high-resolution coupled climate model. *Journal of Climate*, 25(8):2755–2781.

Dlugokencky, E. and Tans, P. (2017). Noaa/esrl. `ftp://aftp.cmdl.noaa.gov/products/trends/co2/co2_annmean_gl.txt`, Accessed: 2017-01-27.

Eby, M., Weaver, A. J., Alexander, K., Zickfeld, K., Abe-Ouchi, A., Cimatoribus, A. A., Crespin, E., Drijfhout, S. S., Edwards, N. R., Eliseev, A. V., Feulner, G., Fichefet, T., Forest, C. E., Goosse, H., Holden, P. B., Joos, F., Kawamiya, M., Kicklighter, D., Kienert, H., Matsumoto, K., Mokhov, I. I., Monier, E., Olsen, S. M., Pedersen, J. O. P., Perrette, M., Philippon-Berthier, G., Ridgwell, A., Schlosser, A., Schneider von Deimling, T., Shaffer, G., Smith, R. S., Spahni, R., Sokolov, A. P., Steinacher, M., Tachiiri, K., Tokos, K., Yoshimori, M., Zeng, N., and Zhao, F. (2013). Historical and idealized climate model experiments: an intercomparison of Earth system models of intermediate complexity. *Climate of the Past*, 9(3):1111–1140.

Eby, M., Zickfeld, K., Montenegro, a., Archer, D., Meissner, K. J., and Weaver, a. J. (2009). Lifetime of anthropogenic climate change: millennial time scales of potential CO2 and surface temperature Perturbations. *Journal of Climate*, 22:2501–2511.

Ewen, T. L., Weaver, A. J., and Eby, M. (2004). Sensitivity of the inorganic ocean carbon cycle to future climate warming in the uvic coupled model. *Atmosphere-Ocean*, 42(1):23–42.

Friedlingstein, P., Cox, P., Betts, R., Bopp, L., von Bloh, W., Brovkin, V., Cadule, P., Doney, S., Eby, M., Fung, I., Bala, G., John, J., Jones, C., Joos, F., Kato, T., Kawamiya, M., Knorr, W., Lindsay, K., Matthews, H. D., Raddatz, T., Rayner, P., Reick, C., Roeckner, E., Schnitzler, K.-G., Schnur, R., Strassmann, K., Weaver, A. J., Yoshikawa, C., and Zeng, N. (2006). Climate–carbon cycle feedback analysis: results from the C4MIP model intercomparison. *Journal of Climate*, 19(14):3337–3353.

Frölicher, T. L. and Joos, F. (2010). Reversible and irreversible impacts of greenhouse gas emissions in multi-century projections with the NCAR global coupled carbon cycle-climate model. *Climate Dynamics*, 35(7):1439–1459.

Frölicher, T. L. and Paynter, D. J. (2015). Extending the relationship between global warming and cumulative carbon emissions to multi-millennial timescales. *Environmental Research Letters*, 10(7):075002.

Frölicher, T. L., Sarmiento, J. L., Paynter, D. J., Dunne, J. P., Krasting, J. P., and Winton, M. (2015). Dominance of the southern ocean in anthropogenic carbon and heat uptake in cmip5 models. *Journal of Climate*, 28(2):862–886.

Frölicher, T. L., Winton, M., and Sarmiento, J. L. (2013). Continued global warming after CO2 emissions stoppage. *Nature Climate Change*, 4(1):40–44.

Fuss, S., Jones, C. D., Kraxner, F., Peters, G. P., Smith, P., Tavoni, M., van Vuuren, D. P., Canadell, J. G., Jackson, R. B., Milne, J., Moreira, J. R., Nakicenovic, N., Sharifi, A., and Yamagata, Y. (2016). Research priorities for negative emissions. *Environmental Research Letters*, 11(11):115007.

Gent, P. R. and Mcwilliams, J. C. (1990). Isopycnal mixing in ocean circulation models. *Journal of Physical Oceanography*, 20(1):150–155.

Gillett, N. P., Arora, V. K., Matthews, D., and Allen, M. R. (2013). Constraining the ratio of global warming to cumulative CO2 emissions using CMIP5 simulations. *Journal of Climate*, 26(18):6844–6858.

Gillett, N. P., Arora, V. K., Zickfeld, K., Marshall, S. J., and Merryfield, W. J. (2011). Ongoing climate change following a complete cessation of carbon dioxide emissions. *Nature Geoscience*, 4(2):83–87.

Gnanadesikan, A. (1999). A simple predictive model for the structure of the oceanic pycnocline. *Science*, 283(5410):2077–2079.

Gnanadesikan, A., Pradal, M.-A., and Abernathey, R. (2015a). Exploring the isopycnal mixing and heliumâĂŞheat paradoxes in a suite of Earth system models. *Ocean Science*, 11(4):591–605.

Gnanadesikan, A., Pradal, M.-A., and Abernathey, R. (2015b). Isopycnal mixing by mesoscale eddies significantly impacts oceanic anthropogenic carbon uptake. *Geophysical Research Letters*, 42(11):4249–4255.

Goes, M., Urban, N. M., Tonkonojenkov, R., Haran, M., Schmittner, A., and Keller, K. (2010). What is the skill of ocean tracers in reducing uncertainties about ocean diapycnal mixing and projections of the atlantic meridional overturning circulation? *Journal of Geophysical Research: Oceans*, 115(C12):C12006.

Goodwin, P., Williams, R. G., and Ridgwell, A. (2015). Sensitivity of climate to cumulative carbon emissions due to compensation of ocean heat and carbon uptake. *Nature Geoscience*, 8(1):29–34.

Gregory, J. M. (2000). Vertical heat transports in the ocean and their effect on time-dependent climate change. *Climate Dynamics*, 16(7):501–515.

Gregory, J. M., Andrews, T., and Good, P. (2015). The inconstancy of the transient climate response parameter under increasing CO2. *Philosophical Transactions of the Royal Society of London A: Mathematical, Physical and Engineering Sciences*, 373(2054).

Hansen, J., Nazarenko, L., Ruedy, R., Sato, M., Willis, J., Del Genio, A., Koch, D., Lacis, A., Lo, K., Menon, S., Novakov, T., Perlwitz, J., Russell, G., Schmidt, G. A., and Tausnev, N. (2005). Earth's energy imbalance: confirmation and implications. *Science (New York, N.Y.)*, 308(5727):1431–1435.

Hansen, J., Russell, G., Lacis, A., Fung, I., Rind, D., and Stone, P. (1985). Climate Response Times: Depedence on Climate Sensitivity and Ocean Mixing. *Science*, 229(4716):857–859.

Hansen, J., Sato, M., Hearty, P., Ruedy, R., Kelley, M., Masson-Delmotte, V., Russell, G., Tselioudis, G., Cao, J., Rignot, E., Velicogna, I., Tormey, B., Donovan, B., Kandiano, E., von Schuckmann, K., Kharecha, P., Legrande, A. N., Bauer, M., and Lo, K.-W. (2016). Ice melt, sea level rise and superstorms: evidence from paleoclimate data, climate modeling, and modern observations that 2°C global warming could be dangerous. *Atmospheric Chemistry and Physics*, 16(6):3761–3812.

Hansen, J., Sato, M., Kharecha, P., and Von Schuckmann, K. (2011). Earth's energy imbalance and implications. *Atmospheric Chemistry and Physics*, 11(24):13421–13449.

Herrington, T. and Zickfeld, K. (2014). Path independence of climate and carbon cycle response over a broad range of cumulative carbon emissions. *Earth System Dynamics*, 5(2):409–422.

IPCC (2013). Summary for policymakers. In Stocker, T., Qin, D., Plattner, G.-K., Tignor, M., Allen, S., Boschung, J., Nauels, A., Xia, Y., Bex, V., and Midgley, P., editors, *Climate Change 2013: The Physical Science Basis. Contribution of Working Group I to the Fifth Assessment Report of the Intergovernmental Panel on Climate Change*, book section SPM, pages 1–30. Cambridge University Press, Cambridge, United Kingdom and New York, NY, USA.

Knutti, R. and Stocker, T. F. (2000). Influence of the thermohaline circulation on projected sea level rise. *Journal of Climate*, 13(12):1997–2001.

Krasting, J. P., Dunne, J. P., Shevliakova, E., and Stouffer, R. J. (2014). Trajectory sensitivity of the transient climate response to cumulative carbon emissions. *Geophysical Research Letters*, 41(7):2520–2527.

Kuhlbrodt, T. and Gregory, J. M. (2012). Ocean heat uptake and its consequences for the magnitude of sea level rise and climate change. *Geophysical Research Letters*, 39(18):1–6.

Kuhlbrodt, T., Gregory, J. M., and Shaffrey, L. C. (2015). A process-based analysis of ocean heat uptake in an AOGCM with an eddy-permitting ocean component. *Climate Dynamics*, 45(11-12):3205–3226.

Le Quéré, C., Andrew, R. M., Canadell, J. G., Sitch, S., Korsbakken, J. I., Peters, G. P., Manning, A. C., Boden, T. A., Tans, P. P., Houghton, R. A., Keeling, R. F., Alin, S., Andrews, O. D., Anthoni, P., Barbero, L., Bopp, L., Chevallier, F., Chini, L. P., Ciais, P., Currie, K., Delire, C., Doney, S. C., Friedlingstein, P., Gkritzalis, T., Harris, I., Hauck, J., Haverd, V., Hoppema, M., Klein Goldewijk, K., Jain, A. K., Kato, E., Körtzinger, A., Landschützer, P., Lefèvre, N., Lenton, A., Lienert, S., Lombardozzi, D., Melton, J. R., Metzl, N., Millero, F., Monteiro, P. M. S., Munro, D. R., Nabel, J. E. M. S., Nakaoka, S.-I., O'Brien, K., Olsen, A., Omar, A. M., Ono, T., Pierrot, D., Poulter, B., Rödenbeck, C., Salisbury, J., Schuster, U., Schwinger, J., Séférian, R., Skjelvan, I., Stocker, B. D., Sutton, A. J., Takahashi, T., Tian, H., Tilbrook, B., van der Laan-Luijkx, I. T., van der Werf, G. R., Viovy, N., Walker, A. P., Wiltshire, A. J., and Zaehle, S. (2016). Global carbon budget 2016. *Earth System Science Data*, 8(2):605–649.

Leduc, M., Matthews, H. D., and de Elía, R. (2015). Quantifying the limits of a linear temperature response to cumulative CO2 emissions. *Journal of Climate*, 28(24):9955–9968.

Levermann, A., Griesel, A., Hofmann, M., Montoya, M., and Rahmstorf, S. (2005). Dynamic sea level changes following changes in the thermohaline circulation. *Climate Dynamics*, 24(4):347–354.

Lowe, J. A., Huntingford, C., Raper, S. C. B., Jones, C. D., Liddicoat, S. K., and Gohar, L. K. (2009). How difficult is it to recover from dangerous levels of global warming? *Environmental Research Letters*, 4(1):014012.

MacDougall, A. H. (2013). Reversing climate warming by artificial atmospheric carbon-dioxide removal: Can a Holocene-like climate be restored? *Geophysical Research Letters*, 40(20):5480–5485.

MacDougall, A. H. and Friedlingstein, P. (2015). The origin and limits of the near proportionality between climate warming and cumulative CO2 emissions. *Journal of Climate*, 28(10):4217–4230.

MacDougall, A. H., Swart, N. C., and Knutti, R. (2017). The uncertainty in the transient climate response to cumulative co2 emissions arising from the uncertainty in physical climate parameters. *Journal of Climate*, 30(2):813–827.

Matthews, H. D. and Caldeira, K. (2008). Stabilizing climate requires near-zero emissions. *Geophysical Research Letters*, 35(4):L04705.

Matthews, H. D., Gillett, N. P., Stott, P. a., and Zickfeld, K. (2009). The proportionality of global warming to cumulative carbon emissions. *Nature*, 459(7248):829–832.

Matthews, H. D. and Zickfeld, K. (2012). Climate response to zeroed emissions of greenhouse gases and aerosols. *Nature Climate Change*, 2(5):338–341.

Meehl, G., Stocker, T. F., Collins, W., Friedlingstein, P., Gaye, A., Gregory, J., Kitoh, A., Knutti, R., Murphy, J., Noda, A., Raper, S. C. B., Watterson, I., Weaver, A., and Zhao, Z.-C. (2007). Global Climate Projections. In Solomon, S., Qin, D., Manning, M., Chen, Z., Marquis, M., K.B. Averyt, K., M., T., and Miller, H., editors, *Climate Change 2007: Contribution of Working Group I to the Fourth Assessment Report of the Intergovernmental Panel on Climate Change*, chapter 10, pages 747–846. Cambridge University Press, Cambridge, United Kingdom and New York, NY, USA.

Meinshausen, M., Smith, S. J., Calvin, K., Daniel, J. S., Kainuma, M. L. T., Lamarque, J.-F., Matsumoto, K., Montzka, S. A., Raper, S. C. B., Riahi, K., Thomson, A., Velders, G. J. M., and Vuuren, D. P. (2011). The RCP greenhouse gas concentrations and their extensions from 1765 to 2300. *Climatic Change*, 109(1-2):213–241.

Meissner, K. J., Eby, M., Weaver, A. J., and Saenko, O. A. (2008). CO2 threshold for millennial-scale oscillations in the climate system: implications for global warming scenarios. *Climate Dynamics*, 30(2):161–174.

Meissner, K. J., Weaver, a. J., Matthews, H. D., and Cox, P. M. (2003). The role of land surface dynamics in glacial inception: a study with the UVic Earth System Model. *Climate Dynamics*, 21(7):515–537.

Munday, D. R., Johnson, H. L., and Marshall, D. P. (2014). Impacts and effects of mesoscale ocean eddies on ocean carbon storage and atmospheric pCO2. *Global Biogeochemical Cycles*, 28(8):877–896.

Newsom, E. R., Bitz, C. M., Bryan, F. O., Abernathey, R., and Gent, P. R. (2016). Southern Ocean Deep Circulation and Heat Uptake in a High-Resolution Climate Model. *Journal of Climate*, 29(7):2597–2619.

Nohara, D., Tsutsui, J., Watanabe, S., Tachiiri, K., Hajima, T., Okajima, H., and Matsuno, T. (2015). Examination of a climate stabilization pathway via zero-emissions using Earth system models. *Environmental Research Letters*, 10(9):095005.

Olson, R., Sriver, R., Goes, M., Urban, N. M., Matthews, H. D., Haran, M., and Keller, K. (2012). A climate sensitivity estimate using Bayesian fusion of instrumental observations and an Earth System model. *Journal of Geophysical Research*, 117(D4):D04103.

Paris Agreement (2015). United Nations Framework Convention on Climate Change, Paris Agreement. `http://unfccc.int/files/essential_background/convention/application/pdf/english_paris_agreement.pdf`, Accessed: Feb 1, 2016.

Peters, G. P., Andrew, R. M., Solomon, S., and Friedlingstein, P. (2015). Measuring a fair and ambitious climate agreement using cumulative emissions. *Environmental Research Letters*, 10(10):105004.

Purkey, S. G. and Johnson, G. C. (2012). Global contraction of Antarctic Bottom Water between the 1980s and 2000s. *Journal of Climate*, 25(17):5830–5844.

Rahmstorf, S. (2006). Thermohaline Ocean Circulation. In Elias, S. A., editor, *Encyclopedia of Quaternary Sciences*, pages 1–10. Elsevier, Amsterdam.

Rahmstorf, S. (2007). A semi-empirical approach to projecting future sea-level rise. *Science*, 315(5810):368–370.

Raupach, M. R., Davis, S. J., Peters, G. P., Andrew, R. M., Canadell, J. G., Ciais, P., Friedlingstein, P., Jotzo, F., van Vuuren, D. P., and Le Quere, C. (2014). Sharing a quota on cumulative carbon emissions. *Nature Climate Change*, 4(10):873–879.

Robinson, A., Calov, R., and Ganopolski, A. (2012). Multistability and critical thresholds of the greenland ice sheet. *Nature Clim. Change*, 2(6):429–432.

Rogelj, J., den Elzen, M., Höhne, N., Fransen, T., Fekete, H., Winkler, H., Schaeffer, R., Sha, F., Riahi, K., and Meinshausen, M. (2016a). Paris Agreement climate proposals need a boost to keep warming well below 2°C. *Nature*, 534(7609):631–639.

Rogelj, J., Schaeffer, M., Friedlingstein, P., Gillett, N. P., van Vuuren, D. P., Riahi, K., Allen, M., and Knutti, R. (2016). Differences between carbon budget estimates unravelled. *Nature Climate Change*, 6(3):245–252.

Ross, A., Matthews, H. D., Schmittner, A., and Kothavala, Z. (2012). Assessing the effects of ocean diffusivity and climate sensitivity on the rate of global climate change. *Tellus B: Chemical and Physical Meteorology*, 64(1):1–10.

Sarmiento, J. and Gruber, N. (2006). *Ocean Biogoechemical Dynamics*. Princeton University Press.

Sarmiento, J., Hughes, T., Stouffer, R., and Manabe, S. (1998). Simulated response of the ocean carbon cycle to anthropogenic climate warming. *Nature*, 393(6682):245–249.

Schimel, D. S. (1995). Terrestrial ecosystems and the carbon cycle. *Global Change Biology*, 1(1):77–91.

Schmittner, A., Oschlies, A., Giraud, X., Eby, M., and Simmons, H. L. (2005). A global model of the marine ecosystem for long-term simulations: Sensitivity to ocean mixing, buoyancy forcing, particle sinking, and dissolved organic matter cycling. *Global Biogeochemical Cycles*, 19(3):GB3004.

Schmittner, A., Urban, N. M., Keller, K., and Matthews, D. (2009). Using tracer observations to reduce the uncertainty of ocean diapycnal mixing and climate-carbon cycle projections. *Global Biogeochemical Cycles*, 23:n/a–n/a. GB4009.

Schmittner, A. and Weaver, A. J. (2001). Dependence of multiple climate states on ocean mixing parameters. *Geophysical Research Letters*, 28(6):1027–1030.

Shine, K. P., Fuglestvedt, J. S., Hailemariam, K., and Stuber, N. (2005). Alternatives to the global warming potential for comparing climate impacts of emissions of greenhouse gases. *Climatic Change*, 68(3):281–302.

Smith, P., Davis, S. J., Creutzig, F., Fuss, S., Minx, J., Gabrielle, B., Kato, E., Jackson, R. B., Cowie, A., Kriegler, E., van Vuuren, D. P., Rogelj, J., Ciais, P., Milne, J., Canadell, J. G., McCollum, D., Peters, G., Andrew, R., Krey, V., Shrestha, G., Friedlingstein, P., Gasser, T., Grübler, A., Heidug, W. K., Jonas, M., Jones, C. D., Kraxner, F., Littleton, E., Lowe, J., Moreira, J. R. J. R., Nakicenovic, N., Obersteiner, M., Patwardhan, A., Rogner, M., Rubin, E., Sharifi, A., Torvanger, A. A., Yamagata, Y., Edmonds, J., Yongsung, C., Grubler, A., Heidug, W. K., Jonas, M., Jones, C. D., Kraxner, F., Littleton, E., Lowe, J., Moreira, J. R. J. R., Nakicenovic, N., Obersteiner, M., Patwardhan, A., Rogner, M., Rubin, E., Sharifi, A., Torvanger, A. A., Yamagata, Y., Edmonds, J., and Yongsung, C. (2016). Biophysical and economic limits to negative CO2 emissions. *Nature Climate Change*, 6(1):42–50.

Smith, S. M., Lowe, J. a., Bowerman, N. H. a., Gohar, L. K., Huntingford, C., and Allen, M. R. (2012). Equivalence of greenhouse-gas emissions for peak temperature limits. *Nature Climate Change*, 2(7):535–538.

Solomon, S., Plattner, G.-K., Knutti, R., and Friedlingstein, P. (2009). Irreversible climate change due to carbon dioxide emissions. *Proceedings of the National Academy of Sciences*, 106(6):1704–1709.

Stocker, T. and Schmittner, A. (1997). Influence of CO2 emission rates on the stability of the thermohaline circulation. *Nature*, 388(6645):862–865.

Tokarska, K. B., Gillett, N. P., Weaver, A. J., Arora, V. K., and Eby, M. (2016). The climate response to five trillion tonnes of carbon. *Nature Climate Change*, 6(9):851–855.

Tokarska, K. B. and Zickfeld, K. (2015). The effectiveness of net negative carbon dioxide emissions in reversing anthropogenic climate change. *Environmental Research Letters*, 10(9):094013.

Trossman, D. S., Palter, J. B., Merlis, T. M., Huang, Y., and Xia, Y. (2016). Large-scale ocean circulation-cloud interactions reduce the pace of transient climate change. *Geophysical Research Letters*, 43(8):3935–3943.

Weaver, A. J., Eby, M., Wiebe, E. C., Bitz, C. M., Duffy, P. B., Ewen, T. L., Fanning, A. F., Holland, M. M., MacFadyen, A., Matthews, H. D., Meissner, K. J., Saenko, O., Schmittner, A., Wang, H., and Yoshimori, M. (2001). The UVic earth system climate model: Model description, climatology, and applications to past, present and future climates. *Atmosphere-Ocean*, 39(4):361–428.

Williams, K., Harris, C., Bodas-Salcedo, A., Camp, J., Comer, R., Copsey, D., Fereday, D., Graham, T., Hill, R., Hinton, T., et al. (2015). The met office global coupled model 2.0 (gc2) configuration. *Geoscientific Model Development*, 8(5):1509–1524.

Williams, R. G., Goodwin, P., Rouusenov, V. M., and Bopp, L. (2016). A framework to understand the transient climate response to emissions. *Environmental Research Letters*, 11(1):15003.

Winton, M., Griffies, S. M., Samuels, B. L., Sarmiento, J. L., and Frölicher, T. L. (2013). Connecting changing ocean circulation with changing climate. *Journal of Climate*, 26(7):2268–2278.

Wu, P., Jackson, L., Pardaens, A., and Schaller, N. (2011). Extended warming of the northern high latitudes due to an overshoot of the Atlantic meridional overturning circulation. *Geophysical Research Letters*, 38(24):1–5.

Zickfeld, K., Arora, V. K., and Gillett, N. P. (2012). Is the climate response to CO2 emissions path dependent? *Geophysical Research Letters*, 39(5):L05703.

Zickfeld, K., Eby, M., Alexander, K., Weaver, A. J., Crespin, E., Fichefet, T., Goosse, H., Philippon-Berthier, G., Edwards, N. R., Holden, P. B., Eliseev, A. V., Mokhov, I. I., Feulner, G., Kienert, H., Perrette, M., Schneider von Deimling, T., Forest, C. E., Friedlingstein, P., Joos, F., Spahni, R., Steinacher, M., Kawamiya, M., Tachiiri, K., Kicklighter, D., Monier, E., Schlosser, A., Sokolov, A., Matsumoto, K., Tokos, K. S., Olsen, S. M., Pedersen, J. O. P., Ridgwell, A., Shaffer, G., Yoshimori, M., Zeng, N., and Zhao, F. (2013). Long-term climate change commitment and reversibility: an EMIC intercomparison. *Journal of Climate*, 26(16):5782–5809.

Zickfeld, K., Eby, M., Matthews, H. D., Schmittner, A., and Weaver, A. J. (2011). Nonlinearity of carbon cycle feedbacks. *Journal of Climate*, 24(16):4255–4275.

Zickfeld, K., Eby, M., Matthews, H. D., and Weaver, A. J. (2009). Setting cumulative emissions targets to reduce the risk of dangerous climate change. *Proceedings of the National Academy of Sciences*, 106(38):16129–16134.

Zickfeld, K., MacDougall, A. H., and Matthews, H. D. (2016). On the proportionality between global temperature change and cumulative CO2 emissions during periods of net negative CO2 emissions. *Environmental Research Letters*, 11(5):055006.

Zickfeld, K., Solomon, S., and Gilford, D. M. (2017). Centuries of thermal sea-level rise due to anthropogenic emissions of short-lived greenhouse gases. *Proceedings of the National Academy of Sciences*, 114(4):657–662.